A STUDY OF FIBRE GLASS GRID REINFORCED HOT MIX ASPHALT CONCRETE

SINA MIRZAPOUR MOUNES

**FACULTY OF ENGINEERING
UNIVERSITY OF MALAYA
KUALA LUMPUR**

2016

A STUDY OF FIBRE GLASS GRID REINFORCED HOT MIX ASPHALT CONCRETE

SINA MIRZAPOUR MOUNES

THESIS SUBMITTED IN FULFILLMENT OF THE REQUIREMENT FOR THE DEGREE OF DOCTOR OF PHILOSOPHY

FACULTY OF ENGINEERING
UNIVERSITY OF MALAYA
KUALA LUMPUR

2016

UNIVERSITY OF MALAYA
ORIGINAL LITERARY WORK DECLARATION

Name of Candidate: SINA MIRZAPOUR MOUNES

Registration/Matric No: KHA080055

Name of Degree: Doctor. of Philosophy

Title of Project Paper/Research Report/Dissertation/Thesis ("this Work"): A STUDY OF FIBRE GLASS GRID REINFORCED HOT MIX ASPHALT CONCRETE

Field of Study: Civil Engineering

 I do solemnly and sincerely declare that:

(1) I am the sole author/writer of this Work;
(2) This Work is original;
(3) Any use of any work in which copyright exists was done by way of fair dealing and for permitted purposes and any excerpt or extract from, or reference to or reproduction of any copyright work has been disclosed expressly and sufficiently and the title of the Work and its authorship have been acknowledged in this Work;
(4) I do not have any actual knowledge nor do I ought reasonably to know that the making of this work constitutes an infringement of any copyright work;
(5) I hereby assign all and every rights in the copyright to this Work to the University of Malaya ("UM"), who henceforth shall be owner of the copyright in this Work and that any reproduction or use in any form or by any means whatsoever is prohibited without the written consent of UM having been first had and obtained;
(6) I am fully aware that if in the course of making this Work I have infringed any copyright whether intentionally or otherwise, I may be subject to legal action or any other action as may be determined by UM.

Candidate's Signature   Date:

Subscribed and solemnly declared before,

Witness's Signature   Date:

Name:

Designation:

ABSTRACT

Asphalt concrete is a viscoelastic material that exhibits time and temperature dependency and, except at low temperatures, viscoplastic non-recoverable strain as well as self-recovery ability in certain conditions. During the last decades, several methods such as geogrid reinforcement of asphalt concrete have been adopted by researchers to improve its characteristics. This thesis seeks to investigate some of the properties of Hot Mix Asphalt (HMA) reinforced by four different types of fibreglass grid, and unreinforced control specimens, on the basis of grid tensile strength and mesh size.

In this study, the dynamic modulus of reinforced and control specimens was measured using a flexural bending beam apparatus, and the master curves for each type of specimen were constructed. The same testing aparatus with other testing conditions were used for determining the possible effect of inlaid fibreglass grids on damage recovery ability of asphalt concrete. Finally, dynamic creep test was used to investigate the behaviour of different types of asphalt concretes utilised in this study, at two different levels of load to rest ratios. In addition, a recently developed creep curve model has been verified and used to study the creep behaviour of the specimens in the primary and secondary regions of the creep curve, as well as determining the boundary point of the regions.

The results of dynamic modulus test showed that, at very high frequencies or very low temperatures, the asphalt mixture bore most of the applied load and the grids were not activated. However, at very low frequencies or very high temperatures, the grids were activated and the load was borne by the grid. Moreover, at very low frequencies or very high temperatures, not only was the tensile strength of the grids effective, but the grid opening sizes also influenced the dynamic moduli of the asphalt concrete. In addition, the smaller mesh sized grids recorded much lower asymptote values. The same

behaviour of grid tensile strength and mesh size was observed for the inflection points of the master curves. In terms of damage recovery ability of grid reinforced and unreinforced specimens, the results show that small mesh sized grids have a significant positive effect on the damage recovery ability of asphalt concrete, while there was little or no difference in recovery performance between the two types of tensile strength grids with large openings or the unreinforced (control) specimens. In addition, the small mesh sized grids with high tensile strength showed a higher damage recovery than the same mesh sized grids with low tensile strength. Finally, the creep test results and analysis suggest that not only grid tensile strength, but also grid mesh size is of great importance in combatting permanent deformation of the fibreglass grid reinforced asphalt concrete within the conditions and grids used in this study. In a nutshell, higher tensile strength and/or smaller mesh size grids lead to overall better performance of grid reinforced specimens. Moreover, great care must be taken when the creep curves are not reached in the tertiary region, and the creep rate must be taken into account to avoid any misinterpretation of the results.

ABSTRAK

Konkrit asfalt adalah bahan viscoelastic yang mempamerkan masa dan suhu pergantungan dan, kecuali pada suhu rendah, tekanan tidak boleh diperolehi semula viscoplastic serta keupayaan pemulihan diri dalam keadaan tertentu. Sepanjang dekad yang lalu, beberapa kaedah seperti tetulang geogrid konkrit asfalt telah digunakan oleh pengkaji untuk meningkatkan ciri-ciri. Tesis ini bertujuan untuk menyiasat beberapa sifat-sifat Hot Mix Asphalt (HMA) diperkukuh oleh empat jenis grid gentian kaca, dan spesimen kawalan tanpa tetulang, berdasarkan grid kekuatan tegangan dan saiz mesh.

Dalam kajian ini, modulus dinamik spesimen diperkukuh dan kawalan diukur menggunakan lenturan lenturan alat rasuk, dan lengkung induk bagi setiap jenis spesimen telah dibina. Radas ujian sama dengan syarat-syarat ujian lain telah digunakan untuk menentukan kesan yang mungkin grid bertatahkan gentian kaca kepada keupayaan pemulihan kerosakan konkrit asfalt. Akhir sekali, ujian rayapan dinamik digunakan untuk menyiasat tingkah laku jenis konkrit asfalt digunakan dalam kajian ini, di dua tahap yang berbeza beban untuk berehat nisbah. Di samping itu, model lengkung rayapan baru-baru ini dibangunkan telah disahkan dan digunakan untuk mengkaji tingkah laku rayapan daripada spesimen di kawasan rendah dan menengah lengkung rayapan, serta menentukan titik sempadan wilayah.

Keputusan ujian modulus dinamik menunjukkan bahawa, pada frekuensi yang sangat tinggi atau suhu yang sangat rendah, campuran asfalt melahirkan sebahagian besar daripada beban yang dikenakan dan grid tidak diaktifkan. Walau bagaimanapun, pada frekuensi yang sangat rendah atau suhu yang sangat tinggi, grid telah diaktifkan dan beban ditanggung oleh grid. Selain itu, pada frekuensi yang sangat rendah atau suhu yang sangat tinggi, bukan sahaja kekuatan tegangan grid berkesan, tetapi grid pembukaan saiz juga dipengaruhi modulus dinamik konkrit asfalt. Di samping itu, mesh kecil grid bersaiz mencatatkan nilai asimptot lebih rendah. Kelakuan sama kekuatan

grid tegangan dan mesh saiz diperhatikan untuk mata lengkok balas lengkung induk. Dari segi keupayaan pemulihan kerosakan grid diperkukuh dan spesimen tanpa tetulang, keputusan menunjukkan bahawa mesh kecil grid bersaiz mempunyai kesan positif yang besar ke atas keupayaan pemulihan kerosakan konkrit asfalt, manakala terdapat sedikit atau tiada perbezaan dalam prestasi pemulihan antara kedua-dua jenis kekuatan tegangan grid dengan bukaan besar atau tanpa tetulang (kawalan) spesimen. Di samping itu, mesh kecil grid bersaiz dengan kekuatan tegangan yang tinggi menunjukkan pemulihan kerosakan yang lebih tinggi daripada mesh grid bersaiz sama dengan kekuatan tegangan yang rendah. Akhirnya, keputusan ujian rayapan dan analisis menunjukkan bahawa bukan sahaja grid kekuatan tegangan, tetapi juga saiz grid mesh adalah amat penting dalam memerangi ubah bentuk kekal grid gentian kaca bertetulang konkrit asfalt dalam keadaan dan grid yang digunakan dalam kajian ini. Secara ringkas, kekuatan tegangan yang lebih tinggi dan / atau lebih kecil grid saiz mesh membawa kepada prestasi keseluruhan yang lebih baik daripada grid bertetulang spesimen. Selain itu, berhati-hati perlu diambil apabila lengkung rayapan tidak dicapai di rantau ini tinggi, dan kadar rayapan yang perlu diambil kira untuk mengelakkan sebarang salah tafsir keputusan.

ACKNOWLEDGEMENT

TABLE OF CONTENTS

LIST OF FIGURES

LIST OF TABLES

CHAPTER 1: INTRODUCTION

1.1 Introduction

Asphalt concrete is a composite material made up of aggregate particles, bitumen, air, and other components such as additives, modifiers, fines, and water in either liquid or vapour form (Kim, 2009). It is a viscoelastic material that exhibits time and temperature dependency and, except at low temperatures, viscoplastic non-recoverable strain. It is also known that, when in its linear viscoelastic range, asphalt concrete is thermorheologically simple (TRS) (Chehab et al., 2002). On the other hand, various types of distresses can affect flexible pavements, such as fatigue cracking and rutting (Bohuslav, 2008). The geosynthetic reinforcement of asphalt concrete is thus one means of tackling fatigue and rutting (Austin & Gilchrist, 1996; Button & Lytton, 2007; Chang et al., 1999; Collin et al., 1996; Laurinavičius & Oginskas, 2006; Leshchinsky & Ling, 2012; Ling & Liu, 2001; Perkins, 1999; Thakur et al., 2012; Yang et al., 2012). In the recent years because of an increase in traffic and heavy vehicles, rutting is one of the most frequent defects in flexible pavements, particularly in hot climates. Geosynthetic reinforcement of asphat concrete was found to be effective in increasing the resistance of asphalt concrete against rutting. In addition, microcrack healing occurring in the course of fatigue leading to the damage to be recovered in the asphalt concrete, can strongly influence fatigue life (Si et al., 2002a). Recovery of an asphalt mixture refers to the behaviour of a deformed material after the load is removed. Before removing the load, the asphalt mixture undergoes a deforming process, in which cracking and permanent deformation are generated in the material if the load is destructive (Luo, 2012). Hence, considering the complex behaviour of asphalt concrete, it can be worthy to study the effects of various types of geosynthetics on the behaviour of asphalt concrete.

1.2 Problem Statement

The main objective of this research is to study certain characteristics of hot mix asphalt reinforced with fibreglass grids.

Rheological measurements such as the dynamic modulus cannot be taken across a wide ranges of temperatures or frequencies by testing instruments, but can be represented by constructing dynamic modulus master curves. Through the latter, the dynamic modulus of asphalt concrete can be assessed and viewed over a broad range of loading times, from a few thousandths of a second to several years. In this study, initially, an effort has been made to construct the master curves of fibreglass grid reinforced and unreinforced asphalt concrete.

The healing phenomenon is an important factor affecting the predicted life of asphalt concrete materials. There are three distinctive stages in the fatigue process: microcrack initiation and growth, macro-crack propagation, and final failure. Throughout this process, fatigue life can be strongly affected by microdamage healing, particularly during the period of microcrack initiation and growth. In fact, asphalt concrete recovery (or the lack of it) is one of the main factors contributing to damage characteristics as well as pavement life prediction. During the recovery phase, microcracks caused by loading start to heal. However, there have been no significant studies conducted on the possible effects of reinforcing geogrids on the damage recovery ability of asphalt concrete. This study also aims to fill that gap, by examining the influence of fibreglass grids on the damage recovery ability of reinforced hot mix asphalt concrete.

In recent years, because of increases in the volume of traffic and of heavy vehicles, rutting is one of the most frequent defects found in flexible pavements, particularly in hot climates. Rutting shows up as depressions formed in the wheel path in a pavement. It normally occurs when a permanent deformation of each layer in the pavement structure accumulates under a repetitive traffic load (Tayfur et al., 2007). Accumulation

of residual strains in wearing course may cause serious problems, particularly through aquaplaning on wet pavements (Fwa et al., 2004; Sivilevičius & Petkevičius, 2002; Verhaeghe et al., 2007, September). Thus, not only does pavement rutting lead to higher road maintenance costs, but it also increases the risk to human life through accidents caused by water accumulating in depressions (ruts) in pavements.

During the past decade or so, there have been a lot of studies by various researchers into how to hinder rutting in pavements through geosynthetic reinforcement (Austin & Gilchrist, 1996; Collin et al., 1996; Laurinavičius & Oginskas, 2006; Leshchinsky & Ling, 2012; Ling & Liu, 2001; Perkins, 1999; Thakur et al., 2012; Yang et al., 2012). However, there are limited studies on separate or combined effects of tensile strength and mesh size of geogrids on asphalt concrete properties. In this study, an effort is finally made to address the separate and combined effects of tensile strength and mesh size of fibreglass grid on dynamic creep behaviour of reinforced asphalt concrete. Furthermore, considering the benefits can be achieved by using an equation to construct the creep curve as an alternative for laboratory dynamic creep test and the gap of previous studies in terms of such equation, it is tried to verify a recently developed creep curve model for geogrid reinforced and unreinforced hot mix asphalt.

1.3 Hypothesis

- There is not significant study on possible effect of geogrids on damage recovery ability of asphalt concrete. We hypothesise that fibreglass grid applied in hot mix asphalt can influence the damage recovery ability of hot mix asphalt concrete.

1.4 Research Questions

- What are the separate and combined effects of geogrid tensile strength and mesh size on permanent deformation of asphalt concrete?

- What creep curve model can be used to draw the creep curve of fibreglass grid reinforced and unreinforced hot mix asphalt concrete?

1.5 Research Objectives

This study aims to investigate certain characteristics of hot mix asphalt concrete reinforced with different types of fibreglass grids. The primary objectives of the study are:

- To construct master curves for unreinforced and fibreglass grid reinforced asphalt concrete specimens and investigate the effects of the grids on these curves.

- To investigate the influence of utilised fibreglass grids on the damage recovery ability of the specimens.

- To determine the separate and combined effects of fibreglass grid tensile strength and aperture size in improving the resistance to permanent deformation of unreinforced and fibreglass grid reinforced asphalt concrete specimens; and

- To model the achieved regions of the creep curves for both unreinforced and fibreglass grid reinforced asphalt concrete specimens, and to estimate the behaviour of the primary and secondary regions and the corresponding boundary points.

1.6 Scope of Thesis

Asphalt concrete is a viscoelastic material which displays complex behaviour in different conditions. The main objective of this research is to study certain characteristics of geogrid reinforced asphalt concrete.

This study seeks to investigate the influence of fibreglass grids on the damage recovery ability of hot mix asphalt. It also examines the separate and combined effects

of grid tensile strength and mesh size on the permanent deformation resistance of the reinforced hot mix asphalt. Finally, it utilises and verifies a recently developed creep curve model for fibreglass grid reinforced and unreinforced hot mix asphalt concrete, including determining the behaviour of the primary and secondary regions and the boundary points of those regions for the applied geogrid specimens. At all of the testing conditions, the grids are applied at mid-depth of the specimens.

1.7 Significance of the Study

Geogrids are one of the means of reinforcing asphalt concrete. A better understanding of the effects of these on the damage recovery of asphalt concrete will help future researchers and practitioners to determine more accurately the fatigue life of geogrid reinforced asphalt concrete. Furthermore, this study seeks to calculate more precisely than hitherto the effects of geogrid tensile strength and mesh size on the resistance to permanent deformation of reinforced asphalt concrete. This should help in the future selection of the optimum type of geogrids for reinforcing purposes, taking into account field conditions and the required rutting resistance – leading to potentially lower maintenance and replacement costs. Finally, modelling creep curves can be a very useful alternative to performing dynamic creep tests in the laboratory.

1.8 Organisation of Thesis

This thesis consists of five chapters. Chapter 1 introduces the focus of the study, including the problem statement, the objectives of the research and the scope of the study, followed by an outline of the thesis. Chapter 2 presents a review of previous literature on subjects related to the study, such as flexible pavement distresses and methods to tackle these. It concludes by explaining the limitations and gaps in previous studies, and argues the need for the current research. Chapter 3 introduces the materials and methodologies used to conduct the laboratory tests. Chapter 4 contains the results of

the study and a discussion of these. Finally, Chapter 5 presents the main conclusions derived from the previous chapters, together with recommendations for future work.

CHAPTER 2: LITERATURE REVIEW

2.1 Introduction

Flexible pavements are composed of bituminous and granular materials (Huang, 1993). Rutting (also called permanent deformation), fatigue cracking, and reflective cracking are three of the most important distresses causing flexible pavement to be deteriorated. Reinforcement of asphalt mixes is a method adopted to enhance the performance of pavement against the distresses. A definition for reinforcement can be stated as to incorporate certain materials having favourable properties within other material lacking those properties (Maurer & Malasheskie, 1989).

In the recent years, high-strength and high stiffness grids as well as fabrics have been used in asphalt concrete overlays in order for minimising cracks and in some of the cases for waterproofing purposes. In was shown that probably the grids and fabrics with high stiffness can change the direction of reflective cracking into horizontal plane under the interlayer and retard indefinitely the reflective cracking, provided they are properly constructed.(Amini, 2005).

In terms of strength determination of asphalt concrete for pavement design purposes, dynamic modulus is one of the parameters which is of great importance for the upcoming Mechanistic Empirical Pavement Design Guide (MEPDG). Dynamic modulus will be used for designing flexible pavements in MEPDG. Asphalt concrete material stiffness is represented by dynamic modulus when it is tested in a compressive-type, repeated load test. In evaluation of rutting and fatigue cracking in the MEPDG one of the key parameters is dynamic modulus (Bennert, 2009). Master curve construction of asphalt mixture through which there would be possibility of integrating traffic speed, climate effects, and ageing for pavement response and distress models, is a key feature in material characterisation (Kim, 2009).

Recovery of an asphalt mixture refers to the behaviour of a deformed material after the load is removed. Before removing the load, the asphalt mixture undergoes a deforming process, in which cracking and permanent deformation are generated in the material if the load is destructive (Luo, 2012). Healing phenomenon in asphalt concrete is one of the factors affecting it in terms of the predicted life of it. In fact, asphalt concrete recovery is one of the main contributing factors of the damage characteristics as well as pavement life prediction. During the recovery phase, the micro cracks caused by loading, starts to heal. Damage recovery decreases cracking damage leading to implying inaccuracy in the prediction of remaining cracks in asphalt mixtures.

According to literature some of the methods used for measuring damage recovery in asphalt concrete are through impact-resonance test, flexural bending beam test, dissipated creep strain energy. Furthermore, some of the factors reported to be effective on healing of asphalt concrete are, binder, aggregates, surface energy, rest periods, waveform, and temperature.

In the recent years because of an increase in traffic and heavy vehicles, rutting is one of the most frequent defects in flexible pavements, particularly in hot climates. Rutting reveals itself as depressions which are formed in the pavement's wheel path. It normally occurs when permanent deformation of each layer in pavement structure accumulates under the repetitive traffic loading (Tayfur et al., 2007).

Various laboratory testing methods are developed to investigate the rutting resistance of asphalt concrete. Some of these methods are static/dynamic creep test, wheel track test, and indirect tensile test. Dynamic creep test developed by Monismith et al. is thought to be one the best assessment methods for evaluating resistance of asphalt concrete against permanent deformation (Kalyoncuoglu & Tigdemir, 2011). One of the most important outputs of dynamic creep test is creep curve, illustrating permanent deformation versus loading cycles. Regardless of type of considered material, this curve

can be divided into three distinct regions, namely primary, secondary, and tertiary region (Witczak et al., 2004).

Since creep curves obtained by dynamic creep test are used to assess the permanent deformation resistance of asphalt concretes, not only is the behaviour of each region of creep curve of great importance, but identification of the boundary points connecting primary to secondary region, and secondary to tertiary region is also of great importance. So, characterising the obtained creep curves from dynamic creep test can help better understanding of permanent deformation resistance of asphalt concrete.

2.2 Flexible Pavements

Bituminous and granular materials are the main materials of which flexible pavements are composed. Newark, New Jersey was the first place at which the first asphalt roadway was constructed in the United States, in 1870. Sheet-asphalt pavement, is a hot mixture of asphalt cement with clean, angular, graded sand and mineral filler. For the first time, this type of asphalt pavement was laid in 1876 on Pennsylvania Avenue in Washington, D.C., with imported asphalt from Trinidad Lake (Huang, 1993).

2.3 Distresses of Flexible Pavement

There are various types of distresses affecting flexible pavements such as rutting, patching, fatigue cracking, Longitudinal/transverse cracking, ravelling, flushing, etc (Bohuslav, 2008). In the following sub-chapters three of the main distresses of flexible pavements are described.

2.3.1 Rutting

Rutting which is often referred as permanent deformation is a common type of distress which occurs in flexible pavements. By movement of truck tyres across an asphalt concrete pavement, there would be a very small amount of deflection in the pavement. The ranges for such deflections are from much less than a tenth of a

millimetre in cold weather-in very stiff pavement and subgrade-to a millimetre or more in warm weather-in hot and very soft pavement surface. After passing the truck tyre over a certain spot on the pavement, the pavement intends to spring back to its original position. Nevertheless, complete recovery will not be achieved on the pavement surface. In lieu of that, in the wheel path, a very small amount of permanent deformation will occur. Rut depth of 20 mm or more can be observed in intensely rutted pavements.

A rough riding surface can be resulted through ruts. Then, during rain or snow events, the water filled in ruts can cause hydroplaning and losing control of the vehicles travelling on the pavement. It was normally considered excessive and a significant safety hazard when the rut depths were about 10 mm or more. The rutting diagram in HMA pavements is illustration in Figure 2.1 (NCHRP, 2011).
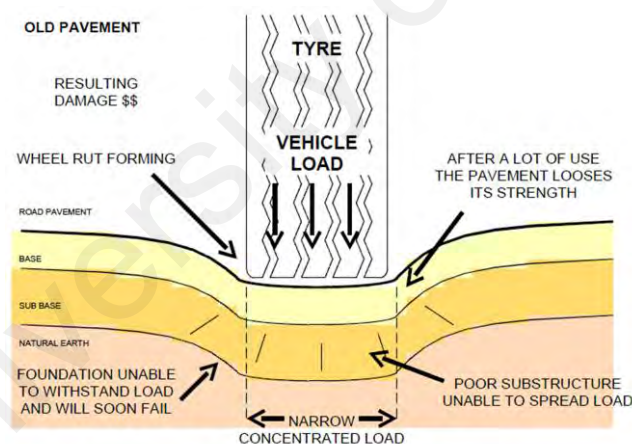
Figure 2.1: Schematic diagram of rutting in a flexible pavement ("Rutting,")

2.3.2 Fatigue Cracking

Another type of the main distresses influencing the design life of asphalt concrete is fatigue cracking which occurs in areas of the pavement subjected to repeated loading such as the areas along the wheel paths. Initially, fatigue cracking occurs as a series of

small isolated microcracks, then with the aid of repeated loading, grow and interconnect yielding the characteristic chicken wire or alligator skin cracking patterns. Cyclic laboratory tests are the typical types of the tests performing on the specimens produced in the laboratory in order for understanding the performance of different asphalt/aggregate combinations in terms of fatigue resistance. Number of cycles to failure is a quantity which has been used traditionally in order to describe the fatigue performance of the tested specimen. Depending on the loading mode such as stress or strain control mode of loading, quite different ranking of the specimens can be obtained (Kutay et al., 2008). Figure 2.2 illustrates the schematic drawing of fatigue cracking.
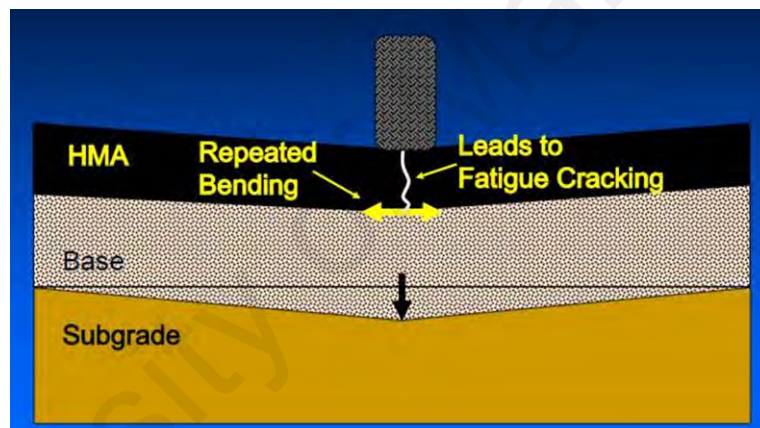
Figure 2.2: Schematic diagram of fatigue in flexible pavements
(M. Signore, 2012)

2.3.3 Reflective Cracks

Reflective cracking is another type of the cracks in the HMA overlay. Such crack type reflects the crack or joint pattern in the underlying pavement. A more detailed description is that reflective cracks are fractures in an HMA overlay or surface course that are a result of, and reflect, the crack or joint pattern in the underlying layer, and may be either environmental or traffic induced. Reflective cracks are a major concern to airport management personnel because they can significantly reduce the service life of HMA overlays of airside airport pavements. After placing HMA overlays over jointed

11

and/or severely cracked rigid and flexible pavements, in a short period of time, the cracks and joints in the existing pavement can reflect to the surface. In order for preventing the generation of loose aggregate and increased roughness that can be harmful to aircraft operations, such reflective cracks needs to be maintained. Because the water will be allowed to penetrate the underlying layers through these cracks which can lead to further damage to the pavement structure (Von Quintus et al., 2009).

2.4 Reinforcement of Flexible Pavements

A definition for reinforcement can be incorporation of certain materials with some favourable properties within other material lacking those properties (Maurer & Malasheskie, 1989). Consequently, fibre reinforcement is considered as a coin with two sides. One side is to directly include the fibres into the matrix of materials such as asphalt concrete, in a random way. Another side comprises the oriented fibrous materials, e.g. geosynthetics family. It is emphasised that the former concept is not as well-known as the second, not only in optimising fibre properties, fibre diameter, length, surface texture etc., but also in reinforcing mechanism (Mahrez et al., 2005).

According to Hongu and Philips (1990) quoted by Abtahi et al. (2009), the idea of using fibres to enhance the material behaviour is an old suggestion. Using of fibres can be traced back to a 4000 year old arch in China constructed with a clay earth mixed with fibres or the Great Wall built 2000 years ago (Abtahi et al., 2009). However, it was reported by Mahrez et al. (2003) that it was early 1960s when the modern developments of fibre reinforcement started.

The pavement sections can be strengthen structurally through geosynthetic materials by changing the response of the pavement to loading only if the geosynthetics has a higher modulus and adequate cross sectional area to considerably strengthen the

overlay. A more uniform load distribution and a reduction in the rut depth at the surface of the asphalt course are provided by geogrid reinforcement.

The resistance of overlay against reflective cracking may be improved by inclusion of a geosynthetic interlayer either by a stress-relief or a reinforcement mechanism, or by a combination of both (Khodaii et al., 2009).

2.5 Asphalt Concrete

Asphalt concrete was defined by Kim (2009) as a composite material composed of aggregate particles, bitumen, air, and other components such as additives, modifiers, fines, and water in either liquid or vapour forms.

Asphalt concrete is a viscoelastic material that exhibits time and temperature dependency, and, except at low temperatures, viscoplastic non-recoverable strain. It is also known that when in its linear viscoelastic range, asphalt concrete is thermorheologically simple (TRS). In other words, given that the asphalt concrete is in its undamaged state, time-temperature superposition can be applied. As an application of that principle, data from complex modulus testing conducted within linear viscoelastic limits at different frequencies and temperatures should yield a single continuous master curve for dynamic modulus and phase angle as a function of frequency at a given reference temperature by horizontally shifting individual curves along the logarithmic frequency axis. That is, the effects of time or frequency and temperature can be expressed through one joint parameter. As such, the same material property values can be obtained either at low temperatures and long times or at high test temperatures but short times (Chehab et al., 2002).

Bitumen is defined as a class of black or dark-coloured (solid, semisolid, or viscous) cementitious substances, natural or manufactured, composed principally of high

molecular weight hydrocarbons, of which asphalts, tars, pitches, and asphaltites are typical (ASTM, 2000b).

2.6 Geosynthetics

According to the definition of geosynthetic in ASTM (2000f) is a planar product manufactured from a variety of synthetic polymer materials that are specifically fabricated to be used in geotechnical, geoenvironmental, hydraulic and transportation engineering related materials as an integral part of a man-made project, structure, or system.

2.6.1 History, Pros and Cons

The utilisation of geosynthetics in roadway pavements has erupted from the 1960s and 1970s, when the materials were utilised for solving problems, to today when geosynthetics are designed into the pavement structure for improving performance and economics (Berg et al., 2000).

It was reported that there would not be much technical difficulty or additional cost in asphalt reproduction processes (i.e. resurfacing or demolition) by the presence of geosynthetics as a reinforcing agent in the asphalt concrete. Rather, the reinforced asphalt concrete can still efficiently be recycled through shredding the polymer geosynthetic during cold milling. Therefore, from a construction view, the reinforced pavement is considered feasible (Ling & Liu, 2001).

One of the most important aspects in constructing and performing of geosynthetic interlayers is the proper selection of tack coat material and its application rate. For that purpose, a consultation should be made with the particular geosynthetic manufacturer's installation manual. Hot asphalt cement is the material which is usually recommended as a tack for geosynthetics. Uniformly application of tack coats at a specified rate is of great importance and it can be achieved through the using of a calibrated asphalt

distributor truck. Also, a tack coat spray of approximately 4 inches wider than the geosynthetic was recommended. Some of the common field problems reported interms of tack coat applications include proper temperature control, clogged or leaking spray bars or nozzles, application of too much or too little material, and nonuniform distribution (Button & Lytton, 2007).

2.6.2 Types of Geosynthetics

Generally geosynthetic consist of seven main classes named geotextiles, geogrids, geonets, geomembranes, geosynthetic clay liners, geofoam, and geocomposites. In terms of soil and asphalt pavement reinforcement, out of the above-menstioned seven classes, geotextiles, geogrids and geocomposites are the ones usually utilised (Hosseini et al., 2009). More details on geogrids were described in the following section.

2.6.2.1 Geogrids

According to ASTM (2000f), geogrid is defined as a geosynthetic formed by a regular network of integrally connected elements with apertures greater than 6.35 mm to allow interlocking with surrounding soil, rock, earth, and other surrounding materials to function primarily as reinforcement. Figure 2.3 shows some types of geogrid. One of the initial researches on geogrid reinforcement of asphalt concrete was in 1981 being a four year programme started to investigate the benefits of using geogrids for asphalt reinforcement (Austin & Gilchrist, 1996).
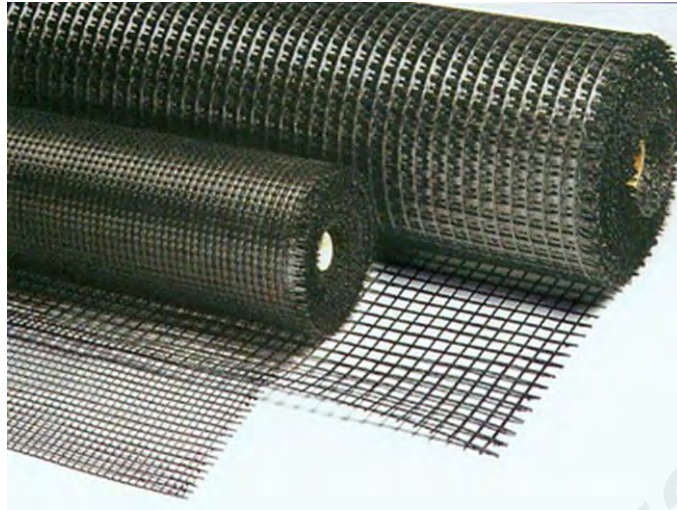
Figure 2.3: Geogrid

According to Barsdale (1991), quoted by Button and Lytton (2007), typically moduli of grids are higher than those of fabrics and logically should take on more stress at low strain levels. That is the reason why grids systems primarily serve as a reinforcing interlayer. In order that the grids act as overlay reinforcement, they must be tightly stretched, or slightly pretensioned, and it must have sufficient stiffness. Stiffness values varying from 80 to >1000 lb/inch were observed in typical grids used as overlay reinforcement. Nevertheless, only the stiffest grids (>1000) can operate as overlay reinforcement.

In terms of reinforcement mechanism by geogrids, it was reported by Chang et al. (1999) that the reinforcing function of geogrids comes from two aspects. One is from the ribs of the geogrid, which restrain the growth of a crack; the other is from the deformation of the geogrid, which absorbs the energy at the tips of the crack and thus stops the crack from growing outward.

2.6.2.2 Geonets

Geonets, also known as geospacers, are another type of geosynthetic materials. Generally, the nets which are used to improve the pavement performance are embedded between the base layer and the sub-base layer. However, in the recent years, the use of steel reinforcement net between the binder layer and the base layer was examined. It was observed that steel reinforcement develops fracture resistance of asphalt pavement at all temperatures, and a 3D-FEM simulation was developed for the experiment, both of which were in accordance with each other (Montepara et al., 2007, September). In addition, the capability of steel reinforcement netting interlayer system for retarding reflective cracks was simulated using 3D finite element method and the ABAQUS cohesive zone model. The results of analysis showed that by means of steel reinforcement netting located between the hot mix asphalt overlay and existing portland cement concrete, reflective crack initiation time increased by seven times (Baek & Al-Qadi, 2008).

2.6.2.3 Geocomposites

Geocomposite, a function of which is reinforcing the pavement structure, consists of geotextile, geogrids, geonets and/or geomembranes, is another type of geosynthetic material. Based on a research, a composite combination of stiff polypropylene geogrid with a geotextile being resistant to normal temperatures of asphalt paving can improve the surface deformation resistance of pavements as well as providing ease in installation of geogrids. Moreover, pavements furnished with this geocomposite can resist large horizontal strains developping in the bituminous material at the same level of the geogrid. In addition, reinforcing composites in the bound layers of the pavement may have an important role in reducing the stresses of subgrade in a pavement on soft foundations (Austin & Gilchrist, 1996). Another research on this matter carried out on large dimension asphalt samples in Poland, showed that by applying repeated loading

test, the samples reinforced with geocomposites functioned better compared with geogrid reinforced samples on fatigue crack resistance behaviour (Grabowski & Pozarycki, 2008). Similarly in comparison with paving fabrics, a study was performed on geocomposite reinforced, paving fabric reinforced, and unreinforced asphalt beams by three different load levels for each set. It was observed that geocomposite reinforced asphalt beams had the best performance and paving fabric inclusion functioned better in comparison with unreinforced set (Saraf et al., 1996).

According to the theory of composites, the effectiveness of reinforcements depends on transfer of load from asphalt layers to reinforcement elements (stiffness of bonding), volume ratio of reinforcement, stiffness modulus of reinforcement to stiffness modulus of asphalt layers ratio, and durability of geosynthetics parameters during usage. Because stiffness modulus of asphalt mixes is strongly dependent on temperature and frequency of load, a given system of interlayer in one condition could be treated as a reinforcement, and in another condition it could not (Zielinski, 2013).

2.6.3 Functions of Geosynthetics in Pavements

The primary functions of a geosynthetic when used in general engineering applications can be identified as being one of separation, filtration, drainage, reinforcement, fluid/gas containment, or erosion control. In some cases the geosynthetic may serve dual functions. The major functions of geosynthetic materials in relation with transportation engineering are separation, reinforcement, filtration, drainage and acting as a liquid barrier (Khodaii et al., 2009), but if the geosynthetics are installed properly in the asphalt layer, their main function is as fluid barrier, cushion, and reinforcement. The reinforcement function of it is discussed in the following section.

2.6.3.1 Reinforcement function

Reinforcement is a function of geosynthetic material in pavements. Such material structurally strengthens the pavement section by changing the response of the pavement to loading, causing to have a chance to re-direct the reflective crack. In general, ribs of the geogrid, which suppress the growth of a crack (Saraf & Majidzadeh, 1973, June), and deforming of geogrid, that absorbs the energy at the tip of the crack (Saraf et al., 1996) are the main causes in stopping growth of the crack. Many researches have been performed for the purpose of achieving an insight to reinforcement characteristic of geogrid. One of the earliest studies in 1982 used stiff biaxial geogrids as the reinforcing agent in asphalt at Canvey Island, near London, England, where 10,000 square metre of geogrid were used for controlling reflective cracking over a cracked concrete pavement (Austin & Gilchrist, 1996). The mechanism of reinforcement can only occur if the geosynthetic properly constructed, has a higher modulus compared to asphalt concrete and sufficient cross sectional area to substantially strengthen the overlay (Khodaii et al., 2009; Lytton, 1989). Similarly, it was concluded that in order to ensure a satisfactory performance of pavement, the bonding condition between geosynthetic reinforcement and asphalt as well as the geogrid stiffness are of great importance (Komatsu et al., 1998; Ling & Liu, 1999). For reinforcement purposes geosynthetics can be placed in both aggregate layers of pavement, and its asphaltic layers.

The main reinforcement mechanism in paved roads is usually called base or sub-base course restraint, and subgrade lateral restraint (Berg et al., 2000). The reinforcement mechanisms in bound layes of pavements are either through fatigue life extension or reduction of layers' thickness Brown et al. (2001), and/or, eliminating or reducing the reflective cracking (Austin & Gilchrist, 1996; Brown et al., 2001; Elseifi & Al-Qadi, 2004; Khodaii et al., 2009; Montestruque et al., 2004), and/or, reducing the rutting and permanent deformation (Komatsu et al., 1998).

In a study conducted through a full-scale accelerated test, the geosynthetic materials were embedded in aggregate layers showed that geogrid can significantly reduce horizontal shear deformation of the aggregate layer, particularly in the traffic direction. Furthermore, pavement structure composition and layer thickness were identified as decisive factors to pavement performance and the distress type developed (Al-Qadi et al., 2008). The results of another full-scale field test which was carried out on a strain-gauge instrumented geogrid reinforced unpaved road in Switzerland indicated that using various geosynthetics have a relevant reinforcing influence provided that a thin aggregate layer is used on a soft subgrade. The stiffness of geosynthetic affects the degree of reinforcement which can be accomplished and is limited by finite lateral anchoring forces (Hufenus et al., 2006). However, in terms of effect of geosynthetics on unbound materials in pavement structure, the dynamic responses of the soil specimens with and without geogrid reinforcement were investigated. It was concluded that geogrids affectd little on increasing the dynamic modulus of the soil specimens, unlike their significant effect on damping ratios of reinforced specimens (Yang et al., 2014).

The performance of pavement structure depends not only on how aggregate layers perform, but the role of asphaltic layers is also important. Extensive studies have been performed on behaviour of geosynthetics in asphalt concrete. Results of a research on geogrid reinforced samples indicated that the crack propagation rate reduced significantly in reinforced samples. In addition, old pavement type whether being concrete or asphalt pavement, geogrid position and temperature were found as factors affecting the type of crack propagation in asphalt overlays (Khodaii et al., 2009).

In terms of effectiveness of geogrids in improving the resistance of asphalt concrete to fatigue failure, the results of one of the earliest studies on reinforcement effect of a kind of high tensile strength plastic geogrid known as Tensar, revealed that by using Tensar, fatigue crack resistance may be developed, thickness savings of asphaltic

materials may be achieved, and number of load repetition may be doubled (Halim et al., 1983).

In addition, a laboratory and case study performed in Taiwan where three types of geogrids, two of which made by glass fibre and the other by high density polyethylene (HDPE) were tested. Based on fatigue test of asphalt concrete beams placed on clearance rubber, fatigue lives of glass grids of 100 kN/m strength and HDPE geogrids were 3 to 5 times greater than those of an unreinforced beam; this value for glass grids of 200 kN/m strength was 5 to 9 times. Besides, obtaining 10 month rutting depth measurements from the site, confirmed the improvement from the geogrids (Chang et al., 1999). This may imply that geosynthetic reinforcement can be used for fatigue related problems of pavements as well. Due to complex behaviour of bituminous materials such as plastic flow, examining such characteristics can be functional and help to have pavements with long performance lives. The effectiveness of high-modulus and high-strength polyoxymethylene fibre geogrid on plastic and crack resistance of asphalt concrete was examined in Japan through wheel tracking machine. The results indicated a remarkable increase in viscosity and durability of reinforced asphalt concrete. Moreover, in that study durability was correlated to geogrid mesh size and degree of adhesion of it to asphalt concrete, meaning that by decreasing size of the mesh and increasing adhesion, the durability improves (Komatsu et al., 1998).

A research was carried out in National University of Singapore to set a logical basis so as to design and analyse the porous asphalt pavement for car parks and roads in Singapore. By means of large scale laboratory wheel tracking tests, using geogrid in the surface course interface, geogrid was found effective in providing rutting resistance under local condition (Ong & Fwa, 2005), implying that geogrid may be utilised not only in hot mix asphalt which is common place, but also in other types of asphalt concrete. Depending on the means pavement structure is used, it may tolerate different

types of loading. In this regard, a research on geogrid reinforced asphalt concrete through monotonic and cyclic static loading as well as dynamic loading under plain strain conditions was conducted. It was found that stiffness and bearing capacity of the asphalt concrete pavement were increased by inclusion of geogrid. This improvement was more significant for dynamic loading compared with static loading (Ling & Liu, 1999). Consequently, it might be said that the amount of success can be achieved in sections of pavement experiencing mostly static loading e.g. parking lots might be less than parts enduring dynamic loading such as on high speed highways.

Mathematical modelling is one of the methods used to estimate the behaviour of materials without performing many expensive tests and spending a lot of time. A research developed a precise model through which the mechanical behaviour of bituminous mixtures can be simulated. It also allows a reliable comparison among the various bituminous systems tested. It was performed by means of four-point flexural test under repeated loading cycles on bi-layer bituminous systems reinforced with three different geosynthetic materials. No fracture was observed in geosynthetic-furnished samples, and it was concluded that the 4PB test can discriminate the differences between treated and untreated specimens (Virgili et al., 2009).

Nowadays, the use of geogrids made by glass in pavement structure is also propounded. Based on an extensive study carried out on glass grid reinforced laboratory pavement sections, and comparing the results with 3D finite element computer modelling output, it was concluded that by including the glass fibre grid, performance of pavement is raised. It was also deduced that glass grid provides a crack propagation resistance for asphalt concrete (Siriwardane et al., 2010). Moreover, a mathematical modelling was carried out by employing theory of fracture mechanics, and the crack growth resistant ability of glass grid reinforced asphalt overlay was determined. Asphalt mix design tests, three-point bending tests, and fatigue crack propagation tests were

carried out. The results showed that glass grid improves crack resistance ability of asphalt concrete through its low rate of elongation and its high tensile strength, and it is able to offer a suitable solution for reflective cracks (Zheng & Aysar, 2007). In another study in South Korea, four types of modifying and three kinds of reinforcing materials were examined. Different combination of them was effective in improving asphalt concrete performance. However, the most remarkable effect took place when modified asphalt was reinforced with a glass fibre grid, leading to an increase in fatigue life and dynamic stability by up to 20-30 folds (Kim et al., 1999).

Furthermore, in terms of ability of geosynthetic reinforcement against permanent deformation, based on investigation of different studies in a review paper by Mirzapour Mounes et al. (2014) in terms of asphalt concrete reinforcement, it appears that geosynthetic reinforcement particularly some certain geogrids positively influences permanent deformation of asphaltic pavements.This influence was stronger in geogrid reinforced samples when the laid location of geogrid was in mid-depth of asphalt concrete compared to embedding at the bottom. In addition, a conclusion was drawn by them that mesh size and adhesion of geogrid to asphalt concrete played important roles in durability improvement.

In summary it can be said that reinforcement of pavement by geosynthetics may increase the resistance of pavement structure against distresses. However, care must be taken that various geosynthetic materials may have different reinforcement levels, meanwhile, the reinforcing ability of a certain geosynthetic may be influenced by several factors (Mirzapour Mounes et al., 2011).

2.6.4 Design Principles of Geosynthetics for Roads

In order to prevent unnecessary differential settlements of the pavement structure during its construction on soft soils a certain bearing capacity of the sub-base is

required. For the subsoil having insufficient bearing capacity, stabilisation is important and necessary. Excavation of the soft material, chemical stabilisation by using chalk or by using geosynthetics are some of the means in order for increasing the bearing capacity. When geosynthetics are utilised in paved road structures (surface layer existing of asphalt or concrete) the long-term behaviour has to be taken into account. That is, the measurements of bearing capacity on top of the base should be maintained during the total service life of the road (Meyer & Elias, 1999, March). The existing design methods for geosynthetic reinforced flexible pavements in the unbound base aggregate layer are mostly empirical (Berg et al., 2000)

Because of various factors as stated below, these existing design methods have been limited in use by many state departments of transportation.

1. Design methods are not part of a nationally recognised pavement design procedure.
2. Design methods are often times applicable to a narrow range of design conditions.
3. Design methods are often times proprietary, making it difficult to directly compare the cost-benefit of several reinforcement products from different manufacturers.

2.6.5 Efficiency Factor of Geosynthetics as Reinforcement

A fabric effective factor (F_{EF}) as a proper factor indicating the performance of the reinforcement was defined as given in Equation 2.1 (Saraf et al., 1996). This factor can be applied to both woven and nonwoven fabrics.

$$F_{EF} = \frac{N_r(reinforced)}{N_{ur}(unreinforced)}$$

Equation (2.1)

where: N_r is the number of cycles to failure of reinforced asphalt concrete, and

N_{ur} is the number of cycles to failure of unreinforced asphalt concrete.

F values as high as 16 was reported in the literature. This indicated that a remarkable increase can be achieved in a pavement lifetime by using the geosynthetic as reinforcement or separation agent in pavement structures. The enhancement in pavement performance achieved by geosynthetic utilisation was confirmed by the results obtained by field observations and research. Figure 2.4 illustrates an improvement of pavement achieved against rutting by using geosynthetics (Palmeira, 2007). As it can be seen in the graph for a certain rut depth, number of load repetitions for geosynthetic reinforced pavements was almost three times higher than those of without geosynthetics.
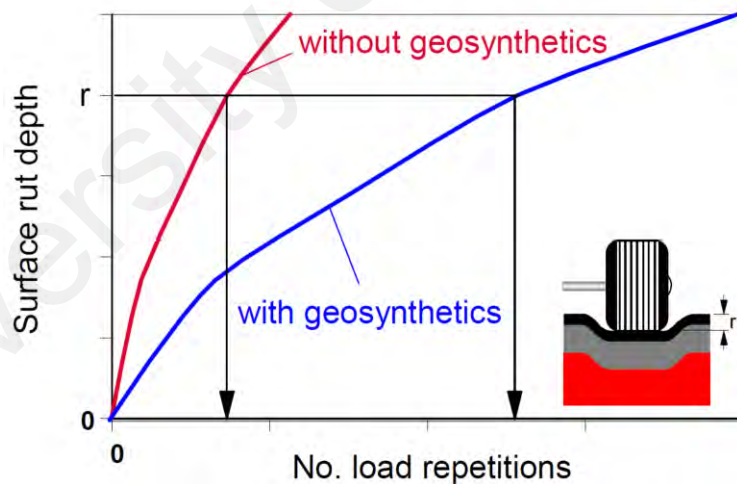
**Figure 2.4: Increase of pavement life time due to the use of
geosynthetic reinforcement
(Palmeira, 2007)**

2.7 Asphalt Concrete Stiffness

Asphalt concrete stiffness is a material property. Precisely, in the stress-strain curve of asphalt concrete, the slope of the curve is asphalt concrete stiffness. What is unique

about a material property is that it is independent of the test apparatus, or the sample size or geometry that is used to measure it. The converse of this is that if a measured result of a test does depend upon the test apparatus or the sample size or geometry, then that measured result is not and cannot be a material property. There are several types of stress-strain curves from which asphalt concrete stiffness can be measured as a material property (Kim, 2009).

2.7.1 Affecting Factros of Asphalt Concrete Stiffness

Asphalt concrete stiffness depends upon the strain rate of loading, the temperature, the moisture content of the bitumen, the stress state, the aggregate particles, the bitumen itself, the fines in the mastic, the water in liquid and vapour form and its location with the mixture, the air in the mixture, its age, and its reactivity with oxygen, and any additives or modifiers that have been added to the mixture (Kim, 2009). Each of these is discussed subsequently.

2.7.1.2 Temperature, moisture, and rate of loading

The stiffness of asphalt concrete is dependent on the temperature and strain rate of loading. At any given temperature, asphalt concrete will deform slowly and permanently if it is loaded slowly, while if it is loaded at a higher rate, it will be much stiffer and will be subject to fracture. At any given strain rate of loading, there is a temperature above which the material will relax quickly enough that no stress will accumulate in the test sample (Kim, 2009).

Moisture has a similar effect on the stiffness and type of damage that occurs in asphalt concrete. Although the mechanisms are distinctively different, high moisture and high temperature both result in plastic flow. At any given strain rate, there is a moisture content in the asphalt, above which the material relaxes faster than the stress can build up in the material (Kim, 2009).

2.7.1.3 Stress state

The state of stress of asphalt concrete modifies its stiffness. In an isotropic mixture, the stiffness depends upon the level of the first and the second deviatoric stress invariants I_1 and J_2'. In an anisotropic mixture, which is the usual case, the stiffness is directional and depends upon both the two stress state invariants just mentioned and the stress tensor components. Because of the shape of the particles and the way that an asphalt concrete mixture is compacted, there is a vertical modulus, a horizontal modulus, and a shear modulus. There are also two Poisson's ratios. One of the Poisson's ratios is located in the vertical plane, while the other one is located in the horizontal plane. Testing and analysis of triaxial test data has been able to determine all five of the moduli of this cross-anisotropic case. The fact of cross-anisotropy has several important implications for the way that pavements resist both fracture and plastic deformation (Kim, 2009).

Figure 2.5 shows Poisson's ratios that rise well above 0.5 which is the maximum that it can be in a material that has a constant elastic modulus. The measurement of Poisson's ratios that are above 0.5 is a common observation in stress-dependent materials such as asphalt concrete and unbound aggregate base course materials. It also varies with the frequency and direction of loading. A typical pattern is shown in Figure 2.5 (Kim, 2009).
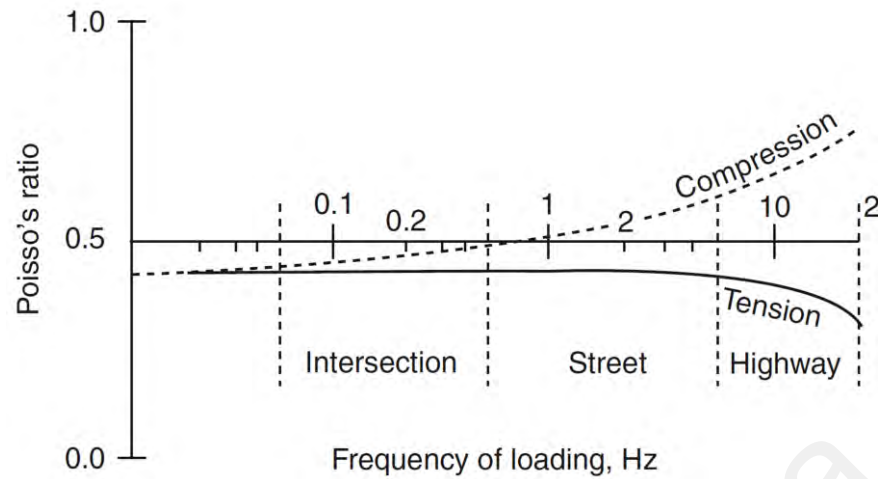
Figure 2.5: Poisson's ratios of asphalt concrete
(Kim, 2009)

The tensile Poisson's ratios remain below 0.5 while the compressive Poisson's ratios rise above 0.5 once the loading frequency rises above about one Hz. Highway traffic loading is typically above 8 Hz and this means that an asphalt concrete layer, when loaded with traffic travelling at normal highway speeds, tries to expand laterally. When prevented from doing so, the asphalt concrete layer builds up a confining pressure that stiffens the asphalt concrete, resists lateral plastic deformation, and presses closed any microcracks that may be growing in the asphalt. This is illustrated in Figure 2.6 (Kim, 2009).
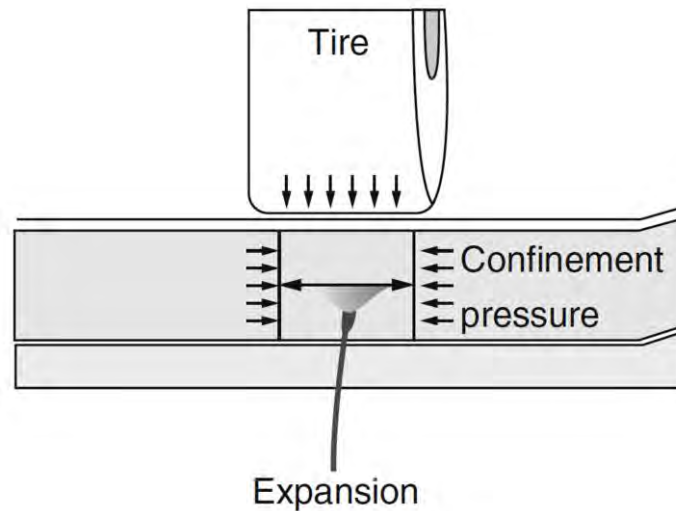
Figure 2.6: Effect of large compressive Poisson's ratios

2.7.1.4 Aggregate particles

Cross-anisotropic is one of the characteristics of asphalt concrete stiffness. The principal reason for the emergence of the cross-anisotropic formulation of the stiffness of asphalt concrete is because of the shape of the aggregate particles. When they are compacted, the oblong particles tend to lie flat resulting in a modulus that is greater in the vertical direction than in the horizontal direction. In addition to the shape, the size and size distribution of the particles and the texture of the particles also have an effect upon the directional stiffness and the effective Poisson's ratio of asphalt concrete. The graph in Figure 2.7 shows qualitatively the effect of particle size distribution on the ―effective‖ Poisson's ratio of the mixture. The closer that the particle size distribution approaches the maximum density distribution line, the higher will be the ―effective‖ Poisson's ratio (Kim, 2009).
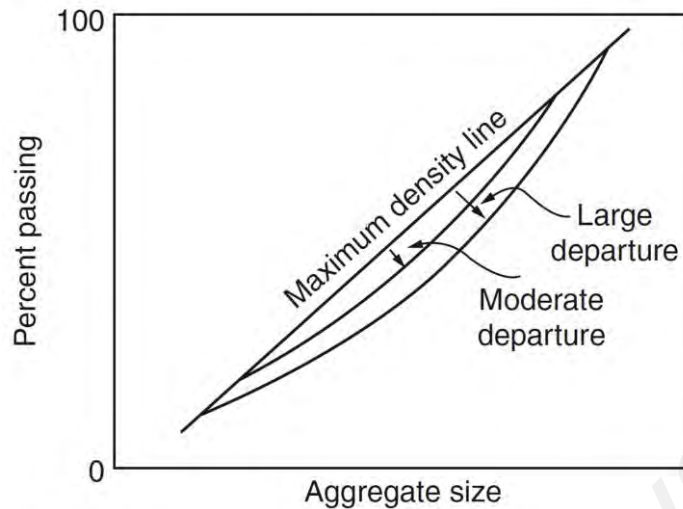
**Figure 2.7: Effect of particle size distribution on the
"effective" Poisson's ratio
(Kim, 2009)**

2.7.1.5 Asphalt binder

The material properties of the asphalt binder which affect the stiffness of asphalt concrete are the compliance, the mastic film thickness, the ageing, and the wetting and the surface energy dewetting components. The compliance is a material response to a constant applied stress. This time-dependent strain divided by the constant stress is the creep compliance. The creep compliance is related to the relaxation modulus. This is determined in a uniaxial test in which a strain is imposed on the material and held constant. The stress in the material then relaxes as the time after the strain was first applied increases. The relaxation modulus is the time-dependent stress divided by the constant strain (Kim, 2009).

2.7.1.6 Surface energies

There are three components of surface energy: the nonpolar or Lifshitz-Van der Waals, and the Lewis acid and Lewis base polar components. There is a hysteresis effect between the wetting and the dewetting surface energies. The wetting surface

energies are associated with the healing of the microfractures in the asphalt while the dewetting surface energies are associated with the fracture of the asphalt (Kim, 2009).

As an asphalt ages, the surface energies change so as to reduce healing and to make fracture easier. Thus, the nonpolar portion of the wetting surface energies grows larger and the polar portions grow smaller as the asphalt ages. At the same time, both of the portions of the dewetting surface energies decrease so as to decrease the work of fracture with age. Once a microcrack, or a crack, forms in the asphalt binder, the surface energies on each face of the crack interact to provide the cohesive bond strength against fracture and to provide the surface energy to promote healing (Kim, 2009).

The aggregate particles also have surface energy components which interact with the surface energies of the asphalt binder to produce the adhesive bonding strength at the interface between the two. It must be noted that when water is on the interface between asphalt and an aggregate surface, the water acts to destroy the adhesive bond (Kim, 2009).

There are two components of moisture damage to asphalt concrete stiffness: one due to soaking and the other due to repeated loading progressively opening adhesive debonding interface zones along the surface of the aggregates in the asphalt concrete mixture. The soaking damage depends upon the rate of moisture diffusion and the water amount that the asphalt film can hold. The rate of moisture diffusion depends upon the relative vapour pressure in the immediate vicinity of each aggregate particle and the thickness of the mastic film surrounding the aggregate (Kim, 2009).

2.7.1.7 Fines

The fines in an asphalt concrete mix are all of the particles that are smaller than 0.075 mm. They make up around half of the volume of the mastic. The stiffness of the mix will be affected significantly by how well the fines bond with the asphalt binder,

the size and size distribution of the fines, how well they are dispersed in the mastic, and their surface energy compatibility with the asphalt both with and without water. The size, size distribution, and dispersion all work together to arrest microcracks when they are small and easier to stop (Kim, 2009).

2.7.1.8 Air voids

Air voids may be viewed with some accuracy as small particles with zero stiffness. Small, well-dispersed air voids in the asphalt concrete mixture will provide several benefits to the mix, including acting as microcrack arresters and providing well-dispersed volumes for the asphalt to expand into at high temperatures. Too much air will accelerate the growth of microcracks and too little air will cause bleeding (or flushing) and promote large plastic deformations. Too much air will also provide ready access of both air and water into the interior of an asphalt concrete layer and will accelerate ageing and moisture damage. As with the fine particles, the air voids must be small and well-dispersed in order to have its desired effect on the stiffness of the mixture (Kim, 2009).

2.7.2 Complex Modulus

Complex Modulus is a computed value defining the relationship between stress and strain for a linear viscoelastic material (Dougan et al., 2003). It consists of two portions called, the real and imaginary portions which can be written as:

$$E^* = E' + iE''$$ Equation (2.2)

E' is generally referred to as the storage or elastic modulus component of the complex modulus; E'' is referred to as the loss or viscous modulus.

2.7.3 Dynamic Modulus

Dynamic Modulus is the absolute value of the complex modulus which is the product of dividing the maximum (peak-to-peak) stress by the recoverable (peak-to peak) axial

strain for a material. The dynamic modulus of a material can be determine by subjecting it to a sinusoidal loading (Dougan et al., 2003). According to Witczak (2002), it can be shown mathematically in Equation 2.3.

$$|E^*| = \frac{\sigma_0}{\varepsilon_0}$$ Equation (2.3)

(ζ_0) is the maximum dynamic stress and (ε_0) is the peak recoverable axial strain.

2.7.4 Phase Angle

Phase angle is the angle in degrees between a sinusoidal applied (peak-to-peak) stress and the resulting (peak-to-peak) strain in a controlled-stress test (Dougan et al., 2003). In other words, the angle by which ε_0 lags behind ζ_0 is the phase angle which is an indicator of the viscous properties of the material being evaluated. Mathematically, this is expressed as the following equations (Kaloush et al., 2002).

$$E^* = |E^*| \cos \varphi + i|E^*|\sin\varphi$$ Equation (2.4)

$$\varphi = \frac{t_i}{t_p} \times (360)$$ Equation (2.5)

where: $t_i =$ time lag between a cycle of stress and strain (s),

$t_p =$ time for a stress cycle (s), and

$i =$ imaginary number.

For a pure elastic material, $\varphi = 0$, and the complex modulus (E*) is equal to the absolute value, or dynamic modulus. For pure viscous materials, $\varphi = 90°$.

2.7.5 Linear Viscoelastic

Linear viscoelastic: within the context of dynamic modulus test linear viscoelastic is a behaviour in which the stress or strain amplitude doesn't have any influence on dynamic modulus (Dougan et al., 2003).

It was quoted by Dougan et al. (2003) that originally Coffman and Pagen at Ohio State University in the 1960's developed a linear viscoelastic test protocol for determining the dynamic modulus of asphaltic materials. It was also reported that the test can be applied in a uniaxial (triaxial) condition in either compression or tension. According to them, over the past 30-35 years the compression mode has been adopted in most of the tests for obtaining the dynamic modulus.

2.7.6 Asphalt Concrete Master Curve

Master curve construction of the mixture is a key feature in the material characterisation. Through the master curve, viscoelastic behaviour of the material can be defined as a function of both temperature and loading time (Kim, 2009). In other words, representing rheological measurements such as dynamic modulus at wide ranges of temperatures or frequencies can be allowed through master curves (Rahimzadeh, 2002). By using the master curve it is possible for integrating traffic speed, climatic effects, and ageing for the pavement response and distress models. Thus, in order for fully characterising asphalt mixtures, master curve construction is required (Kim, 2009).

According to Anderson et al. (1991), Christensen and Anderson (1992), and Hayton (1998), quoted by Rahimzadeh (2002) in order to construct a master curve over a range of frequencies and temperatures time-temperature superposition is utilised.

2.7.6.1 Time-temperature superposition principle

It has been shown in earlier research by Goodrich (1991) and Kim and Lee (1995), quoted byChehab et al. (2002) that asphalt concrete is a thermorheologically simple material when it is in linear viscoelastic state. That is, given that the asphalt concrete is in its undamaged state, time-temperature superposition can be applied. As an application of that principle, data from complex modulus testing conducted within linear viscoelastic limits at different frequencies and temperatures should yield a single

continuous master curve for dynamic modulus and phase angle as a function of frequency at a given reference temperature by horizontally shifting individual curves along the logarithmic frequency axis. In other words, one joint parameter can express the effects of time or frequency and temperature. As such, either at low temperatures and long times or at high test temperatures but short times the same values of material property can be obtained (Chehab et al., 2002).

2.7.6.2 Shift factor

The collected test data at various temperatures can be shifted relative to the time of loading or frequency, in order that the various curves can be aligned to form a single master curve. The requires shift can be defined as a shift factor a(T) at a given temperature. This shift factor is a constant by which the time must be divided so as to obtain a reduced time for the master curve. In frequency domain, the frequency must be multiplied by shift factor a(T) to obtain reduced frequency ξ as shown in Equation 2.6 (Kim, 2009).

$$\xi = f.\,a(T) \quad \text{or} \quad \log(\xi) + \log[a(T)] \qquad \text{Equation (2.6)}$$

In terms of the bituminous viscoelastic materials, there are three different commonly used functions in order to model the time-temperature superposition relationship. Those functions are log-linear, Arrhenius, and Williams-Landel-Ferry equations. Arrhenius and Williams-Landel-Ferry (WLF) equations are presented as the following:

-   **Arrhenius type equation:**

    An Arrhenius type equation is a commonly used formula for the shift factor used by various researchers such as Francken and Clauwaert (1987, July) and Jacobs (Jacobs, 1995), quoted by Medani and Huurman (2003), as well as by Lytton et al. (1993). It is shown in Equation 2.7.

$$\log a_T = C.\left(\frac{1}{T} - \frac{1}{T_{ref}}\right) = \log e.\frac{\Delta H}{R}\left(\frac{1}{T} - \frac{1}{T_{ref}}\right) \qquad \text{Equation (2.7)}$$

where:
T = the experimental temperature (K),
T_{ref} = the reference temperature (K),
C = a constant (K),
ΔH = activation energy (J/mol), and
R = ideal gas constant, 8.314 J/(mol.K).

Some of the values reported for the constatnt C based on the literature are as the following.

1) C=10920 K, by Francken and Clauwaert (1987, July).

2) C=13060 K, by Lytton et al. (1993).

3) C=7680 K, by Jacobs (1995).

- **Williams-Landel-Ferry (WLF) equation**

Another formula for calculating the shift factor is the Williams-Landel-Ferry (WLF) equation developed by Williams et al. (1955), quoted by Medani and Huurman (2003). It can be shown as in Equation 2.8.

$$log f_{fict} - log f = log \alpha_T = -\frac{C_1.(T - T_{ref})}{C_2 + T - T_{ref}} \qquad \text{Equation (2.8)}$$

where:
f_{fict} = the frequency where the master curve should be read (Hz),
f = loading frequency (Hz), and
C_1, C_2 = empirical constants.

and other variables as previously defined.

It was quoted by Medani and Huurman (2003), that Sayegh (1967, January) reported C1 and C2, 9.5 and 95, respectively; however, those constants were reported as 19 and 92 by Lytton et al. (1993).

For the purpose of mathematically modelling of the bituminous mixtures' response to construct the master curve, there are two different functional forms that mainly have been used by different researchers. One of the functional forms is generalised power law, and the other is Sigmoidal function (Kim, 2009).

For time or frequency dependency, the generalised power-law has been used at low to intermediate temperatures when shifting creep or relaxation test data for asphalt mixtures. As the higher temperature data is included, polynomial fitting functions have been used to capture the form of master curve initiated by the material behaviour (Kim, 2009).

In terms of shifting the dynamic modulus test data, the best method is Sigmoidal Fitting Function (Equation 2.9) to fit the dynamic modulus test data obtained from temperatures ranging from -18°C to 55°C (Kim, 2009).

$$\log(|E^*|) = \delta + \frac{\alpha}{1 + e^{\beta - \gamma \log(\xi)}}$$
Equation (2.9)

where: $|E^*|$ =   dynamic modulus,

ξ =   reduced frequency,

δ =   minimum modulus value,

α =   span of modulus values, and

β, γ =   shape parameters.

2.8 Recovery and Healing in Asphalt Concrete

Recovery of an asphalt mixture refers to the behaviour of a deformed material after the load is removed. Before removing the load, the asphalt mixture undergoes a deforming process, in which cracking and permanent deformation are generated in the material if the load is destructive (Luo, 2012). On the other hand, in some of the materials such as polymers there is another phenomenon taking place during deforming process which is called healing, the mechanism of which is described by Prager and Tirrell (1981), quoted by Carpenter and Shen (Carpenter & Shen, 2006) as follows:

When two pieces of the same amorphous polymeric material are brought into contact at a temperature above the glass transition, the junction surface gradually develops increasing mechanical strength until at long enough contact time, the full fracture strength of the virgin material is reached. At this point the junction surface has in all respects become indistinguishable from any other surface that might be located within the bulk material: we say the junction has healed.

The composition of asphalt mixture, including bitumen content, aggregate structure characteristicas and gradation, affects the healing phenomenon which can take place in the asphalt concrete (Liu, 2012).

2.8.1 Mechanism of Fatigue Cracking

As it was stated in Section 2.3.2 fatigue is a process in which microscopic flaws in a material under repeated loading grow in size and become more densely concentrated until flaws of a visible size develop (Si et al., 2002a). The repetitive nature of traffic loading is the main reason of fatigue; longitudinal cracks in the wheel path appear on the pavement surface and by continuing of the loading the cracks propagate into alligator cracking patterns. The surface cracks can be created through shear and tensile

forces, respectively at the pavement surface and at the bottom of the asphalt layer (Daniel & Kim, 2001).

Three distinctive stages have been identified in the fatigue process: microcrack initiation and growth, macro-crack-propagation, and final failure. During the whole process, fatigue life can be strongly affected by microdamage healing, particularly during the period of microcrack initiation and growth. The fatigue's process is defined as a balance between fatigue fracture during loading cycles and recovery of healing due to rest periods (Si et al., 2002b).

At temperatures below about 25°C, the dominant mechanism in the damage process is one of microcrack development and growth and ultimately coalescence of microcracks and propagation in the form of macrocracks (Si et al., 2002a).

It was quoted by Castro and Sánchez (2006) that on the basis of the results of fatigue tests conducted by De La Roche (1996), as well as several laboratories in the RILEM Inter-Laboratory Programme on Fatigue (Francken & Verstraeten, 1998), two distinct fatigue mechanisms seem to be confirmed. Those two mechanisms had already been suggested by Verstraeten (1991), as the following:

- Thixotropic effect: At relatively high temperatures (>15°C), fatigue is mainly caused by the thixotropic behaviour of bitumen. Under repeated loads, bitumen changes progressively from a gel to a sol structure.

- Structural damage: At relatively low temperatures (< 5°C), fatigue is mainly caused by the appearance of structural damage in the mixtures.

Based on the literature, the healing of the mixture during rest periods would be explained by these fatigue mechanisms. At high temperatures, healing occurs because of a return of bitumen from a sol to a gel structure and, if the rest time is sufficient, this sol to gel structure return would be almost total. However, at low temperatures, rest periods

do not allow the healing of the structural damage created by the loading cycles and recovery would only be partial (Castro & Sánchez, 2006).

2.8.2 Healing Mechanism and Determination Methods

Extensive studies of healing have been carried out in the field of polymer science. A comprehensive review on this subject is given in Kausch et al. (1987) with eighty references, quoted by Luo (2012). One of these theories that is applied to asphalt materials is Wool and O'Connor's theory (1981) quoted by Luo (2012), which states that healing is combination of two processes: wetting of two crack surfaces (―wetting") and an increase of the joint strength of the two crack surfaces. ―Wetting" is a process in which contact and adhesion are established between two crack surfaces. Increase of the joint strength of the two crack surfaces that are in complete contact is a process in which strength is developed through molecular interchange across the interface and random entanglement formation. It is a diffusion process characterised by molecular motion (Luo, 2012).

It was quoted by Carpenter and Shen in (2006) and (2007) that most of the researchers such as Bazin and Saunier (1967, January), Mc Elvaney and Pell (1973), Raithby and Sterling (Raithby & Sterling, 1970), as well as Sias (1996) used an interrupted type of fatigue test to investigate about healing. Furthermore, Zhang et al. (2001), and Kim et al. (2003) used interrupted fatigue test to study healing phenomenon. In the interrupted fatigue tests various lengths of resting periods after a certain number of cyclic loadings is inserted for showing a modulus or energy recovery when the next sequence of loading cycles begins (Carpenter & Shen, 2006).

In the following sections, some of the methods for determining the healing ability of asphalt concrete are described.

2.8.2.1 Nonlinear viscoelastic correspondence principle

The so-called elastic-viscoelastic correspondence principle is an excellent method to evaluate and model the hysteretic behaviour of viscoelastic media. This principle simply states that a viscoelastic (time-dependent) problem can be reduced to an elastic (time-independent) problem only by working in an appropriately transformed domain and substituting elastic moduli. The nonlinear viscoelastic correspondence principle was developed by Schapery (1984), quoted by Kim et al. (1994). He proposed that the constitutive equations for certain nonlinear viscoelastic media are identical to those for the nonlinear elastic case, but stresses and strains are not necessarily physical quantities in the viscoelastic body. Rather, they are "pseudo" parameters in the form of a convolution integral. Kim et al. (1990), quoted Kim et al. (1994), used this method successfully in differentiating the healing potentials of different binders. According to Kim et al. (1994), it was proved that this principle is an excellent means to model the growthing damage and healing in asphalt concrete under complex cyclic loading.

The advantage of introducing pseuqostrains is that they can be related to stresses through Hooke's law. Therefore, the viscoelastic behaviour of the material can be eliminated. Thus, if a linear elastic solution is known for a particular geometry, determination of the corresponding linear viscoelastic solution is possible through a convolution integral. The measured stress against pseudostrain plot can be obtained through using pseudostrain for damaged nonlinear asphalt concrete. Then, the pseudo stiffness is determined with a linear regression technique, and dissipated pseudostrain energy for damaged nonlinear viscoelastic asphalt concrete can be calculated by computing the area within the pseudohysteresis loops. This dissipated pseudostrain energy describes the real damage, such as plastic deformation, heat dissipation, fracture, and healing, because both the time-dependent linear viscoelastic effects and the non-linearity of the material have been eliminated from the time-dependent damage process

by using a nonlinear pseudo strain instead of a physical strain. The dissipated pseudostrain energy is a real damage indicator and should be related to fatigue fracture and healing (Si et al., 2002a). The slope of the linear regression of the pseudohysteresis loop is defined as pseudostiffness. It is an unambiguous indicator to evaluate the effect of rest periods on micro damage and healing (Si et al., 2002b).

It was reported by Si et al. (2002b) that pseudostiffness is appropriate and efficient method for evaluating microdamage and healing during the fatigue damage process. Pseudostiffness decreases consistently with an increasing number of loading cycles, which indicates that the micro damage occurs during the fatigue test. The significant recovery of pseudostiffness after rest periods indicates that there is a strong healing due to rest periods.

2.8.2.2 Impact resonance test method

It was reported by Whitmoyer and Kim (1994), quoted by Kim et al. (1994) that the impact-resonance method which was described in modified version of ASTM C215 (2000d) can produce very repetitive, consistent results for portland cement concrete and for asphalt concrete. Two most important characteristics of this method are low equipment costs and the small amount of time. In a study by Kim et al. (1994), three modes of testing, so-called longitudinal, transverse, and torsional were conducted. For determining whether the increase in moduli of the damaged specimens after exposure to heat was caused by healing or some type of ageing phenomenon, the number of loading cycles is varied among the specimens. Test results demonstrated that the impact-resonance test is able to determine varying magnitudes of structural regain of asphaltic mixtures after rest periods at higher temperatures. Also, healing ratios, defined as the ratio between the moduli obtained before and after exposure to heat (Kim et al., 1994).

In another case, two types of asphalt mixtures were adopted and three-point bending beam fatigue machine was utilised in order to induce flexural bottom up fatigue damage. Thereafter, the stiffness of the specimens through cycles of damage and healing was evaluated by using impact-resonance method through which the stiffness changes of two asphalt concrete mixtures were evaluated because of temperature, fatigue damage growth, and healing during rest periods. It was observed that as the temperature increases and as microcrack damage growth occurs in the specimen due to fatigue, the dynamic modulus of elasticity in the specimen decreases. Furthermore, an increase in dynamic modulus of elasticity was detected in the specimens after rest periods. In their study, they also observed an increase in flexural stiffness from measurements and such increase was attributed to closure of microcracks or healing during the rest period. It appeared that the amount of healing or stiffness gain increases when the rest periods were applied to specimens at higher temperatures (Daniel & Kim, 2001).

2.8.2.3 Flexural bending beam test method

In a study short constant rest periods varying from zero to nine seconds was applied after each haversine load pulse for simulating a rest period between loads through four-point bending machine with an intermediate strain level of 500 microstrains. The load cycles in that test were individually associated with a specific rest period; so,the dissipated energy were uniquely related to the total load cycle sequence (load plus rest period) which occured before the current load. All test setups followed the standard four-point bending beam fatigue test procedure specified in AASHTO T321 (2003), except that rest periods inserted after each load pulse (Carpenter & Shen, 2006).

It was reported by Little et al. (2001) that the rest period of 24 h in traditional flexural beam bending test could result in 100% increase in the fatigue life, depending on the binder type used.

In another study, in order to study healing phenomenon in asphalt concrete, three-point bending tests were conducted on the specimens by applying intermittent loading modality with and without rest periods, and the corresponding fatigue curves were obtained. According to the experience, ten times the loading time were adopted as the rest period duration. Based on the results of the experiment, an increase of five to ten times fatigue strength was obtained through application of rest periods (Castro & Sánchez, 2006).

In another study quoted by Shen and Carpenter (2007), a rolled asphalt base course mixture was tested by Van Dijk and Visser (1977) using a three-point bending apparatus in a constant strain mode, frequency of 40Hz, and at the temperature of 20ºC. In was also quoted by Shen and Carpenter (2007), that Bonnaure et al. (1982) used an intermittent loading in order to investigate the rest period influence on fatigue life. Three-point bending tests were carried out on rectangular beam shaped specimens with dimensions of $230 \times 30 \times 20$ *mm*. Both constant stress and constant strain loading modes were used with, three temperatures (5ºC, 20ºC, and 25ºC), frequency of 40Hz, and various rest periods. Beneficial effect of rest periods on fatigue life was found from their results. The maximum advantageous effect seemed to reach around the maximum rest period (Shen & Carpenter, 2007).

2.8.2.4 Dissipated creep strain energy (DCSE)

Kim and Roque (2006) developed a healing test which was basically in accordance with AASHTO TP 31 (1994). In that study the rate of healing in asphalt mixtures was determined in terms of recovered DCSE per unit time, and a normalised healing rate in terms of $DCSE/DCSE_{applied}$ was defined for evaluating the healing properties independent of the amount of damage occured in the mixture. The test was carried out by application of a repeated loading test followed by periodic resilient modulus tests.

Based on the results, it was determined that above 10°C the rates of healing in the tested asphalt mixtures increased significantly and were more influenced by the aggregate structural characteristics such as aggregate interlock, film thickness, voids in mineral aggregate of the mixtures than by polymer modification. Therefore, it appears that the overall healing rate as well as the rate of damage recovery of these mixtures is more affected by the aggregate structural characteristics of the mixtures than by polymer modification (Kim & Roque, 2006). It was hypothesised by Little et al. (1998) that the polymer acts as a filler system that interrupts the ability of pure bitumen to re-establish contact and heal.

2.8.3 Affecting Factors of Healing in Asphalt Concrete

According to the literature, the factors affecting the healing phenomenon in asphalt concrete can be categorised as in Tabe 2.1.

Table 2.1: influencial factors on asphalt mixture healing (Liu, 2012)

Factors influencing healing	Bitumen properties	Bitumen type
		Chemical compositions
		Viscoelastic properties
		Surface free energy
		Ageing
		Diffusion
		Modifiers
	Asphalt mixture compositions	Bitumen content
		Aggregate structure
		Gradation
		Thickness
	Environments	Temperature
		Loading history
		Rest period
		Water / moisture

In the following section, the description of some of the factors is presented.

2.8.3.1 Binder

Asphalt binder itself indicates excellent healing capability due to its nature. It was discovered that the healing property of asphalt concrete is influenced by the types of asphalt and the asphalt content. In the studies of Van Gooswilligen et al. (1994) and Molenaar (2009), quoted by Jiang et al. (2010) a soft asphalt binder of 80/100 penetration grade shows higher healing capacity than a hard asphalt binder of 40/60 penetration grade. In addition , high asphalt content also shows advantage on healing.

According to Bonnaure et al. (1983) and Francken and Clauwaert (1987, July), quoted by Castro and Sánchez (2006), in the mixtures with softer bitumen the recovery is greater, and generally in the mixtures with softer bitumen and higher binder content,

the beneficial effect of rest periods is greater. However, in a study by Kim and Roque (2006), mixtures with lower asphalt content (6.1 % for both the unmodified and the modified) exhibited higher normalised healing rates than mixtures with 7.2% asphalt content. This increased healing rate can be partially explained by the fact that these mixtures with lower asphalt content were compacted more to reach 7.0% air voids than were the mixtures with higher asphalt content, which resulted in the increased capacity for healing. This trend is apparently related to the results of fracture tests, in which the mixtures with lower binder content showed greater resistance to fatigue-type crack growth in these particular types of mixtures.

2.8.3.2 Aggregates

Kim and Roque (2006) reported that the healing of these mixtures at low to intermediate temperature (0°C to 20°C) is more influenced by the aggregate structural characteristics of the mixture such as aggregate interlock, film thickness, and voids in mineral aggregate (VMA) than by polymer modification. .

The aggregate structure within the asphalt mixture was described by quantifying the aggregate orientation and the aggregate segregation, as well as aggregate-to-aggregate contact points (Partl et al., 2013).

2.8.3.3 Surface energy

Fatigue fracture and healing of asphalt concrete depend largely on surface energy. Two components of thermodynamic surface energy of either wetting or dewetting have been identified, namely, Lifshitz- Van der Waals (Γ^{LW}) and Lewis acid-base (Γ^{AB}). These two components can be used to explain cohesive and adhesive bonding interactions within the asphalt concrete specimen. Actually, both cohesive and adhesive fracture and healing can and do occur. The cohesive fracture and healing are where the crack advances and heals in the binder or mastic region and the adhesive fracture and

healing are where the crack advances and heals at the asphalt-aggregate interface. Most healing occurs in cohesive regions between two mastic surfaces. A key representation in Schapery's equation of healing rate to the consideration of microcrack healing in asphalt mixtures is the direct relationship between surface energy and the rate of micro fracture healing; that is, a greater surface energy implicates a greater potential for healing, with all other components remaining the same (Si et al., 2002b).

The laboratory observations indicated that both, theories were correct. Schapery predicated his theory on forces acting perpendicular to the crack face and actively pulling the crack faces together. This is typical of hydrogen bonding, which takes a longer time to form. Lytton's theory applies to the tensile short-term Lifshitz-Van der Waals forces, which act in the crack face plane. They form rapidly and pull the molecules in the plane of the crack face together. The stronger these bonds, the slower will be the initial healing that occurs (Si et al., 2002b).

By analogy with rate process theory and consistent with the form of Schapery's fracture theory, Little et al. (1998), quoted by Si et al. (2002b) proposed another healing speed relation. The results showed that the lower the surface energy density, the greater is the degree of healing that will proceed under otherwise equal conditions. This proposes that surface energy density acts as an inhibitor to the healing process. In fact, Little et al. (1998) viewed surface energy not as acting as an attractive force between asphalt surfaces on either side of a crack face but as an impedance towards closure or re-formation of the cracked surface. In the course of analysing the measured healing data, it was discovered that the actual rate of healing is governed by two separate healing mechanisms, one of which is controlled by the nonpolar (Lifschitz-Van der Waals) components, which dominate in the short-term healing process; the other is controlled by the polar (Lewis acid-base) components of the surface energy densities, which dominate in the long-term healing process.

In another research by Little et al. (1998) the mechanism of fracture and healing of asphalt mixtures based on surface energy was studied. Based on the results, an inverse relationship between healing potential and Lifshitz-Van der Waals surface energy was found; while a direct relationship between acid-base surface energy and healing potential was found.

In general, based on a research by Si et al. (2002b) it was reported that the nonpolar surface energy and polar surface energy governed, respectively, the initial healing rate, and the final healing rate (Si et al., 2002b).

2.8.3.4 Rest periods

Healing can be measured either by measuring the storage recovery of mechanical properties over a period of rest time when the sample is not subject to loading; or by intermittent loading in which the rest periods are inserted after each load cycle and the fatigue life increase is measured. (Castro & Sánchez, 2006; Matthew et al., 2013; Shen & Carpenter, 2007). Two different types of fatigue test are shown in Figure 2.8.

In the researches using rest intervals, the rest periods are usually minutes or hours and sometimes they are used for varying the test temperature (Figure 2.8(a)). However, in the tests with intermittent loadings as shown in Figure 2.8(b), the duration of the rest period is several seconds and it is a multiple of the duration of the immediately preceding set of loading cycles. The tests with intermittent loads are more modern and the true traffic load can be reflected better compared to that can be by rest intervals. Nevertheless, tests with rest intervals continue to be performed when, e g., it is deemed necessary to change the temperature during the rest period or in order to study the microcracking healing by means of microscopy (Castro & Sánchez, 2006).
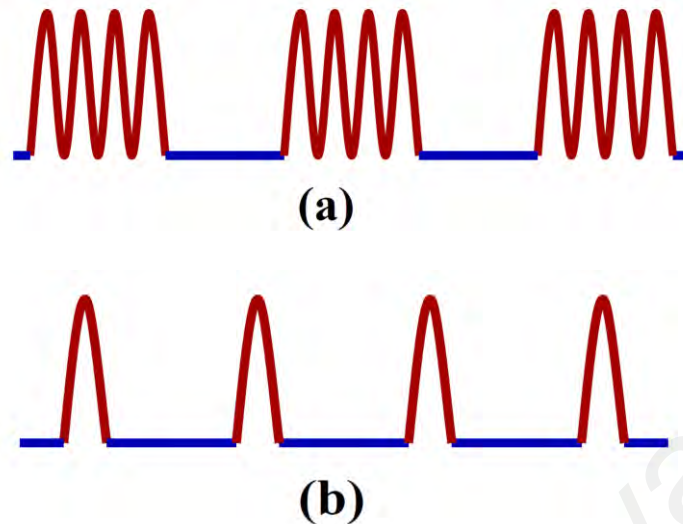
Figure 2.8: Fatigue tests (a) with rest intervals; (b) with intermittent loads (Matthew et al., 2013)

Van Dijk and Vesser (1977), quoted by Shen and Carpenter (2007) used a loading ratio (1/i) for describing the intermittent loading used in a three-point bending fatigue tests with rest times, where i was the length of the rest time declared in the length of one loading cycle.. Furthermore, Bonnaure et al. (1982), quoted by Shen and Carpenter (2007) used an intermittent loading on rectangular beams inserting different rest periods being 0, 3, 5, 10, and 25 times the length of the loading cycle. In other research by Si et al. (2002a) the fatigue damage and healing of various types of asphalt concrete mixtures were evaluated using strain controlled fatigue test by inserting a series of rest periods at 1,000 cycle intervals after the first 10,000 cycles.

2.8.3.5 Wave form

Based on Raithby and Sterling (1970), quoted by Castro and Sánchez (2006). the sinusoidal wave is the usual type of the waveform being more reality in fatigue tests with rest periods. Furthermore, it must be noted that the effect of waveform is very limited, particularly if it is compared to the effect of the rest periods.

2.8.3.6 Temperature

Daniel and Kim (2001) reported that at 60°C healing periods, dynamic modulus of elasticity and flexural stiffness of tested asphalt concrete mixtures increase were generally greater the corresponding increases at 20°C healing periods, even though it was not observed in every cases. This followed the intuitive thought that the healing capacity of the asphalt cement should be improved as a result of its increased ability to flow and further close more microcracks at higher temperatures.

2.9 Permanent Deformation and its Mechanism

In the recent years because of an increase in traffic and heavy vehicles, rutting is one of the most frequent defects in flexible pavements, particularly in hot climates. Rutting reveals itself as depressions which are formed in the pavement's wheel path. It normally occurs when permanent deformation of each layer in pavement structure accumulates under the repetitive traffic loading (Tayfur et al., 2007). Accumulation of residual strains in wearing course particularly in wet pavements may cause serious problems through aquaplaning (Fwa et al., 2004; Sivilevičius & Petkevičius, 2002; Verhaeghe et al., 2007, September). So, not only does pavement rutting increase the road maintenance cost, but also it increases human life's risk through causing an accident when water accumulates in pavement depressions.

There are generally two modes of ruts that occur on pavements, namely, compactive, and plastic. The first mode is when permanent deformation happens because of densification (consolidation). An indication of compactive mode is where the deformed surface is lower than the original surface. In plastic mode (also called shape distortaion), permanent deformation occurs due to shear failure and flow. Unlike the former mode, it is recognised as plastic mode where the deformed surface is higher than the original surface. The uplift typically occurs both between and outside the wheel paths (Gabra &

Horvli, 2006). Generally, plastic mode in hot mix asphalt pavements occurs in the top 100mm (Lee et al., 2010). Figure 2.9 shows schematically both forms of deformations.
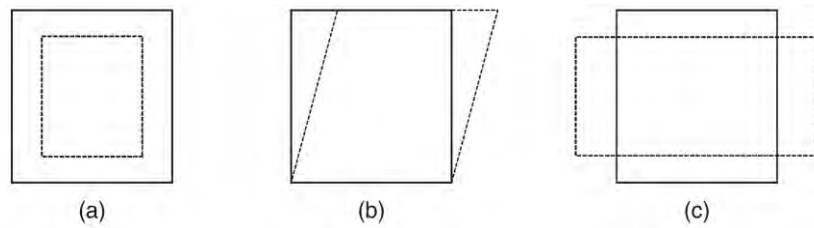
**Figure 2.9: Schematic representations of volume change,
(a.), and shape distortion (b., c.)
(Kim, 2009)**

Rutting resistance of a paving asphalt mixture is one of the important considerations in asphalt mix design, as a large part of accumulated rutting in pavement structure occurs in the surface layer. Formation of ruts, having started in the initial stage of pavement operation, increases with the growth of the flow of heavy traffic. The main cause of rut initiation is shear strains in asphalt. There are several causes of such deformations. Some of them are high temperature, unsuitable mixture, and traffic loads (Bertuliene et al., 2011, May). In general, rutting at higher temperatures occurs due to pavement consolidation and/or HMA experiences lateral movement which is a shear failure (Kim & Park, 2013). Moreover, analysing the rutting behaviour of composite pavements in the State of Louisiana depicted that cumulative ESAL, thickness of the portland cement concrete layer, highway functional classification, and surface age can highly influence permanent deformation (Nur et al., 2013).

2.9.1 Measurement of Asphalt Concrete Permanent Deformation

Various laboratory testing methods have been developed to investigate the asphalt concrete resistance to rutting. These include the static and dynamic creep test, wheel track test, and indirect tensile test. Monismith et al. (1975, January), quoted by Kalyoncuoglu and Tigdemir (2011), developed the dynamic creep test which is thought

to be one the best methods to evaluate the resistance of asphalt concrete to permanent deformation. Furthermore,a report by the NCHRP (Cominsky et al., 1998), quoted by Kaloush and Witczak (2002), identified the dynamic creep test as having the potential to be utilised as a field quality control. Dynamic creep test is relevant to this study, so the detailed description of it is here.

2.9.1.1 Dynamic creep test output

One of the most important outputs of dynamic creep test is creep curve, illustrating permanent deformation versus loading cycles. Regardless of type of considered material, this curve can be divided into three distinct regions, namely primary, secondary, and tertiary region, as in Figure 2.10. The high level (rate) of permanent deformation in the primary stage with decreasing rate of shear deformation is dominantly associated with volumetric change. There is a small and constant permanent deformation rate in the secondary stage which is also related to volumetric changes. But, in this stage shear deformation increases at an increasing rate unlike the primary stage. Finally, the high permanent deformation level in the tertiary stage is dominantly associated with shear deformation under no densification (Witczak et al., 2004).
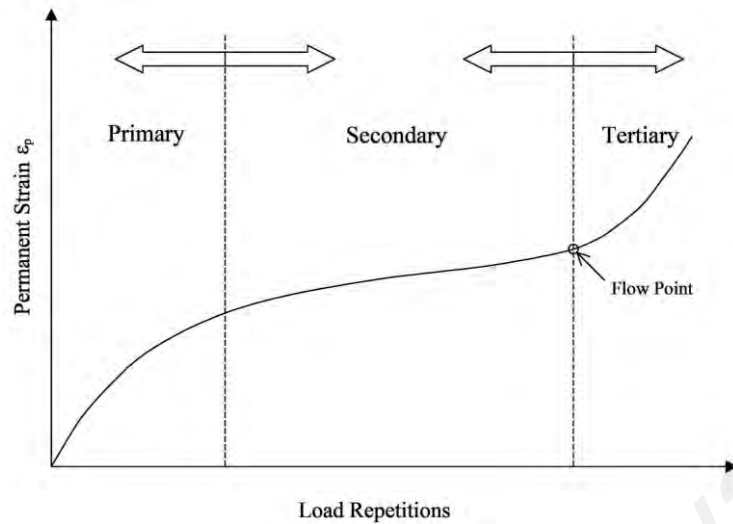
**Figure 2.10: Typical creep curve of pavement materials
(Witczak et al., 2004)**

The creep modulus being one of the most important outputs of dynamic creep test indicating the sample resistance to permanent deformation could be obtained from the following equations (Alataş et al., 2012; EN_CEN, 2005):

$$\varepsilon_c = (L3_n - L1)/G \qquad\qquad \text{Equation (2.10)}$$

$$\sigma = F/A \qquad\qquad \text{Equation (2.11)}$$

$$E_c = \sigma/\varepsilon_c \qquad\qquad \text{Equation (2.12)}$$

where: ε_c: is the total permanent (plastic) strain (%),
E_c: is the creep modulus (MPa),
G: is the initial height of the sample (mm),
$L1$:   is the initial reference displacement of LVDT (mm),
$L3_n$:   is the level of displacement prior to the application of (n + 1)th load pulse (mm),
σ: is the maximum vertical stress(MPa),
F: is the maximum vertical load (N), and
A: denotes the cross-section area of the sample (mm2).

2.9.1.2 Creep curve models

Since creep curves obtained by dynamic creep test are used to assess the permanent deformation resistance of asphalt concretes, not only is the behaviour of each region of creep curve of great importance, but identification of the boundary points connecting primary to secondary region, and secondary to tertiary region is also of great importance. So, characterising the obtained creep curves from dynamic creep test can help better understanding of permanent deformation resistance of asphalt concrete.

As quoted by Zhou et al. (2004), different mathematical models such as Barksdale's Semi-log model (1972, September), Power-law models based on the Monismith model (1975, January), and Tseng and Lytton's model (1989), have been developed in order to fit the creep curve and estimate the flow number parameter in asphalt mixtures. For fitting and distinguishing between regions of the unmodified asphalt mixture creep curve, a three-stage model was proposed by Zhou et al. (2004). In their model a power model was considered for the primary region, a linear model for the secondary region, and for tertiary region an exponential model was proposed . In other words, they modelled each region of the creep curve separately. At the same time , some other researchers believe that the logarithmic model can more accurately simulate the primary region of the creep curves in SBS modified asphalt mixtures (Ahari et al., 2013; Kalyoncuoglu & Tigdemir, 2011).

The Semi-log model proposed by Barksdale (1972, September), quoted by Zhou et al. (2004) has been shown in the following equation.

$$\varepsilon_p = a_1 + b_1 logN \qquad \text{Equation (2.13)}$$

$$\varepsilon_{pn} = \frac{b_1}{N} \ (N > 1) \qquad \text{Equation (2.14)}$$

where: ε_p: is accumulated permanent strain,

N: is number of load repetitions,

ε_{pn}: is permanent strain due to a single load application, i.e., at the N_{th} application, and

a_1, b_1: are positive regression constants.

It was quoted by Zhou et al. (2004) that the Power-law model proposed by Monismith et al. (1975, January), *VESYS* model (Kenis, 1978), Ohio State model (Majidzadeh et al.), Superpave model (Lytton et al., 1993), and AASHTO 2002 model (Witczak, 2001), are as the following:

$$Power\ law\ model: \quad \varepsilon_p = aN^b \qquad \text{Equation (2.15)}$$

$$VESYS\ model: \quad \varepsilon_{pn} = \mu.\varepsilon_r N^{-\alpha} \qquad \text{Equation (2.16)}$$

$$Ohio\ State\ model: \quad \varepsilon_p = aN^{1-m} \qquad \text{Equation (2.17)}$$

$$Superpave\ model: \quad log\varepsilon_p = log\varepsilon_p(1) + SlogN \qquad \text{Equation (2.18)}$$

$$AASHTO\ 2002\ model: \quad log\frac{\varepsilon_p}{\varepsilon_r} = logC + 0.4262logN \qquad \text{Equation (2.19)}$$

where:
ε_p = accumulated permanent strain,

N = number of load repetitions,

ε_{pn} = permanent strain due to a single load application, i.e., at the N_{th} application,

ε_r = resilient strain, generally assumed to be independent of the load repetition (N),

$\varepsilon_p(1)$ = the permanent strain at the first load application,

$a,b,m,$ and S are positive regression constants,

a = 1-b; permanent deformation parameter indicating the rate of decrease in incremental permanent deformation as the number of load repetitions increases. Normally, α > 0, and

C = $T^{2.02755}/5615.391$; is a function of temperature (°F).

It was also quoted by Zhou et al. (2004), the Tseng and Lytton's model (Tseng & Lytton, 1989) as follows:

$$\varepsilon_p = \varepsilon_0 e^{-(\frac{\rho}{N})^\beta}$$
Equation (2.20)

$$\varepsilon_{pn} = \varepsilon_0 \beta \rho^\beta \frac{N^\beta \sqrt{A}}{N^{(\beta+1)}}$$
Equation (2.21)

where:
ε_p = accumulated permanent strain,

N = number of load repetitions,

ε_{pn} = permanent strain due to a single load application, i.e., at the Nth application,

ε_r = resilient strain, generally assumed to be independent of the load repetition (N),

ε_0 , β, and ρ are the positive regression constants, and

A = $1/e^{\rho^\beta}$ is a constant and less than 1.

An extensive research was carried out by Zhou et al. (2004) for developing a model that was able to fit the creep curve and estimate its boundary points accurately. For modelling 1-3 regions of the creep curve they used, respectively, a power-law function, a linear function and an exponential function. The equations illustrated below were used for modelling each regions of the creep curve.

$Primary\ stage$: $\quad \varepsilon_p = aN^b, \quad N < N_{PS}$ Equation (2.22)

$Secondary\ stage$: $\quad \varepsilon_p = \varepsilon_{PS} + c(N - N_{PS}), \quad N_{PS} \leq N < N_{ST}$ Equation (2.23)

$Tertiary\ stage$: $\quad \varepsilon_p = \varepsilon_{ST} + d\left(e^{f(N-N_{ST})} - 1\right), \quad N \geq N_{ST}$ Equation (2.24)

where: a and $b =$ material constant,

$N_{PS} =$ number of load repetitions corresponding to the initiation of the secondary stage,

$c =$ material constant,

$N_{ST} =$ flow number which is the number of load repetitions corresponding to the initiation of the tertiary stage,

$\varepsilon_{PS} =$ permanent strain corresponding to the initiation of the secondary stage,

d and $f =$ material constants, and

$\varepsilon_{ST} =$ permanent strain corresponding to the initiation of the tertiary stage.

The model proposed by Zhou et al. (2004) was evaluated by Khodaii and Mehrara (2009) and an improved model for the tertiary region of the creep curves was proposed for SBS modified asphalt mixtures. A second order parabolic function as shown in Equation 2.25 was proposed which can be more precisely model the tertiary region of the creep curves of SBS modified asphalt mixtures than the exponential function proposed by Zhou et al. (2004).

$$\varepsilon_p = \varepsilon_{ST} + d(N - N_{ST})^2 + f(N - N_{ST}), N \geq N_{ST} \ and \ \varepsilon_{ST} = \varepsilon_{PS} + c(N_{ST} - N_{PS})$$
Equation (2.25)

In another study by Mirzahosseini et al. (2011), computational methods was used for analysing permanent deformation of dense graded asphalt mixtures. These researchers gathered a comprehensive laboratory database using the dynamic creep tests on the

dynamic creep laboratory test results of up to 270 asphalt mixture specimens were used and the Equation 2.24 was suggested for determining the flow number.

$$Log(F_N) = \frac{\frac{C}{S}}{(\frac{2C}{S} - 5)(-2VMA - 5)} + \frac{\frac{M}{F}}{(\frac{2C}{S} - 4)(BP - VMA)} + Exp(\frac{\frac{C}{S} - VMA + 1}{\frac{M}{F} - VMA - 4})$$

Equation (2.26)

where:

$\frac{C}{S} =$ weight percent of coarse aggregates to that of fine aggregates,

$BP =$ bitumen content (%),

$VMA =$ voids in mineral aggregates (%), and

$\frac{M}{F} =$ ratio of Marshall Stability to flow.

At the same time , some other researchers believe that the logarithmic model simulates more accurately the primary region of the creep curves in SBS modified asphalt mixtures (Ahari et al., 2013; Kalyoncuoglu & Tigdemir, 2011). Moreover, Ahari et al. (2013) developed a two-stage model for the primary and secondary regions of creep curves in SBS modified asphalt mixtures. They proposed two different approaches for modelling the primary and secondary regions of the creep curve.

2.10 Gap of the Previous Studies and Necessity for Further Research

Significant studies are not conducted on the effect of geogrids on damage recovery ability of asphalt concrete. By understanding and considering the damage recovery effect of geogrids in asphalt concrete the fatigue life of geogrid reinforced samples can be determined more accurately.

Researchers generally agree that geogrid reinforced asphalt concrete is more resistant to surface deformation than unreinforced concrete (Austin & Gilchrist, 1996; Bertuliene et al., 2011, May; Komatsu et al., 1998; Siriwardane et al., 2010; Sobhan et al., 2005, June). Yet very few researchers have provided a full-range comparison of the effects of the mesh size and tensile strength of such grids on the permanent deformation of bituminous systems. Tests of asphalt concrete plastic flow resistance suggest that durability increases when the size of grid openings decreases (Komatsu et al., 1998). Similarly, Jenkins et al. (2004, September) observed slightly less rutting in grids reinforced with smaller grid mesh sizes than those with larger mesh sizes.

Thus, in this study, an effort has been made to conduct a study on investigating the possible effect of fibreglass grid applied in asphalt concrete on the damage recovery ability of it. Moreover, it was tried to study the separate and combined effects of grid tensile strength and mesh size on permanent deformation of the fibreglass grid reinforced asphalt concrete. In addition a recently developed creep curve model has been verified to be used for the conditions and materials adopted in this study.

2.11 Summary of the Chapter

This chapter reviewed the literature in the area of flexible pavements and some of its main related distress such as rutting, fatigue cracking and reflective cracks. Asphalt concrete is one the layers in flexible pavements which can be affected by such distresses, and leads to premature deterioration of flexible pavements. As was mentioned, geosynthetics can be categorised into seven main categories. Geotextiles, geogrids and geocomposites are the main geosynthetics being utilised in soils and asphalt pavement reinforcement for separation, reinforcement, filtration, drainage and acting as a liquid barrier purposes. In order to encounter some of the above-mentioned distresses the geogrid reinforcement and the mechanism of reinforcement were discussed.

Then, the definition of asphalt concrete stiffness being a slope of a stress-strain curve of the asphalt concrete, and the main factors affecting this stiffness were discussed. Some of such factors were, temperature, rate of loading, aggregate particles, air voids, etc. Thereafter, some of the definitions relating to asphalt concrete stiffness such as complex and dynamic moduli, etc. were provided. It was followed by discussion on master curve and some of the methods for its construction.

Then, the healing and damage recovery ability of asphalt mixtures were discussed, including mechanisms, methods of measurements, and factors that can affect the healing or damage recovery ability of asphalt concrete. According to the literature, the composition of asphalt mixture, including bitumen content, aggregate structure characteristics and gradation, affects the healing phenomenon which can take place in the asphalt concrete.

Finally, the permanent deformation and its mechanism in asphalt concrete is discussed in more details, followed by measurement methods of it. Dynamic creep test developed by Monismith et al. is thought to be one the best assessment methods for evaluating the resistance of asphalt concrete against permanent deformation. It was followed by discussion on creep curves and some of the developed models for creep curve. Then, some of the gaps of previous studies that there is still need for further research are presented. The next chapter considers the modelling of the study and its methodology procedure.

CHAPTER 3: METHODOLOGY

3.1 Introduction

The material characteristics and experimental tests used in this study for investigating some of the characteristics and effects of fibreglass grids with two different tensile strengths and opening sizes on bituminous mixtures are presented in this chapter. The physical properties of both fibreglass grids reinforced and unreinforced specimens were determined from the relevant tests. It was conducted using some laboratory tests in accordance with American Society of Testing and Materials (ASTM), British Standards (BS EN), and Association of State Highway and Transportation Officials (AASHTO). These laboratory testing methods determine a number of parameters and structural properties of specimens in order to optimise the warrant of required material characteristic fulfillment. The flow chart of this research methodology is illustrated in Figure 3.1. The methodology can be described briefly as follows:

After selecting the materials, firstly the optimum binder content (OBC) was determined for the mixture by means of Marshall method; then using the determined OBC, the asphalt mixture was prepared and compacted using roller compactor to the slab shaped grid reinforced and unreinforced specimens. Afterwards, the slabs were cut and cored to the the beams and cores with certain dimensions specified in the related test standards. Before starting the tests on the obtained beams and cores, it must be noted that the specimens need be conditioned for a certain period in a room temperature to be dried. Three types of tests were conducted on the specimens in different conditions as it can be seen in the chart. Finaly, the data analysis were performed on the acquired data and the conclusions were made. More details on the tests can be found the sunsequent sections.
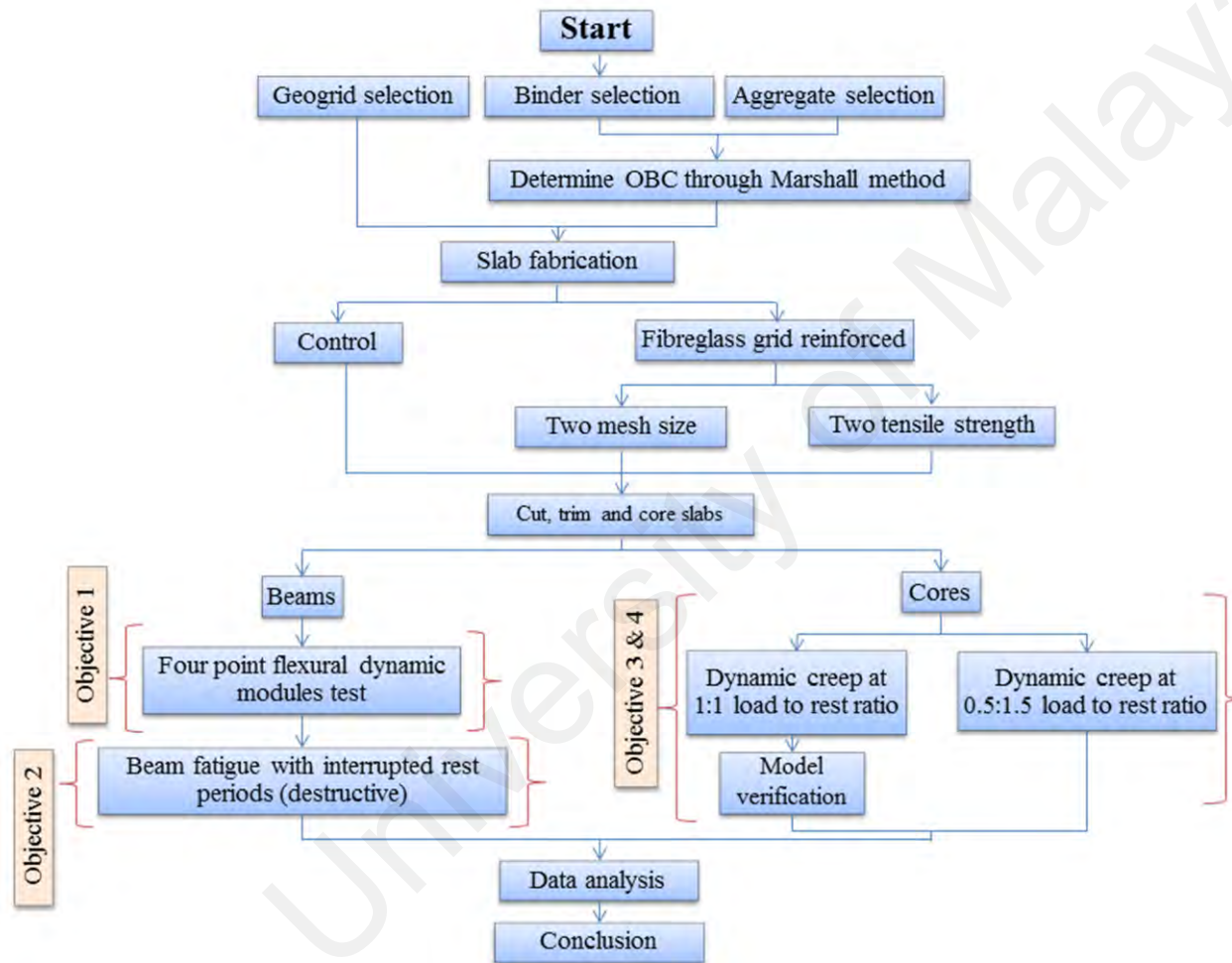
Figure 3.1: Flowchart of the research methodology

3.2 Materials

To ensure for consistency of material characteristics, all of the materials utilised in this study come from the same source. The detailed descriptions of the materials are presented in the subsequent sections.

3.2.1 Bitumen Selection

The bitumen used in this study supplied by Asphalt Technology sdn. bhd in Malaysia. Table 3.1 shows some of the properties of this bitumen (Asphalt Technology, 2003).

Table 3.1: Thechnical specification of bitumen

TYPICAL PROPERTY	Min	Max	Test Method
Penetration at 25ºC, 0.1mm	80	100	ASTM D5
Softening Point (R & B) ºC	45	52	ASTM D36
Flash Point (Cleveland Open Cup), ºC, min	225	-	ASTM D92
Relative Density at 25ºC, g/cm³	1.00	1.05	ASTM D71
Ductility at 25°C, cm, min	100	-	ASTM D113
Loss on heating, % wt., max	-	0.5	ASTM D6
Solubility in trichloroethylene, % wt.,min.	99	-	ASTM D2042
Drop in penetration after heating, %,max.	-	20	ASTM D5
Application temperatures, mixing at ºC	140	160	-

3.2.2 Aggregate Selection

Crushed granite supplied from Kajang region of Selangor state in Malaysia was used as aggregates in this study. Table 3.2 and Figure 3.2 show the aggregate gradation for dense graded mixture utilised in this research according to ASTM D3515 (2000) with nominal maximum aggregate size of 9.5mm. Considering the opening size of fibreglass grids used in this study, selecting this aggregate gradation allowed grids to provide better interlocking with asphalt concrete.

Table 3.2 : Mix gradation, optimum asphalt, and maximum relative density

| Sieve Sizes (mm) | Percent passing | | | Retained | |
	Min	Max	Adopted	%	weight (gr)
12.5	100	100	100	0	-
9.5	90	100	95.00	5	975
4.75	55	85	68.00	27	5256
2.36	32	67	45.50	22.5	4380
0.30	7	23	11.00	34.5	6714
0.075	2	10	4.00	7	1362
Pan	-	-	-	4	780
Total	-	-	-	100	19467
Optimum Asphalt Content (% of total mix)	-	-	-	5	1023
Maximum theoretical specific gravity		2.430			
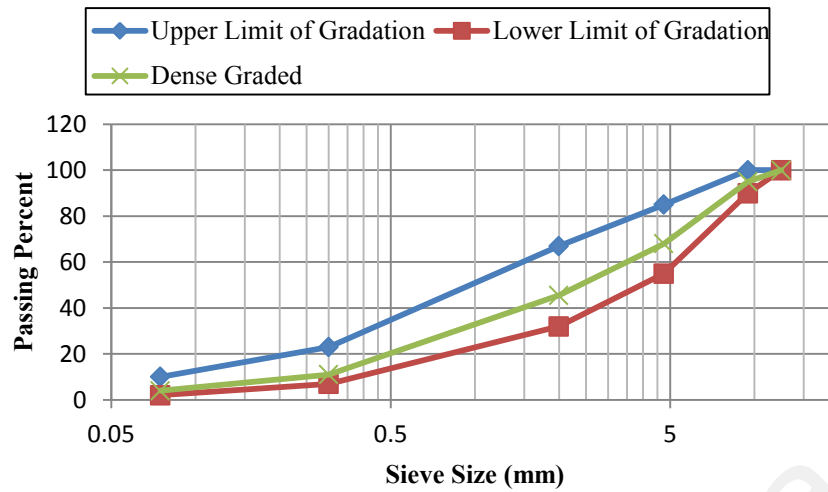
Figure 3.2 : Grading curves for the crushed aggregate

3.2.3 Fibreglass Grid Selection

Four types of fibreglass grid manufactured by a European corporation with two different tensile strengths and two different opening sizes were used as the reinforcing material applied at mid-depth of reinforced specimens between two lifts. The basic properties of these reinforcement agents are presented in Table 3.3 and they are illustrated in Figure 3.3.

Table 3.3: Basic properties of fibreglass grid applied

Code	R1	R2	R3	R4	
Identification					Test Method
Tensile strength (kN/m) (MD ×XD)	115 × 115 +/- 15	115 × 115 +/- 15	115 × 215 +/- 15	115 × 215 +/- 15	ASTM D6637-10 EN-ISO 10319:2008
Grid size (mm) (centre to centre of strand)	12.5 × 12.5	25 × 25	12.5 × 12.5	25 × 19	-
Tensile Elongation (Ultimate) (%)	2.5	2.5	2.5	2.5	ASTM D6637-10 EN-ISO 10319:2008
Secant stiffness EA@ 1% Strain (MD x XD) (N/mm)	4600 × 4600	4600 × 4600	4600 × 8600	4600 × 8600	ASTM D6637-10 EN-ISO 10319:2008
Mass per Unit Area (g/m^2)	405	405	610	610	ASTM D5261-92 ISO 9864
Melting Point	>232℃	>232℃	>232℃	>232℃	ASTM D267-00 EN-ISO 3146

MD: Machine direction

XD: Cross machine direction
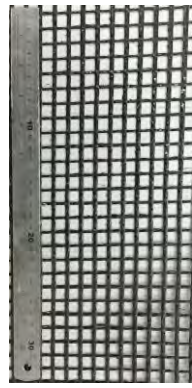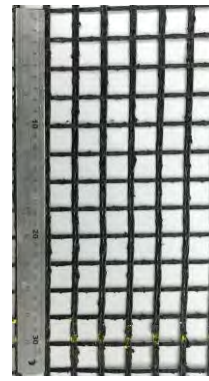
(R1 Grid)   (R2 Grid)
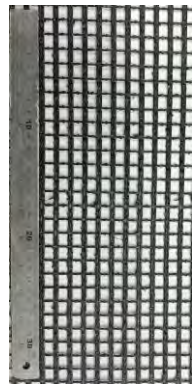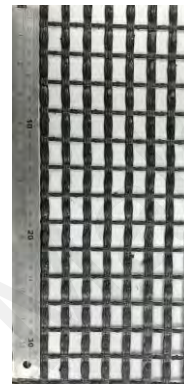
(R3 Grid)   (R4 Grid)

Figure 3.3: Utilized fibreglass grids

3.3 Materials and Slab Preparation

Proper specimen preparation is one of the most important stages for achieving consistency and homogeneity in intrinsic properties of hot mix asphalt (HMA) in order that the design life of pavement is fulfilled. The asphalt concrete slab production process of the slabs for testing is described in this section.

According to the selected aggregate gradation for this research shown in Section 3.2.2, and bearing in mind the opening size of the fibreglass grids used in this study, selecting this aggregate gradation should allow the grids to provide better interlocking with the asphalt concrete. Furthermore, the applied bitumen was 80/100 penetration grade, and the optimum asphalt content of the dense graded asphalt mixture was

determined to be 5% by mass of the total mixture, using the Marshall Test. The asphalt concrete slabs were compacted using a roller compactor in accordance with EN 12697-33 (2003) in two lifts to the target air void of 8%, in order to simulate compaction at the time of field construction (Kandhal & Chakraborty, 1996). The layer thickness of each lift of the slabs was 40-mm, resulting in 80mm thick compacted slabs. Four types of fibreglass grid, with two different tensile strengths and two different opening sizes, were employed as the reinforcing material applied at mid-depth in the reinforced specimens with few centimeters extra grid in length of the mold which is folded properly and attached to the side parts of the mold. This extra length of grid were imposed in order to make sure that at least two grid openings in large mesh size grids and equal number of openings in small mesh size grids can be fit during cutting process of the slabs to beams. However, the adopted grids are coated with a self-adhesive glue through which the grids can be attached tightly on the surface. This study compares two levels (high and low) of grid tensile strength and two levels (large and small) of grid opening size. It should be noted that the dimensions of the girds with large opening sizes differed slightly from those with small opening sizes; however, since the difference was very small, this study assumes that they were of identical size. In addition, as it can be seen in Table 3.3, MD and XD strength of R3 and R4 are not same; therefore, in the process of slab preparation these grids were applied so that the direction with higher strength was located along the length of the beams after cutting the slabs.

In order for achieving the target air void, the following equation was used for calculating the mass of mixture for each of the slabs according to EN 12697-33(2003).

$$M = 10^{-6} \times L \times l \times \rho_m \times \left(\frac{100 - v}{100}\right) \qquad \text{Equation (3.1)}$$

where: M: is the mass of slab, in kilograms (kg),

L: is the interior length of mould, in millimetres (mm),

l: is the interior width of mould, in millimetres (mm),

e: is the final thickness of slab, in millimetres (mm),

ρ_m: is the maxim um density of a bituminous mixture, in kilograms per cubic metre (kg/m³), and

v: is the voids content in slab, in percent (%).

Although no fibreglass grid is applied in unreinforced (control) specimens, control slabs are also fabricated in two lifts in order to maximise the consistency between different specimens.

Since consistent air void is one of the main factors in asphalt concrete mixture design, an effort was made in order to make sure that the air void is distributed consistently in the mixture. For that purpose, after lineation of the slab (as shown in Figure 3.4 (a)), it was firstly cut into three beams (as shown in Figure 3.4 (b), and after trimming top, bottom and sides of the it, the beam was cut into two pieces from mid-depth so that in the reinforced specimens the applied fibreglass grid is cut and removed by sawing machine (considering different specific gravity of asphalt concrete and fibreglass grids, this was carried out in order to minimise the inaccuracy in air void measurement through ASTM D3203, after obtaining the bulk specific gravity and theoretical maximum specific gravity of the mixture according to ASTM D2726 and ASTM D2041). Thereafter, each of the cut beams was cut into three blocks with almost same dimensions. In other words, each slab was cut into 18 blocks - 9 blocks from the top lift of slab and 9 blocks from bottom lift of the slab- as shown in Figure 3.4 (c). Figure 3.5 and 3.6 show the air void distribution respectively, for top and bottom lifts of a slab.

(a)   (b)

(c)

Figure 3.4: Cutting process of the specimens for air void measurement, respectively from (a) to (c)
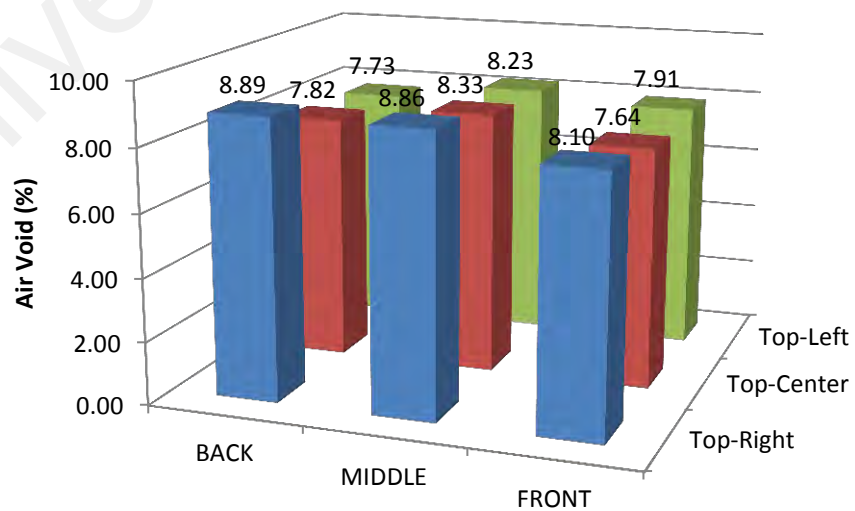
Figure 3.5: Air void distribution in the top lift of slab
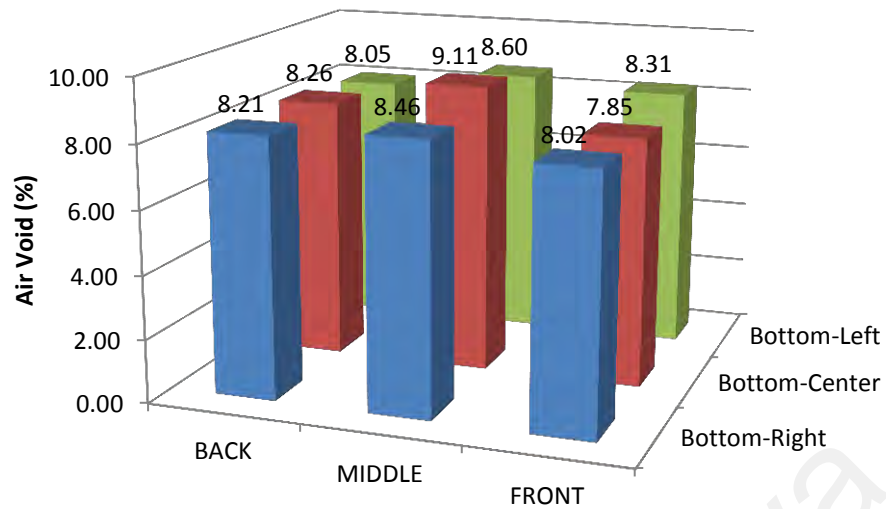
Figure 3.6: Air void distribution in the bottom lift of slab

3.4 Dynamic Modulus Determination

The following three sub-section include the specimen preparation and methodology of dynamic modulus determination as well as the construction of the master curves for fibreglass reinforced and unreinforced hot mix asphalt concrete utilised in this study.

3.4.1 Specimen Preparation

In order to measure dynamic moduli of reinforced and control specimens the procedure was followed in accordance with BS EN 12697-26 (2004). The slabs were cut and trimmed into prismatic shaped beams with dimensions of 380±6 mm in length, 50±6 mm in height, and 63±6 mm in width. The trrimming process was carried our so that the boundary plane of top and bottom lifts was located at mid-depth of each beam. To put it in another way, the grids were located at mid-depth of the beams.

3.4.2 Dynamic Modulus Measurement

Dynamic moduli of different types of beam specimens at various temperatures and frequencies were determined using the UTM-5P from IPC beam fatigue testing machine in accordance with BS EN 12697-26 (2004) except that due to experimental limitations,

only limited ranges of frequencies and temperatures were adopted. The test arrangement in four-point bending apparatus is shown in Figure 3.7 The test condition was:

Type of test:	displacement controlled
Frequencies:	0.5, 1, 2, 5 and 10 Hz
Temperatures:	5, 20, and 35 °C
Strain amplitudes:	25 μm/m
Loading wave:	sine wave
Stiffness measurement:	after 100 pulses

Figure 3.7: Test arrangement in four point bending apparatus

3.4.3 Master Curve Construction

Solver function of Excel was used for obtaining the shift factors and constructing master curve for each type of specimens using Witczak dynamic modulus model and Williams-Landel-Ferry (WLF) equation (Doucet & Auger, 2010; Medani & Huurman, 2003; Rowe et al., 2008, July; Williams et al., 1955). The Witczak model and shift factor equations are:

$$\log|E^*| = \delta + \frac{\alpha}{e^{\beta + \gamma.\log(f_{red})}} \text{(Witczak dynamic modulus model)} \qquad \text{Equation (3.2)}$$

while:

$$log(f_{red}) = log(f) + log(a_T) \qquad\qquad\qquad\qquad \text{Equation (3.3)}$$
and,

$$\log(a_T) = -\frac{C_1.(T - T_{ref})}{C_2 + T - T_{ref}} \qquad \text{(WLF equation)} \qquad \text{Equation (3.4)}$$

where:

f :	loading frequency (Hz),
f_{red} :	reduced frequency after shifting (Hz),
T :	testing temperature (°C),
T_{ref}:	reference temperature (°C),
C_1, C_2:	empirical constants,
$\delta,\ \alpha,\ \beta,\ \gamma$:	Parameters,
10^δ :	lower asymptote (MPa),
$10^{\alpha + \delta}$:	upper asymptote (MPa), and
$10^{-(\beta/\gamma)}$:	inflection point (Hz).

3.5 Damage Recovery Measurement

In this section the methodology through which the damage recovery ability of different types of specimens were measured are presented.

3.5.1 Specimen Preparation

The same specimens of which their dynamic moduli were measured were utilised in this testing process to determine the possible effect of fibreglass grids on asphalt concrete's damage recovery capability. The geogrids are applied at mid-depth of asphalt concrete beams, because application of sinusoidal loads along with locating the grids at mid-depth would cause to initiation of microcracks from both top and bottom of the beams and providing same conditions in terms of damage for both top and bottom lifts. If the asphalt concrete beams are considered as a homogenuous material, mid-depth of

them will be the neutral axis. In the field, however, it must be noted that mid-depth would not be neutral axis anymore.

3.5.2 Determining Damage Recovery Capability

All test procedure in this study followed the standard four-point bending beam fatigue test procedure specified in AASHTO T 321 (2007), except that it was an interrupted fatigue test and some certain rest periods were introduced after the specimens reached to a specific reduction in stiffness as presented in Table 3.4. In the current study, due to limitation of laboratory instruments, rest intervals were adopted. Furthermore, based on Raithby and Sterling (1970), quoted by Castro and Sánchez (2006), the usual waveform in fatigue tests with rest periods is the sinusoidal waveform reflecting more reality which occurs in the field; so, sinusoidal waveform was used in this study.

In the constant strain mode, the most widely used definition of failure in fatigue damage is 50% reduction in the initial stiffness (Matthew et al., 2013). However, three regions of assumed damaged regions - low, intermediate and highly damaged regions – with the same number of steps with 2% stiffness reduction in each step, could not be achieved by splitting 50% reduction into the three target regions. Therefore, instead of using 50% reduction in stiffness as fatigue failure, 54% reduction in initial stiffness is considered as the failure stiffness of the specimens. The first initial stiffness of the specimens being determined at 50th load cycle was called global initial stiffness as shown in Table 3.4.

3.5.2.1 Phase I damage recovery measurement

Due to limitations of laboratory instruments to be able to apply an intermittent rest periods, interrupted fatigue test was used with applications of 2, 4, and 8 minutes as rest periods after every 2% reduction in stiffness. The initial stiffness at the 50th load cycle

of each step after corresponding rest time was used to determine the Damage Recovery Indices (DRI) in Phase I according to the Equation 3.5. Thereafter, those DRI(s) were analysed so as to determine the possible effect of various fibreglass grids applied at mid-depth of asphalt concrete beams after the rest periods on damage recovery capability of asphalt concrete.

$$DRI \ (I)_n = \frac{S_{ini(n+1)} - S_{t(n)}}{S_{global \ initial}}$$ Equation (3.5)

where: $DRI \ (I)_n$: Damage Recovery Index at step *n in phase I,*

$S_{ini(n+1)}$: Stiffness at 50th cycle at step number $(n + 1)$ (MPa)

, $S_{t(n)}$: Terminated stiffness at step *n,*(MPa)

$S_{global \ initial}$: Global Initial Stiffness at the first 50th cycle (MPa), and

n: Step number.

The testing condition in Phase I was:

Type of test:	displacement controlled
Frequencies:	10 Hz
Temperatures:	20 °C
Strain amplitudes:	700 μm/m
Loading wave:	sine wave
Step termination stiffness:	as shown in Table 3.4

Due to a rapid stiffness reduction in the first three steps as shown in Table 3.4, all of the test results from various types of specimens were considered for analysis from step 4 onwards. As it is illustrated in Table 3.4, stiffness decrement of specimens by 2%, followed by random rest times shown in the table was continued up to 54% reduction of global initial stiffness including 27 steps, and this part of the testing procedure is called Phase I damage recovery capability test. Because of manually controlling and time limitation, to be able to finish each specimen within a reasonable time, 700με was selected as the strain to be used in all 27 steps,. These 27 steps are divided into three

ranges, called low, intermediate, and high damage ranges (as shown in Table 3.4). It must be noted that two steps of Phase II damage recovery capability test were conducted during Phase I test process as shown in Table 3.4 and described below.

3.5.2.2 Phase II damage recovery measurement

At the end point of each assumed damaged region (low, intermediately, & highly damaged region) described in previous section, a longer rest time of up to 32 minutes was applied on specimens when the stiffness of the them reached to 18%, 36%, and 54% of the global initial stiffness corresponding to assumed low, intermediate and high damage levels. During that 32-minute rest period the dynamic moduli of the specimens were measured in 2, 4, 8, 16, and 32 minutes with very low strain not to cause any further damage to the specimens. The measured dynamic moduli were used for defining another Damage Recovery Index (DRI_{II}) for Phase II as shown in Equation 3.6. Then, in terms of damage recovery capability, the possible effects of fibreglass grids on asphalt concrete at each of the three assumed damaged region were studied over 32-minute rest period through $DRI_{II}(s)$.

$$DRI_{L/I/H} (II)_n = (\frac{DM_{L/I/H\,(n)}}{DM_{L/I/H\,(2)}} - 1) \times 100 \qquad \text{Equation (3.6)}$$

where:
L: Low damage range,
I: Intermediate damage range,
H: High damage range,
$DRI\,(II)_n$ Damage Recovery Index after n minutes in phase II,
DM_n: Dynamic modulus after n minutes (log MPa),
n: Rest time (minute).

As can be observed in Equation 3.6, DRI(s) in phase II were calculated for three different damage ranges called, Low (L), Intermediate (I), and High (H) damaged, individually after same rest periods (2, 4, 8, 16, and 32 minutes). However, it must be

noted that due to the reason that initially all of the measured dynamic moduli after each rest time in each damage range were normalised by the measured dynamic modulus after 2 minutes of rest time at the corresponding damage region, according to Equation 3.6, $DRI_{II}(s)$ after 2 minutes for all three damage regions equal to zero. Therefore, the analysis excluded DRI_{II} after 2 minutes and only $DRI_{II}(s)$ after 4, 8, 16, and 32 minutes were taken into account. Phase II was conducted in the following conditions:

Type of test:	displacement controlled
Frequencies:	10 Hz
Temperatures:	20 °C
Strain amplitudes:	25 μm/m
Loading wave:	sine wave
Stiffness measurement:	after 100 pulses

Table 3.4: Experimental design of damage recovery measurement

Damage ranges	Step	Initial stiffness of step (S_{ini})	Terminated stiffness (S_t)	Rest time (min)
Considered as low damage range (Phase I)	1	$S_{initial}$	$S_{t1} = 0.98 \times S_{initial}$	4
	2	S_{ini2}	$S_{t2} = 0.96 \times S_{initial}$	2
	3	S_{ini3}	$S_{t3} = 0.94 \times S_{initial}$	8
	4	S_{ini4}	$S_{t4} = 0.92 \times S_{initial}$	8
	5	S_{ini5}	$S_{t5} = 0.90 \times S_{initial}$	4
	6	S_{ini6}	$S_{t6} = 0.88 \times S_{initial}$	2
	7	S_{ini7}	$S_{t7} = 0.86 \times S_{initial}$	2
	8	S_{ini8}	$S_{t8} = 0.84 \times S_{initial}$	4
	9	S_{ini9}	$S_{t9} = 0.82 \times S_{initial}$	8
		$S_{ini9'}$	50 cycles applied only	
		Refer to Phase II damage recovery (Low damaged)		
Considered as intermediate damage range (Phase I)	10	S_{ini10}	$S_{t10} = 0.80 \times S_{initial}$	4
	11	S_{ini11}	$S_{t11} = 0.78 \times S_{initial}$	2
	12	S_{ini12}	$S_{t12} = 0.76 \times S_{initial}$	8
	13	S_{ini13}	$S_{t13} = 0.74 \times S_{initial}$	8
	14	S_{ini14}	$S_{t14} = 0.72 \times S_{initial}$	4
	15	S_{ini15}	$S_{t15} = 0.7 \times S_{initial}$	2
	16	S_{ini16}	$S_{t16} = 0.68 \times S_{initial}$	2
	17	S_{ini17}	$S_{t17} = 0.66 \times S_{initial}$	4
	18	S_{ini18}	$S_{t18} = 0.64 \times S_{initial}$	8
		$S_{ini18'}$	50 cycles applied only	
		Refer to Phase II damage recovery (Intermediately damaged)		
Considered as Highly damage range (Phase I)	19	$S_{ini\ 19}$	$S_{t19} = 0.62 * S_{initial}$	4
	20	$S_{ini\ 20}$	$S_{t20} = 0.60 \times S_{initial}$	2
	21	$S_{ini\ 21}$	$S_{t21} = 0.58 \times S_{initial}$	8
	22	$S_{ini\ 22}$	$S_{t22} = 0.56 \times S_{initial}$	8
	23	$S_{ini\ 23}$	$S_{t23} = 0.54 \times S_{initial}$	4
	24	$S_{ini\ 24}$	$S_{t24} = 0.52 \times S_{initial}$	2
	25	$S_{ini\ 25}$	$S_{t25} = 0.50 \times S_{initial}$	2
	26	$S_{ini\ 26}$	$S_{t26} = 0.48 \times S_{initial}$	4
	27	$S_{ini\ 27}$	$S_{t27} = 0.46 \times S_{initial}$	8
		$S_{ini\ 27}$	50 cycles applied only	
		Refer to Phase II damage recovery (Highly damaged)		

Phase II damage recovery (Low damaged)

Damage range	Rest period (min)	Dynamic modulus
Low (18% of global initial stiffness)	2	$DM_{L\ 2}$
	4	$DM_{L\ 4}$
	8	$DM_{L\ 8}$
	16	$DM_{L\ 16}$
	32	$DM_{L\ 32}$

Phase II damage recovery (Intermediately damaged)

Damage range	Rest period (min)	Dynamic modulus
Intermediate (36% of global initial stiffness)	2	$DM_{I\ 2}$
	4	$DM_{I\ 4}$
	8	$DM_{I\ 8}$
	16	$DM_{I\ 16}$
	32	$DM_{I\ 32}$

Phase II damage recovery (Highly damaged)

Damage range	Rest period (min)	Dynamic modulus
High (54% of global initial stiffness)	2	$DM_{H\ 2}$
	4	$DM_{H\ 4}$
	8	$DM_{H\ 8}$
	16	$DM_{H\ 16}$
	32	$DM_{H\ 32}$

3.6 Dynamic Creep Test Procedure

The specimen preparation and test procedure for dynamic creep test are presented in the following sections.

3.6.1 Specimen Prepration

The specimens to be cored and trimmed into cylindrical shapes had dimensions of 150-mm diameter and 60-mm height as recommended by EN 12697-25 (2005) so that the applied fibreglass grid was placed at mid-depth of the specimen (Figure 3.8).

(a)

(b)

Figure 3.8: Coring (a) and a final cored specimen (b) for dynamic creep test

3.6.2 Dynamic Creep Test

The creep test was conducted using a uniaxial cyclic compression test with the confinement method, as recommended by EN 12697-25 (2005). However, since only three cores were attainable from each slab, three test repetitions were carried out so as to minimise any variability among replicates of one type of specimen. For that purpose, UTM-5P from IPC was used to apply a constant dynamic load at a certain periodic rate onto the cylindrical asphalt specimens, and vertical deformation was measured using a Linear Variable Displacement Transducer (LVDTs). The servo-pneumatic UTM-5P machine has integrated software that allows the operator to select several input parameters such as loading function, stress, frequency and seating stress static pre-loading for a certain period of time can also be applied to the specimens before cyclic loading is started. The loading jig is moreover located in an environmental chamber so as to control the testing temperature.

In the present study, in accordance with EN 12697-25 (2005), the test was performed for both reinforced and control specimens at 40˚C, at a cyclic stress level of 100kPa and a frequency of 0.5Hz, at two resting time ratios 1 and 3. The rest time ratio 1 was called ―Level A" load to rest ratio with 1000 milliseconds allocated for each cycle width and the corresponding rest period, and the rest time ratio 3 was called ―Level B" load to rest ratio with 500 milliseconds allocated for each cycle width and 1500 millisecond allocated for the corresponding rest period. For all the specimens, a constant stress of 100 kPa was applied for up to 10000 cycles due to time limitations. Moreover, a static pre-loading stress of 10kPa was applied to all the specimens for a period of 10 minutes prior to initiating the dynamic load, in order to ensure proper contact between the core surface and loading platen. Before starting of the test, all the specimens were conditioned at 40˚C for about 4 hours in a temperature chamber to

make sure that they had reached the testing temperature. The testing arrangement of the specimens for the dynamic creep test is illustrated in Figure 3.9.

Figure 3.9: Dynamic creep test arrangement

3.6.3 Dynamic Creep Curve Modelling

Ahari et al. (2013) two-stage model was adopted to model the creep curves in this study. They developed a two-stage model for the primary and secondary regions of creep curves in SBS modified asphalt mixtures. They proposed two different approaches for modelling the primary and secondary regions of the creep curve as follows:

Approach 1:

Both the primary and secondary regions of the creep curve can be modelled simultaneously using the following logarithmic function:

$$\varepsilon_P = a \times Ln(X) + b \qquad \text{Equation (3.7)}$$

where: X: is loading cycle,

ε_P: is accumulated permanent strain at loading cycle X, and

a, b: are constants.

Then, in order to check if the developed logarithmic function fits well with both regions, the deviation errors of all the points, re calculated as below, must be less than or equal to 1%:

$$D_e = \frac{\left|\varepsilon_{P(Calculated)} - \varepsilon_{P(Measured)}\right|}{\varepsilon_{P(Measured)}} \times 100$$ Equation (3.8)

where: D_e: is deviation error (%)

Approach 2:

In order to identify the boundary points of the primary and secondary regions of the creep curve, the following steps are taken:

1- Visual selection of loading cycles among the initial loading cycles of the secondary region [It must be noted that this loading cycle is not necessarily the boundary point].

2- Removal of the loading cycles before the selected loading cycles, and plotting a new graph representing the approximate secondary linear region.

3- Fitting a linear model to the approximate secondary region and determining the model coefficients.

4- Calculating the accumulated permanent strain for all the loading cycles of the approximate secondary region, based on obtaining model coefficients.

5- Determining the deviation error (D_e) for all of the calculated accumulated permanent strains.

6- If simultaneously all the $D_e(s) \leq 1\% \rightarrow$ the criterion is met and the linear model is assumed to be representative.

If at least one of the $D_e(s) > 1\% \rightarrow$ go to the next loading cycle and repeat steps 2-6 until the former criterion is met.

7- Fitting the logarithmic function resulting from approach 1 to the primary region.

8- Solving the set of simultaneous equations, called logarithmic and linear, respectively, for the results of the primary and secondary regions, in order to identify the accumulated permanent strain and its corresponding loading cycle, where the primary region is connected to the secondary region.

3.7 Summary of the Chapter

This chapter has discussed the materials and methodologies adopted in this study. Firstly, materials used for fabricating asphalt concrete slabs are described. Then, we discuss dynamic modulus measurement test using four-point bending apparatus followed by describing on dynamic moduli master curve construction of the specimens. It is followed by the method used for studying any possible effect of fibreglass grids on damage recovery ability of asphalt concrete in two phases. Finally, the dynamic creep test has been discussed and the method which was used for modelling the creep curves is described. The following chapter would discuss the results of the analyses for the objectives of the study.

CHAPTER 4: RESULTS AND DISCUSSION

4.1 Introduction

Asphalt concrete is a material which can exhibit both elastic and viscous behaviour. In addition, the bitumen used in asphalt concrete has a self-recovery ability in certain conditions. However, due to the increase in traffic on the roads, the pavements are becoming highly prone to destruction by various types of distresses. Thus, several methods have been adopted by researchers in order to improve the characteristics of asphalt concrete. One of these methods is geogrid reinforcement of asphalt concrete. Bearing in mind the complex behaviour of asphalt concrete, it would be worthwhile to study some of the characteristics of asphalt concrete before and after introducing other materials such as geogrids. In this thesis, an effort has been made to study the dynamic stiffness, damage recovery ability, and creep behaviour of fiberglass grid reinforced and unreinforced hot mix asphalt specimens.

This chapter first presents the results of the laboratory tests conducted on fibreglass grid reinforced and unreinforced hot mix asphalt concrete. It then analyses and discusses these. Each of the main results, together with a discussion of each type of test, is presented in separate sub-sections of this chapter.

The statistical analysis of the results was carried out by a computer program coded in R programming software, run on a Pentium IV 1.9 GHz CPU with 8 GB RAM.

4.2 Dynamic Modulus

Bearing in mind the complex behaviour of asphalt concrete, the main purpose of this experiment was to perform a dynamic modulus test on both unreinforced (control) asphalt concrete specimens and asphalt concrete specimens reinforced with four different types of fibreglass grids. Table 3.3 in Chapter 3 illustrated the four types of glass grids used. Solver function of Excel was used to construct the master curve for

each type of mix. Three replicates were used for each mix, and the average of the parameters was taken to construct the master curve.

The parameters obtained based on the Witczak dynamic modulus model (Equations 3.2-3.4) are given in Table 4.1. Figures 4.1 to 4.5 illustrate the master curves constructed for each type of unreinforced and geogrid reinforced asphalt concrete specimen, including stiffness moduli before and after shifting of the data.

Table 4.1: Regression coefficients for Witczak dynamic modulus model at 20°C

Specimen code	δ	α	β	γ	C_1	C_2	R^2
C	0.896	3.402	-1.785	-0.563	15.302	101.742	0.999
R1	2.014	2.226	-1.235	-0.707	15.111	101.692	0.999
R2	1.737	2.579	-1.354	-0.583	15.690	100.746	0.999
R3	2.228	1.951	-1.323	-0.736	15.692	103.644	0.999
R4	1.908	2.326	-1.463	-0.695	15.759	101.657	0.999
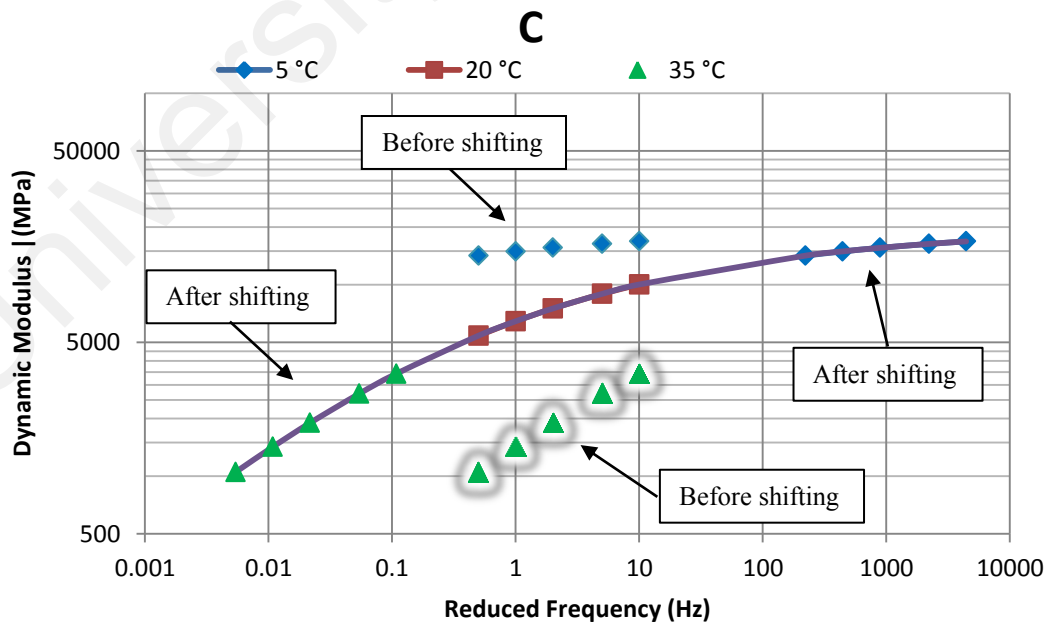
Figure 4.1: Master curve of control specimen

R1
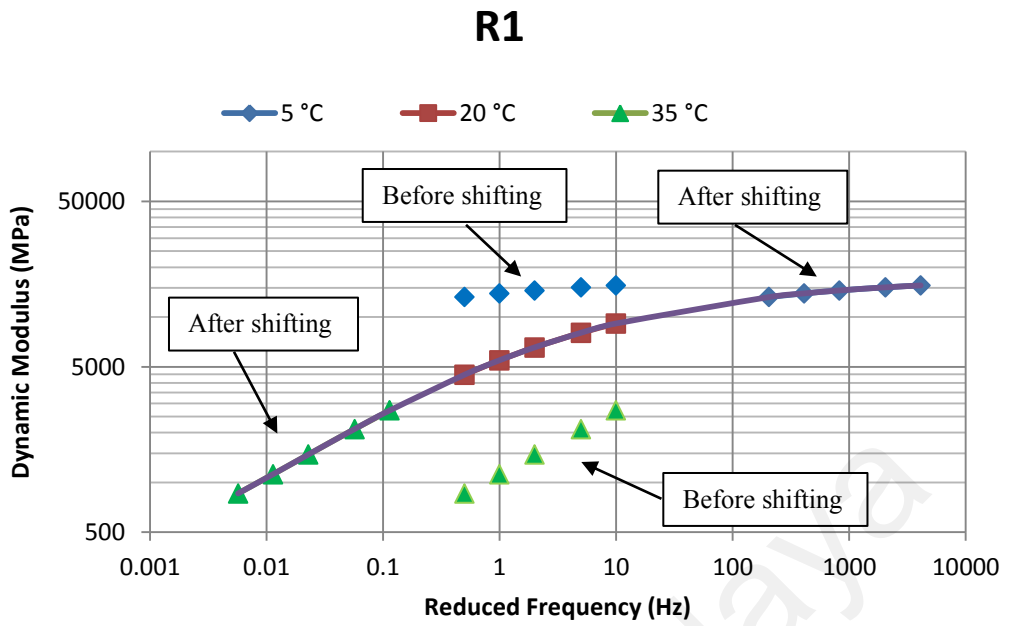
Figure 4.2: Master curve of R1 specimens

R2
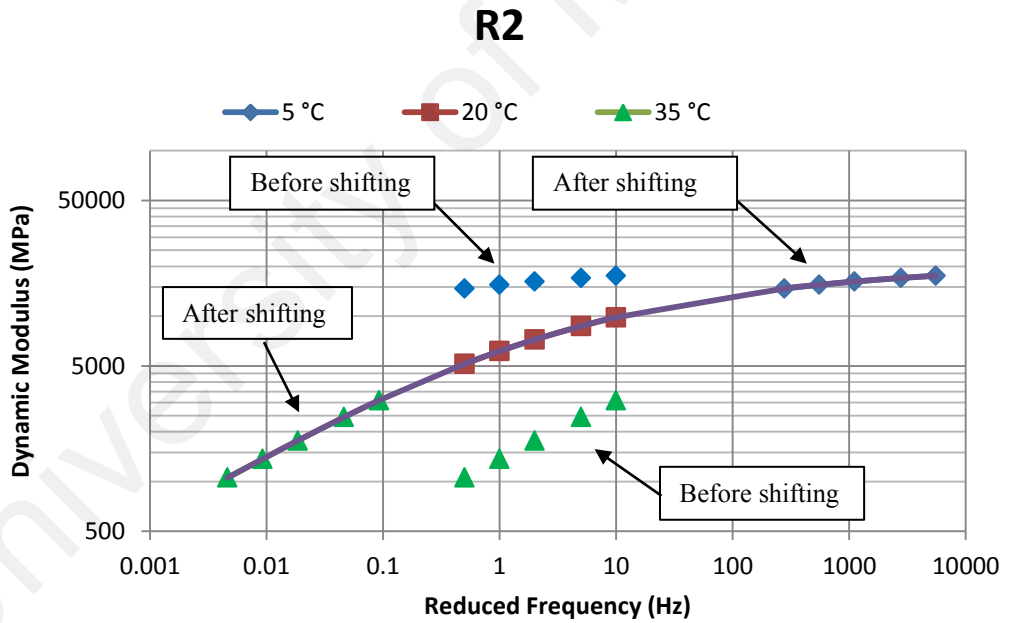
Figure 4.3: Master curve of R2 specimens

R3
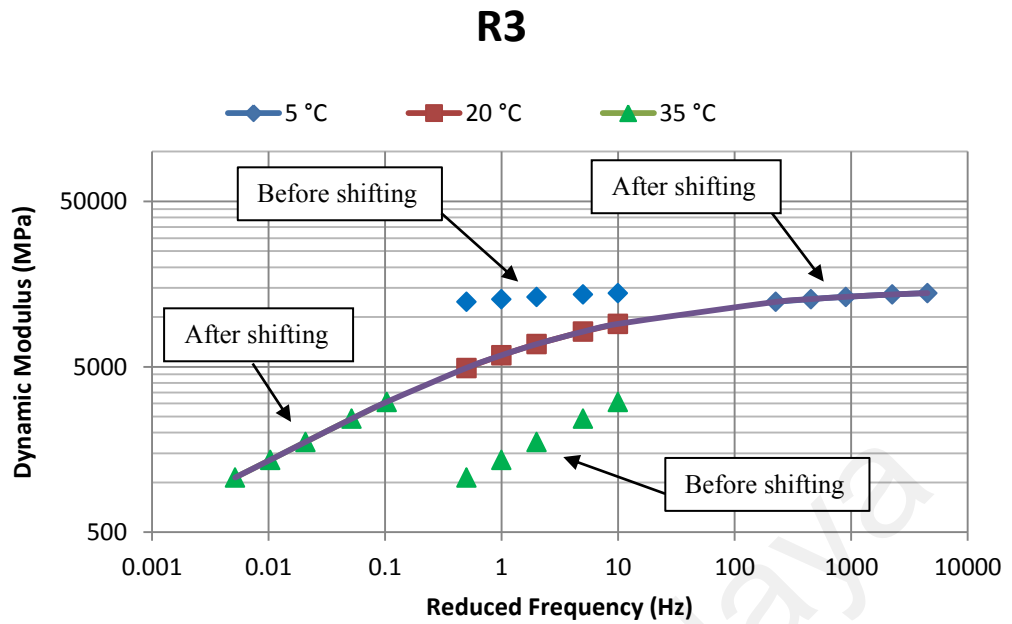
Figure 4.4: Master curve of R3 specimens

R4
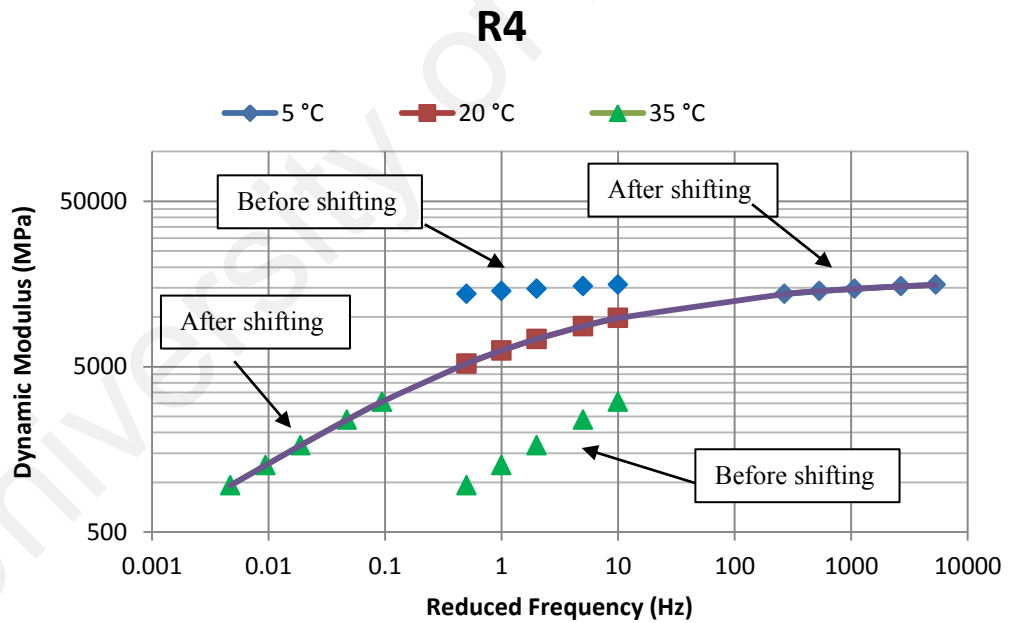
Figure 4.5: Master curve of R4 specimens

From a visual inspection of the constructed master curves, there seem to be no remarkable differences between the various types of specimen within the obtained frequency ranges in the constructed master curves. This results are almost in line with what the results concluded by Canestrari et. al. (2015). Those curves constructed from

the experimental results do not cover the asymptotes of S-curve. Hence, we need to try to analyse further the parameters in Equations 3.2-3.4 (shown in Table 4.1), particularly the lower/upper asymptotes and inflection points of the constructed S-curve for various types of specimens.

This experiment assumes that there are two levels (high and low) of grid tensile strength and two levels (large and small) of grid opening size. However, it should be noted that in large grid opening size level the dimensions are slightly different. Based on this assumption the separate and combined effects of the two different tensile strengths and two mesh sizes on the lower/upper asymptotes and inflection points of the specimens. This comparison is shown in Table 4.2.

Table 4.2: Comparison of upper asymptote, lower asymptote &
inflection points of tested mix types

Specimen code	C	R1	R2	R3	R4
Tensile strength (kN/m) (MD ×XD)	-	$115×115^{*L}$ +/- 15	$115×115^{*L}$ +/- 15	$115×215^{*H}$ +/- 15	$115×215^{*H}$ +/- 15
Grid mesh size (mm) Center to center of strand)	-	$12.5×12.5^{**S}$	$25×25^{**OL}$	$12.5×12.5^{**S}$	$25×19^{**OL}$
Lower asymptote value (MPa)	7.86	103.33	54.63	169	80.85
Improved lower asymptote value compared to control specimen (Times)	1	13.14	6.95	21.49	10.28
Upper asymptote value (MPa)	19860.78	17377.86	20741.57	15111.25	17116.88
Improved upper asymptote value compared to control specimen (Times)	1	0.87	1.04	0.76	0.86
Inflection point (Hz)	0.0006709	0.017955	0.0047507	0.015982	0.007858
Improved inflection point value compared to control specimen (%)	1	26.76	7.08	23.82	11.71

^{*L}: Low level for grid tensile strength ^{**S}: Small level for grid opening size

^{*H}: High level for grid tensile strength ^{**OL}: Large level for grid opening size

The detailed analysis of the parameters of the Witczak dynamic modulus model in Table 4.2 above shows that there is not much difference between the upper asymptotes of the specimens. This may be because at very low temperatures or very high frequencies, when the mix is in its hardest state (near to glassy modulus) and is quite elastic, the load is taken by the mix and since the grids are laid at mid-depth of the beams they are not activated. In other words, grid reinforcement does not increase the hot mix asphalt dynamic modulus at very low temperatures or very high frequencies in which the mixture is highly hard and elastic. The slight differences among the glassy modulus of the various specimens may also be attributed to measurement errors by the testing instruments at cold temperatures and high frequencies.

On the other hand, as again shown in Table 4.2, there are big differences between the lower asymptotes (near to the equilibrium moduli) where the specimens are at their highly viscous range. Moreover, the most significant differences are between the various reinforced specimens and the control ones, with the lower asymptote values of the reinforced specimens being much higher than those of the unreinforced specimens. This suggests that, even although the grids are applied at mid-depth of the beam specimens, the grids are still effective and help to take the load at very low frequencies, perhaps because of the viscoelastic and non-homogeneious nature of the asphalt mixtures. Comparing the lower asymptotes of the various reinforced specimens, it can be seen that those asymptotes of R1 and R3 (small mesh size grids) specimens are higher than those of R2 and R4 (large mesh size grids). Moreover, the lower asymptotes of the high tensile strength grid reinforced specimens (R3 and R4) are higher than those of the corresponding mesh size grids with low tensile strength (R1 and R2).

In terms of the inflection points at which the rate of the dynamic modulus increase/decrease changes by frequency, almost the same differences can be observed as with the lower asymptote. The control (unreinforced) specimens have the lowest

inflection point (although it must be noted that the estimated inflection point of the control specimen was extrapolated since it fell outside of the range after shifting testing frequencies). The second smallest inflection point can be found in the R2 and R4 (large opening size) grids; and finally the largest inflection points occur with the R1 and R3 (small opening size) grids.

The conclusion to be drawn from the above is that the positive effect of the small opening size grids on the inflection point is greater than that of the large opening size grids. In other words, as seen in Table 4.2, the master curves of the small mesh size grid reinforced specimens reached their inflection points on the reduced frequency axis (the frequency at which the dynamic moduli shift from increasing rate to decreasing one) faster than those of large mesh size grid reinforced specimens. Also, at the corresponding dynamic moduli of those frequencies, the small mesh size grid reinforced specimens showed higher moduli compared with those of large mesh size grid reinforced specimens..

From the above discussion, the conclusion can be drawn that reducing the grid mesh size while keeping the tensile strength the same, and increasing the tensile strength while keeping the mesh size grids the same, both lead to higher dynamic moduli in the fibreglass grid reinforced specimens at very low frequencies (corresponding to very high temperatures).

In order to display these differences visually, the data points beyond those actually achieved in the experiment are extrapolated and illustrated in Figure 4.6 below.
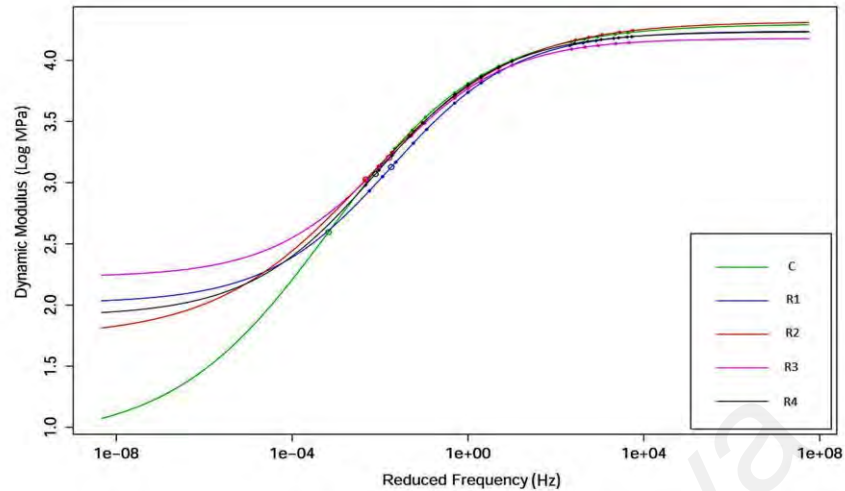
Figure 4.6: Master curves of testing specimens in extrapolated reduced frequencies

(Filled circles show the shifted frequencies, while blank circles show the inflection points of the relevant specimens)

From Figure 4.6 it can also be seen that, at very low frequencies, the lower asymptotes differ substantially between the various specimens. According to Goodrich (1991), quoted by Rahimzadeh (2002), asphalt mixture rheology at high temperatures above 50℃ is predominantly affected by aggregates. The above results suggest that, as the bitumen in the asphalt mixture shifts from the elastic towards the viscous phase and the mixture's rheology properties become predominantly affected by aggregates, the grids are activated even although they are located at the mid-depth of the beams.

.

4.3 Damage Recovery

As noted earlier (see Table 3.3), four types of glass grid reinforced plus one set of control specimens were used in this experiment. This section looks at the damage recovery capability of these. The term damage recovery is used, rather than healing, because net healed amount cannot be obtained in a four-point bending beam apparatus, since the time-dependent linear viscoelastic effects and the non-linearity of the asphalt concrete, as a viscoelastic material, cannot be eliminated from the recovered stiffness (Kim et al., 1994; Si et al., 2002b).

Damage recovery measurements were performed in two phases. Both phases involved four-point bending tests. However, in Phase I, a set of high load levels followed by a rest period after each load level was applied and the stiffness was measured in certain time periods. In Phase II, on the other hand, the specimens were given a 32-minute rest period at certain levels of damege during which time the recovery (if any) of the beam specimens was determined after, respectively, 2, 4, 8, 16, and finally 32 minutes, through applying very low load levels. The procedures to determine damage recovery in both phases were described in more detail in Section 3.5.

An analysis of variance (ANOVA) was used to examine the differences between the Damage recovery Index (DRI) values of the studied specimen types. The significance of the differences was tested at the 0.05% level of error. R software was used to perform the statistical analysis.

Parametric statistical tests such as ANOVA, used to compare the average responses of various treatment groups as well as for a pairwise comparison, are based on three main assumptions: namely the normality, homoscedasticity and continuity of the dependent variables. These assumptions therefore need to be checked before running the statistical tests, since if the assumptions do not hold, the results may be misleading. We duly checked the assumptions and applied corrective measures where needed.

4.3.1 Phase I Damage Recovery Analysis

In this phase of the experiment, an interrupted fatigue test was utilised, with rest times of 2, 4 and 8 minutes being applied randomly after certain amounts of stiffness reduction. Thereafter, the fatigue test was resumed. The stiffness was measured after each of the rest times (see Table 3.4). The average value of the three replicates was used for data analysis in this part of the experiment.

In order to assess how far the Phase I results violated the assumptions for statistical analysis, numerical and graphical analysis were utilised. The descriptive statistics for the various tested specimens are shown in Table 4.3.

Table 4.3: Descriptive statistics of tested specimen's determined DRI (Phase I)

Specimen code	C	R1	R2	R3	R4
Tensile strength (kN/m) (MD×XD)	-	$115 \times 115^{*L}$ +/- 15	$115 \times 115^{*L}$ +/- 15	$115 \times 215^{*H}$ +/- 15	$115 \times 215^{*H}$ +/- 15
Grid mesh size (mm)	-	$12.5 \times 12.5^{**S}$	$25 \times 25^{**OL}$	$12.5 \times 12.5^{**S}$	$25 \times 19^{**OL}$
No.of data	24	24	24	24	24
DRI mean	0.062	0.079	0.061	0.096	0.063
Standard deviation	0.023	0.021	0.019	0.021	0.017
Median	0.068	0.078	0.059	0.093	0.064
Min	0.025	0.038	0.025	0.065	0.026
Max	0.107	0.116	0.091	0.144	0.087
Skew	0.06	-0.01	-0.15	0.33	-0.29
kurtosis	-1.15	-0.75	-1.08	-0.69	-0.93

^{*L}: Low level for grid tensile strength ^{**S}: Small level for grid opening size

^{*H}: High level for grid tensile strength ^{**OL}: Large level for grid opening size

A Shapiro-Wilk normality test, histogram and Q-Q normality plot were used as numerical and graphical tools to check the normality of data. The resulting data shows that the DRI values were indeed normally distributed. The Shapiro-Wilk normality test produced a Shapiro-Wilk statistic of 0.989 and a p-value of 0.410. The histogram and Q-Q plot of the DRI values are illustrated in Figures 4.7 and Figure 4.8, respectively.
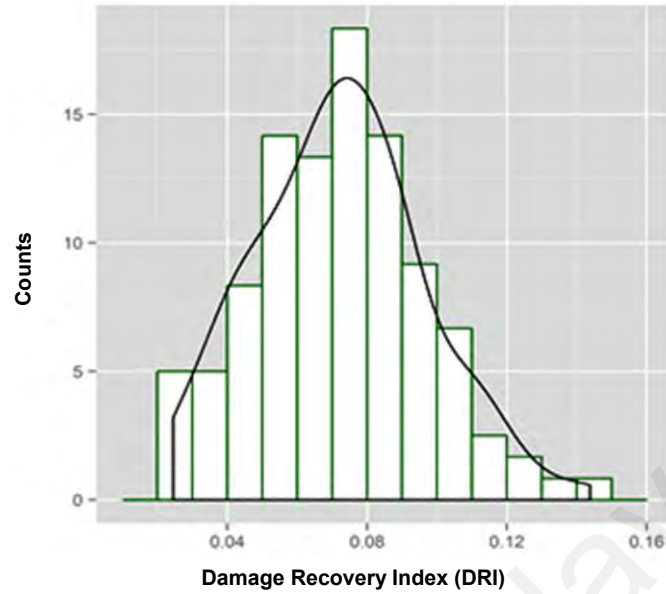
**Figure 4.7: Histogram of damage recovery indices (DRI)
(Phase I)**
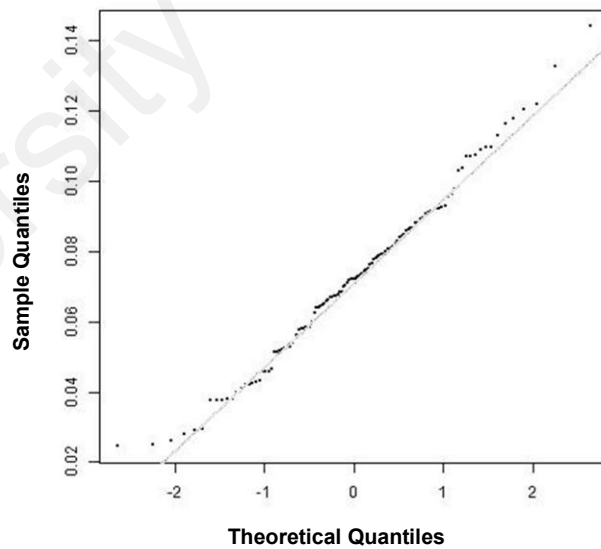
**Figure 4.8: Quantile-Quantile plot of
damage recovery indices (DRI) (Phase I)**

In order to check the homoscedasticity (homogeneity of variance) of the response

values, a Levene's test and box plot were utilised. Running the Levene's test resulted in

an F-value of 0.731 and a p-value of 0.573. Figure 4.9 shows the box plot for each type of specimens. Overall, these show that the homogeneity of variance holds.
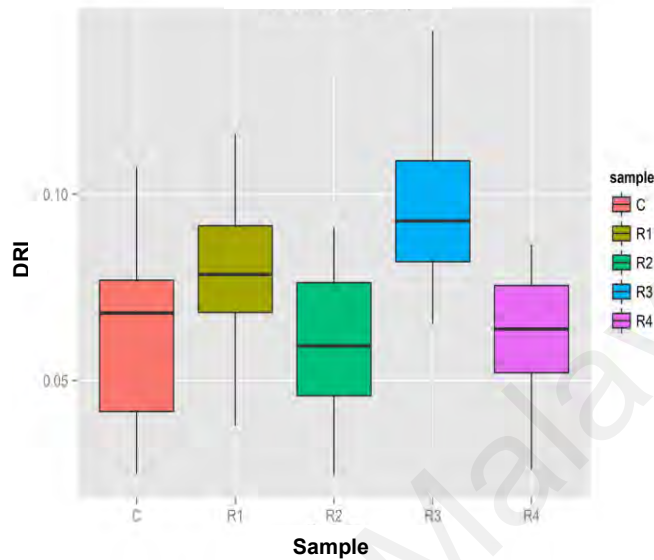
Figure 4.9: Box plot of damage recovery indices (DRI)
(Phase I)

Since all the assumptions proved valid, we proceeded to apply the parametric statistics analysis. Figure 4.10 below contains a bar chart of the overall means of the DRI values for each type of specimen.
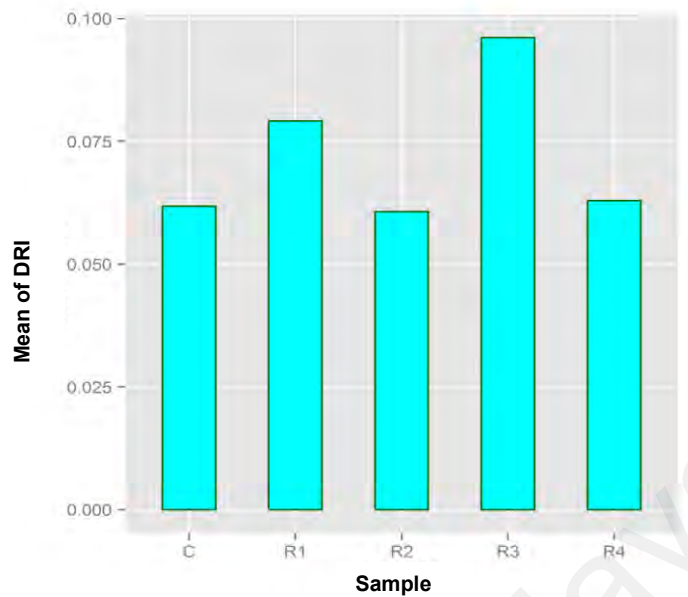
Figure 4.10: Bar chart of mean damage recovery indices (DRI)
(Phase I)

As can be seen from Figure 4.10, specimen R3 and R2, respectively, had the highest and lowest DRI mean values, at 0.096 and 0.061. A further analysis using a one-way ANOVA with an F-value of 13.8 confirmed that these differences were significant at least to the 0.05 level, but did not provide any further information on the differences in DRI between each of the specimens. In order to detect these differences, a post-hoc test was performed using Tukey's procedure for multiple pairwise comparisons without an increase in the probability of a Type I error. The results, including the mean differences, lower and upper confidence intervals, and adjusted p-values are presented numerically in Table 4.4 and graphically in Figure 4.11.

Table 4.4: Mean DRI beween various specimens (one-way ANOVA)

Specimen	Specimen characteristics	Mean difference	Lower C.I.	Upper C.I.	Adjusted p-value
R1 & C	100:0.5[*] & unreinforced	0.0174	0.0011	0.0336	0.0299
R2 & C	100:1[*] & unreinforced	-0.0011	-0.0174	0.0151	0.9997
R3 & C	200:0.5[*] & unreinforced	0.0343	0.0181	0.0505	0.0000
R4 & C	200:1[*] & unreinforced	0.0011	-0.0151	0.0173	0.9997
R2 & R1	100:1[*] & 100:0.5[*]	-0.0185	-0.0347	-0.0022	0.0173
R3 & R1	200:0.5[*] & 100:0.5[*]	0.0170	0.0007	0.0332	0.0360
R4 & R1	200:1[*] & 100:0.5[*]	-0.0163	-0.0325	0.0000	0.0497
R3 & R2	200:0.5[*] & 100:1[*]	0.0354	0.0192	0.0516	0.0000
R4 & R2	200:1[*] & 100:1[*]	0.0022	-0.0140	0.0184	0.9956
R4 & R3	200:1[*] & 200:0.5[*]	-0.0332	-0.04943	-1.70E-02	1.1E-06

Based on adjusted p-values at less than 0.05 and also the lower and upper confidence intervals not including zero in Table 4.4 and Figure 4.11, we can conclude that there is a significant difference between R1 & C, R3 & C, R2 & R1, R3 & R1, R3 & R2, R4 & R1 and R4 & R3, while the differences between R2 & C, R4 & C and R4 & R2 are not significant.

95% family-wise confidence level

Differences in mean levels of sample
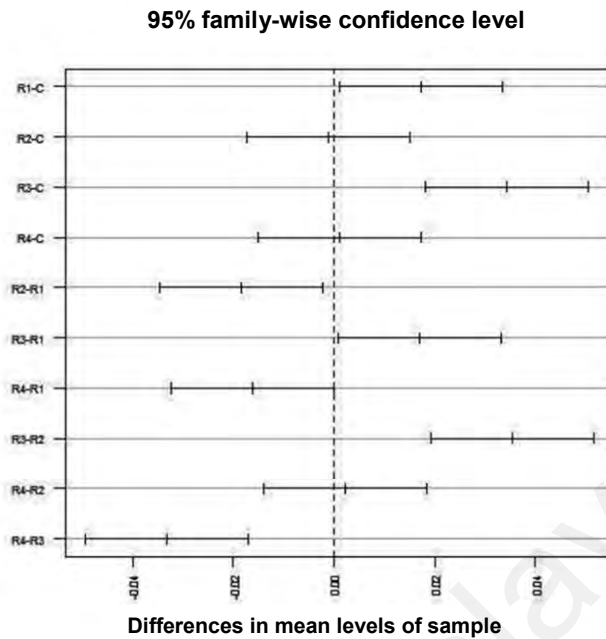
**Figure 4.11: Mean differences and confidence
interval of pairwise comparisons (Phase I)**

An initial look at the data in Table 4.4 suggests that both the grid tensile strength and mesh size influenced the DRI mean, apart from with the unreinforced (control) specimen. To ascertain which were the main effects, a further analysis was carried out using a two-way ANOVA with two independent variables (IVs), namely tensile strength at two levels – high (200KN) and low (100KN); and grid opening size also at two levels – large (1 inch) and small (0.5 inch)). The results of this are presented in Table 4.5, while Figure 4.12 illustrates the DRI means for each level of the two grid factors.
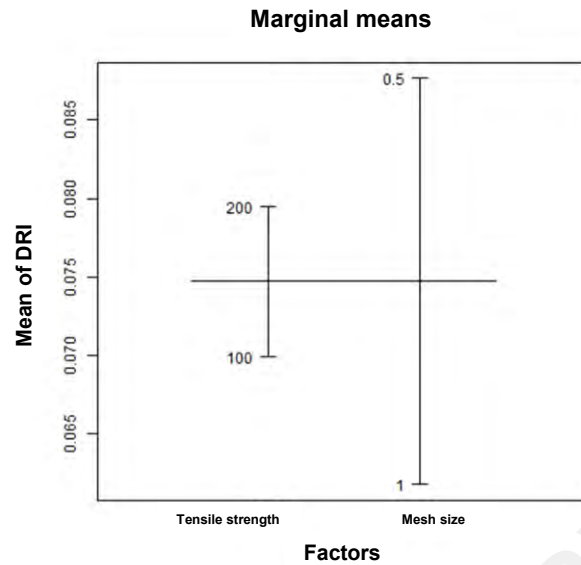
Figure 4.12: Univariate effects of grid tensile strength and mesh size (Phase I)

Table 4.5: Results of two-way ANOVA

Effect Source	F value	Significance level	Effect size
Grid tensile strength	5.77980	0.01822	0.05911
Grid mesh size	41.98970	0.00000	0.31338
Interaction between grid tensile strength & mesh size	3.41630	0.06777	0.03580

Both grid tensile strength and mesh size emerged as main effects at the 0.05 level. Moreover, the effect sizes of both were larger than those of the interaction between them, which does not seem to be a main effect at this level. Furthermore, a similar conclusion can be drawn from Figure 4.13 showing the pattern of DRI means graphically: while the gap between the DRI means becomes narrower as we move from small to large mesh size, the lines depicting tensile strength levels do not touch at any point – an indication that there was no interaction effect.
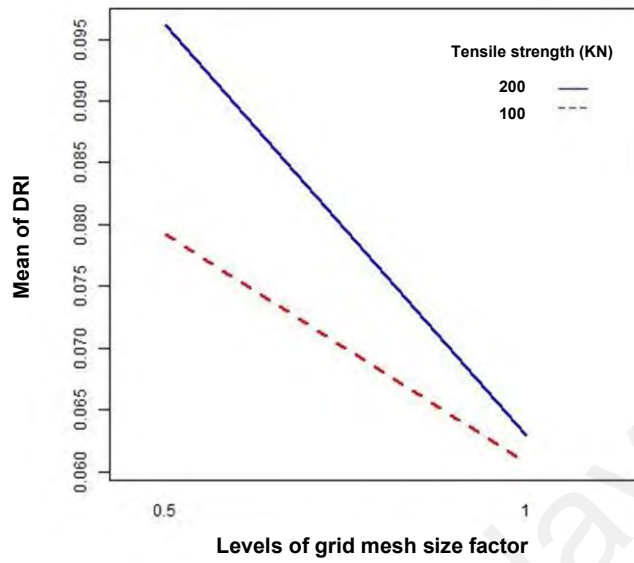
Figure 4.13 Effect size graph (Phase I)
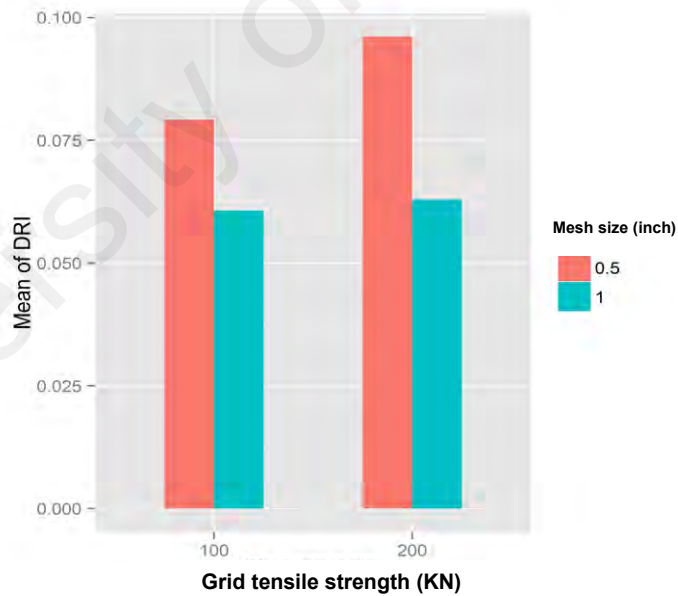
**Figure 4.14 Bar chart of damage recovery indices'(DRI) means
(Phase I)**

Figure 4.14, a bar chart derived from Table 4.4, points to the same conclusion. It shows clearly that the difference in tensile strength is much more significant for the small opening size grids than the large ones.

Table 4.6 contains the results of Tukey's multiple comparison, illustrating the upper and lower confidence intervals of the main effects with a significant influence on DRI in the first two rows of the table. All the remaining data in Table 4.6 again points to the same conclusion as Table 4.4.

Table 4.6: Mean DRI differences among various specimens
(two-way ANOVA)

Specimen	Mean difference	Lower C.I.	Upper C.I.	Adjusted p-value
200^{**} & 100^{**}	0.009584	0.001666	0.017501	0.018216
1^{***} & 0.5^{***}	-0.025830	-0.033750	-0.017910	0.000000
$200{:}0.5^{*}$ & $100{:}0.5^{*}$	0.016952	0.002200	0.031704	0.017595
$100{:}1^{*}$ & $100{:}0.5^{*}$	-0.018460	-0.033220	-0.003710	0.007986
$200{:}1^{*}$ & $100{:}0.5^{*}$	-0.016250	-0.031000	-0.001500	0.024926
$100{:}1^{*}$ & $200{:}0.5^{*}$	-0.035420	-0.050170	-0.020660	0.000000
$200{:}1^{*}$ & $200{:}0.5^{*}$	-0.033200	-0.047950	-0.018450	0.000000
$200{:}1^{*}$ & $100{:}1^{*}$	0.002216	-0.012540	0.016967	0.979289

Note: * Tensile strength (KN) : Mesh size (inch)

** Tensile strength (KN)

*** Mesh size (inch)

As can be seen from Table 4.6, only the difference between 200:1 (R4) and 100:1 (R2) is not significant, and there are significant differences between all the other reinforced specimens.

Below is a summary of the Phase I damage recovery statistical analysis:

- Comparing the reinforced specimens and the control ones, there were significant differences only between R1, R3 and the control specimens.

- Comparing the reinforced specimens only:

  o For the small opening size grids (0.5 inch), the difference between the high and low tensile strengths was significant, unlike for the large

opening size grids. The high tensile strength grids with a small opening size showed a much higher DRI than the equivalent low tensile strength grids.

o For both the high and low tensile strength grids (200 & 100 KN), the differences between the small and large grid opening sizes were significant. Specimens reinforced with small opening size grids experienced greater recovery than those reinforced with large opening size grids.

o There was a significant difference between the high tensile strength in the small mesh size grid reinforced specimens and the low tensile strength in the large mesh size ones.

o There was a significant difference between the low tensile strength in the small mesh size grid reinforced specimens and the high tensile strength in the large mesh size ones.

o R3 produced the highest DRI (see Figures 4.8 and 4.9).

o Moving from 100KN tensile strength grids to 200KN ones, the small mesh size became more effective (Figure 4.12).

o Moving from 0.5 inch (small) mesh size to 1 inch (large) mesh size, the 200KN tensile strength became more effective (Figure 4.13).

From the above analysis, the small mesh size grid with high tensile strength (R3) emerged with the best damage recovery ability, followed by the small mesh size grid with low tensile strength (R1). There were no significant differences in terms of DRI between the remaining specimens (control, and reinforced low and high grid tensile strength with large opening size). To put it another way, small mesh size grids would help to have a longer pavement life through damage recovery effect of them. In addition, between the two types of small mesh size grids with two tensile strength,

according to table 4.3, it can be seen that the damage recovery index of higher strength grid (R3) is almost 1.2 larger than small ones (R1).

The fact that only small mesh size fibreglass grids have a significant impact on DRI can be probabily attributed to the aggregate structure of reinforced asphalt concrete. Other researchers have found that aggregate structural characteristics, such as aggregate orientation/segregation and aggregate-to-aggregate contact points, are factors that can affect the damage recovery ability of asphalt concrete (Kim & Roque, 2006; Liu, 2012). Moreover, Partl et al. (2013) suggested that only large size aggregates significantly affect the aggregate structure. The insertion of fibreglass grids into the asphalt concrete may lead to some modification of the structure of the aggregates in the asphalt concrete, which in turn impacts positively on the DRI. In other words, the aggregates coming into direct contact with the grid threads and modification of aggregate structure adjacent to the plane at which the grid is applied can probabily caused such significant impact.

As was shown earlier in Table 3.3, the mass per unit areas of the low tensile strength grids (405 g/m^2) is about 66 percent of the mass per unit area for high tensile strength ones (610 g/m^2). Consequently, the area covered by the grids at the applied depth in the high tensile strength grid reinforced specimens is higher. The higher DRI in higher tensile strength grids may be attributed to this difference in the area covered by the geogrids.

Although the mass per unit areas of both the large and small mesh size grids with the same tensile strength are equal, the small mesh size grids are much more evenly distributed within the applied surface due to their smaller aperture size. To put it another way, the probability of aggregates, particularly large ones coming into direct contact with the grid threads in large mesh size grids is much lower than with small mesh size grids. This may be why there was no significant difference between the specimens reinforced with large mesh size grids and the control specimens.

At the same time, as the previous literature states, there are many factors that can affect the damage recovery ability of asphalt mixtures. Moreover, in this study the testing was conducted in one set of circumstances and with only one material. Further research is therefore needed on the damage recovery ability of geogrid reinforced asphalt concrete, and specifically on the mechanisms and processes by which small mesh size grids increase the damage recovery ability of asphalt concrete.

4.3.2 Phase II Damage Recovery Analysis

In Phase II, the specimens were given a 32-minute rest period at certain levels of damage during which time the recovery (if any) of the beam specimens was determined after 2, 4, 8, 16, and finally 32 minutes, respetively, through applying very low load levels so as not to cause any more damage. An almost identical statistical analysis as in Phase I was then applied to the results of Phase II.

The analysis of data revealed that the DRI values in Phase II violated normality assumption and departed from normality. To cope with this, the dependent variables were shifted to a different scale through square rooting, and all the other data was similarly transformed to this new scale. Table 4.7 presents the descriptive statistics for Phase II damage recovery after this transformation of the data.

Table 4.7: Descriptive statistics of tested specimen's determined DRI (Phase II)

Specimen code	C	R1	R2	R3	R4
Tensile strength (kN/m) (MD×XD)	-	$115 \times 115^{*L}$ +/- 15	$115 \times 115^{*L}$ +/- 15	$115 \times 215^{*H}$ +/- 15	$115 \times 215^{*H}$ +/- 15
Grid mesh size (mm)	-	$12.5 \times 12.5^{**S}$	$25 \times 25^{**OL}$	$12.5 \times 12.5^{**S}$	$25 \times 19^{**OL}$
No. of data	12	12	12	12	12
DRI	2.114	2.482	2.129	2.774	2.205
Standard deviation	0.693	0.842	0.694	1.123	0.736
Median	1.913	2.611	2.135	2.599	2.319
Min	1.131	1.239	1.038	0.997	1.082
Max	3.434	3.884	3.391	4.745	3.503
Skew	0.594	0.011	-0.006	0.23	0.087
kurtosis	-0.838	-1.495	-1.05	-1.122	-1.091

*L: Low level for grid tensile strength   **S: Small level for grid opening size

Figures 4.15 and 4.16 are the histogram and Q-Q plot of the transformed DRI values in Phase II.
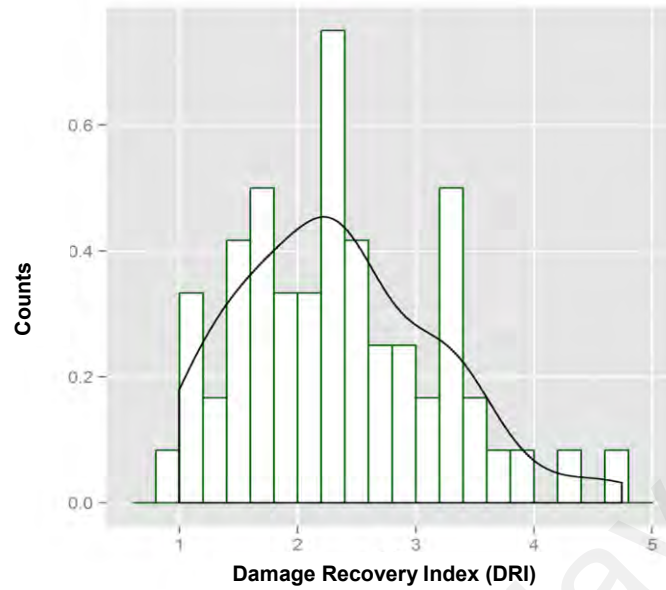
**Figure 4.15: Histogram of damage recovery indices (DRI)
(Phase II)**
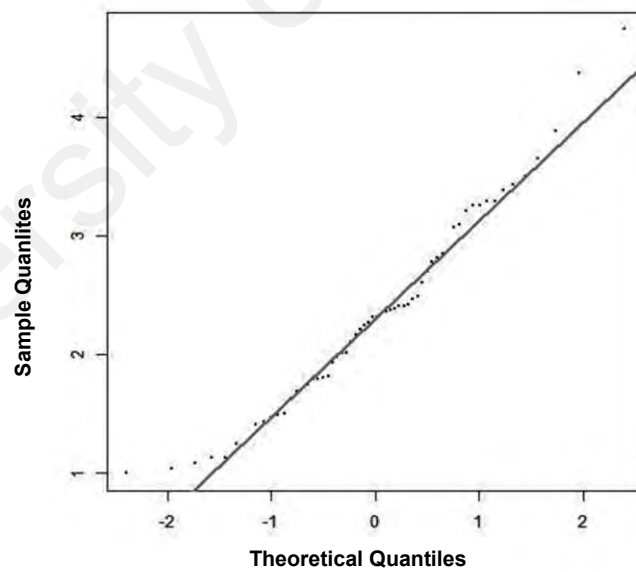
**Figure 4.16: Quantile-Quantile plot of
damage recovery indices (DRI) (Phase II)**

In order to check homoscedasticity (homogeneity of variance) of the response values,

a Levene's test and box plot were utilised. The Levene's test resulted in an F-value of

1.309 and p-value of 0.278, showing that there are insufficient evidence to claim that the variances are not equal. Moreover, as can be seen from Figure 4.17, the homogeneity of variance was not violated.
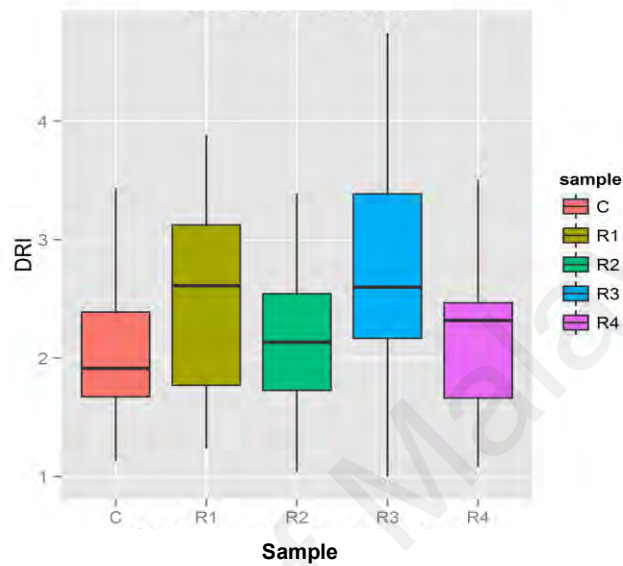
Figure 4.17: Box plot of damage recovery indices (DRI) (Phase II)

The overall DRI mean values of the specimens are illustrated by a bar chart in Figure 4.18.
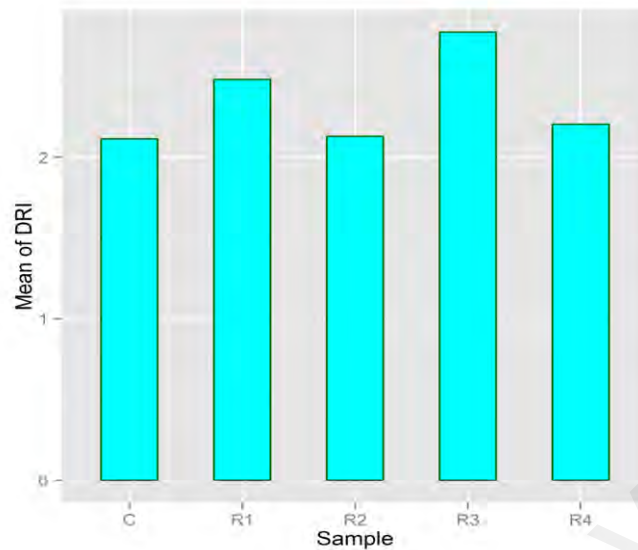
**Figure 4.18: Bar chart of mean damage recovery
indices (DRI) (Phase II)**

As the above graph shows, the R3 specimen came out with the highest DRI, followed by R1, with the remaining specimens having largely similar DRI values. This pattern is very similar to the one in the Phase I damage recovery measurement. In order to check the significance of the differences between the DRI of the specimens, a one-way ANOVA was run at the 0.05 significance level. This produced an F-value of 1.394 and a p-value of 0.248, suggesting that the differences between the DRI of the specimens was not significant. In other words, the various types of fibreglass grids did not induce significantly different levels of damage recovery in the asphalt concrete during the longer rest times tested in this phase of the experiment.

More specifically, the results over the 32min rest time revealed no significant differences in the damage recovery of the different specimens at the $\alpha=0.05$ significance level. This suggests that, when there was no load to cause continuous microcracks to the beams, there was no damage recovery during the 32 minute rest period. In other words, the damage recovery ability achieved in the Phase I test could not possibly have been

due to any type of chemical reaction between the geogrid material and the asphalt mixture.

4.4 Dynamic Creep

In this part, based on the results of dynamic creep test conducted on various types of fibreglass grid reinforced and unreinforced hot mix asphalt concrete, the influence of grid tensile strength and opening size on creep behaviour is investigated. Moreover, a recently developed creep curve model which was verified to be used for modelling the primary and secondary regions of the materials used in this study, is presented.

4.4.1 Permanent Strain Comparison

The permanent deformation potentials of asphalt concrete reinforced with four different types of fibreglass grids as indicated in Table 3.3, at two rest time ratios, so-called 1 and 3 times the loading time were compared with each other, as well as with unreinforced (control) specimens in order to identify which type had the highest resistance to permanent deformation. Afterwards, permanent deformation potential of each specimen type at one load to rest ratio level was compared with its corresponding permanent deformation potential at the other level of load to rest ratio. Considering that there are three replicates for each type of specimen, the diagrams were derived from the average amount of parameters. Figure 4.19 illustrates the comparison results for the specimens in two load to rest ratio, being 1000 millisecond loading time and 1000 millisecond rest time, and 500 millisecond loading time and 1500 millisecond rest time, respectively, denoted as level A, and level B. Thereafter, the creep curve stepwise model developed by Ahari et al. (2013) was verified for the materials used in this study and then used to fit the creep curves and determine the connecting points between the primary and secondary phases. This method consisted of eight steps as shown in Section 3.6.3 (Ahari et al., 2013).
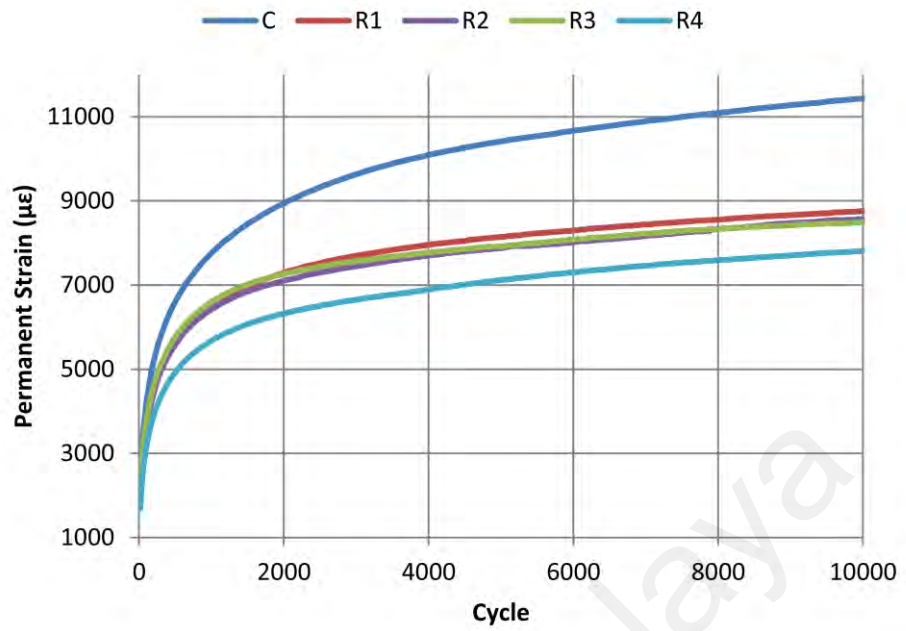
(Level A)
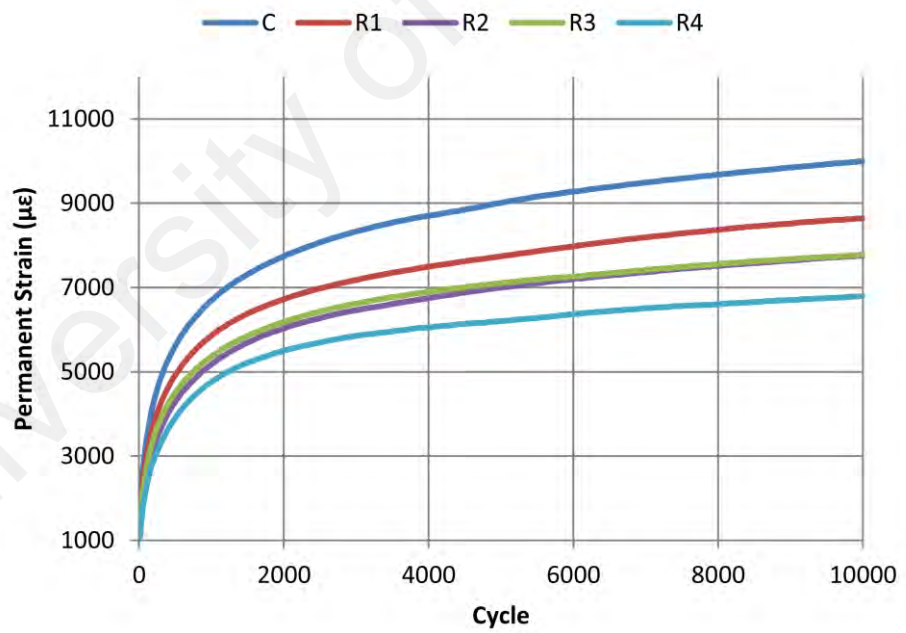
(Level B)

Figure 4.19: Creep curves of tested mixtures including reinforced and control specimens

The application of fibreglass grids at the mid-depth of the specimens of asphalt concrete, notably increased their resistance to permanent deformation over that of the unreinforced specimens at both ―level A‖ and ―level B‖ load to rest ratios. Moreover, as can be seen from Figure 4.19, the specimens reinforced by fibreglass grids with greater tensile strength and greater mesh size (R4) showed the lowest permanent deformation throughout all the cycles conducted in this study.

Figure 4.19 also clearly shows that the control (unreinforced) specimens had substantially higher permanent deformation and accumulation rates of permanent deformation than the reinforced ones – due presumably to the tensile forces and lateral confinement provided by the grids.

A further important finding is that the specimens of identical mesh size reinforced by grids of lower tensile strength experienced more permanent deformation than those reinforced by grids with a higher tensile strength. Furthermore, the difference between the permanent deformations in specimens reinforced with large mesh size was higher than for specimens reinforced with smaller mesh size grids. In other words, increasing the tensile strength of grids with a large mesh size had a greater impact on their ability to resist permanent deformation than such increase in small mesh size grids within the test conditions performed in this study. However, such impact in ―Level B‖is not as remarkable as it in ―Level A‖. In addition, by applying 10000 loading cycles in this experiment, we found that larger permanent deformation occurred in specimens with small rather than large mesh sizes, regardless of whether they had high or low tensile strength grids (Figure 4.19).

Table 4.8 illustrates the results of a quantitative comparison between the measured permanent strain and grid tensile strength and grid opening size respectively, during the last loading cycle of the tests carried out in this study. In this table, reinforced specimens with the same size of opening (mesh) are compared in terms of their grid

tensile strength, and those with the same tensile strength in terms of their grid opening size. The improvements in resistance to permanent deformation shown in Table 4.8 were all determined based on the permanent deformation of the control specimens. The clear conclusion from Table 4.8 is that, based on testing through 10000 cycles, specimens reinforced by grids with greater tensile strength and with larger mesh size achieve the best performance at both levels of A and B.

Table 4.8: Comparison of permanent strains in the last cycle

Specimen code	Tensile strength (kN/m) (MD ×XD)	Grid meah size (mm) Center to center of strand)	Measured last cycle permanent strain (µε)	Improved permanent strain resistance compared to control specimen (%)	Measured last cycle permanent strain (µε)	Improved permanent strain resistance compared to control specimen (%)
			Level A		Level B	
C	-	-	11438	0	9993	0
R1	115×115[*L] +/- 15	12.5×12.5[**S]	8756	31	8647	16
R2	115×115[*L] +/- 15	25 ×25[**OL]	8564	34	7752	29
R3	115×215[*H] +/- 15	12.5×12.5[**S]	8495	35	7783	28
R4	115×215[*H] +/- 15	25 × 19[**OL]	7819	46	6793	47

[*L]: Low level for grid tensile strength   [**S]: Small level for grid opening size

[*H]: High level for grid tensile strength   [**OL]: Large level for grid opening size

In can also be seen from Table 4.8 that increasing the tensile strength in specimens with small grid openings from R1 to R3 leads to a 4% and 12% improvement in permanent strain resistance by the last loading cycle, respectively at level A and B. However, doing the same thing with grids with a large grid opening size from R2 to R4 leads to a 12% and 18% improvement, ie three times as much in level A.

Conversely, comparing the specimens with grids of the same tensile strength, but different size of opening (mesh), it emerges that in specimens with low tensile strength

grids, an increase in grid opening size from small to large (R1 to R2) leads to a 3% and 13% improvement in permanent strain resistance in level A and B, respectively; while doing the same (R3 to R4) with specimens with grids of high tensile strength grids leads to a much larger, 11% and 19% increase in such resistances, ie more than three times as much in level A.

In a research studying the shear behaviour of bi-layer asphalt concrete specimens, geogrid reinforced specimens showed less interlayer shear resistance than unreinforced ones, even though some of the geogrid surface coatings were found to be able to maximise bonding between the interlayer and asphalt concrete (Ferrotti et al., 2012). It may be, therefore, concluded that the effects of the smaller mesh size observed in the current testing condition of this study were due to reduced bonding between the lower and upper lift of the asphalt concrete, leading to the development of higher shear deformation. Comparing the specimens reinforced by small mesh grids and the control ones, it should be noted that, although the bonding of two lifts was important in the reinforced specimens, the reinforcing effect of the grid was much more significant than its effect on the bonding condition of the lifts; the upper and lower lifts in fact remained in full contact in the control specimens. It can likewise be seen that the more the tensile strength increases, the greater the effect of mesh size on strength and resistance.

It can be observed in Table 4.8 that the enhancement in permanent deformation resistance by fibreglass grid reinforcement at load to rest ratio B (500 ms loading time and 1500 ms rest time) is less than that of load to rest ratio A, and only the enhancements in specimen R4 at two load to rest ration are comparable. However, at load to rest ratio B at which the loading time is smaller and resting time is longer, logically such enhancements by grid must not be at least less than those at larger load to rest ratio. Thus, it may be concluded that load to rest ratio B is not suitable for the

current testing condition and materials. Thus, the results of load to rest ratio A is only considered for creep curve modelling in the next section.

In sum, if we look merely at the accumulated permanent strain up to the last cycle of the creep test conducted in this work, this leads to the conclusion that not only increasing the tensile strength, but also enlarging the mesh size of glass grid reinforced asphalt concrete can increase its resistance to permanent deformation. However, it should be noted that the flow point was not reached in the performed test conditions, and that closer investigation of the creep curves after model fitting resulted in rather inferences from the ones drawn in this section. .

4.4.2 Fitted Models Comparison

Unfortunately, none of tested specimens reached the third phase of the creep curve in the course of the 10000 loading cycles conducted in this experiment. Also, it was concluded in the previous section that rest time ratio 3 (Level B) may not be suitable for current test condition and materials. As a results, only the primary and secondary phases of rest ratio 1 (level A) was modelled; the two regions for which Ahari's model was developed. Table 4.9 presents the results of mathematical functions and estimated permanent strains at the boundary points at the last cycle for each phase of testing specimens. Based on Figures 4.20 - 4.22, and the coefficients of determination in Table 4.9, it can be seen that the fitted models, both for the logarithmic and linear regions, fit acceptably with the measured creep curves. Thus, it can be concluded that Ahari's model is suitable for modelling the primary and secondary regions of the creep curve for both the fibreglass grid reinforced specimens and unreinforced hot mix asphalt specimens. The slopes of both the primary and secondary regions are important, particularly the secondary region generally known as the creep rate. In Ahari's proposed model, a ―linear logarithmic model‖ is utilised to model the primary region of the creep curve as shown bellow:

$$y = a + b(\ln(x)) \hspace{4cm} \text{Equation (4.1)}$$

b is the ratio of absolute change in y to the relative change in x. In other words, if x changes by 1%, then the absolute change in y is $0.01b$ unit (Thomas et al., 2001). However, the slope of the primary region is not as important as that of the secondary region. In our study, the slope of the fitted curve in the primary and secondary regions was determined for each individual specimen type. The extend of improvement for each (in terms of smaller permanent strain accumulation rates) was then determined based on the control specimen. These results are shown in Table 4.10. It is worth noting that the control specimens in this table have their maximum slopes in both primary and secondary regions of the creep curves.

Table 4.9 Creep curve models based on Ahari's model and estimated critical values

| Code | First stage model | End of first stage | | | Second stage model | Last cycle | | |
		Cycle (N)	ε_p (modeled)	Improved ε_p compared to control specimen (%)		Cycle (N)	ε_p (modeled)	Improved ε_p compared to control specimen (%)
C_A	$\varepsilon_p = 1523.945\,Ln(N) - 2653.456$ $R^2 = 0.9842$	7072	10863	0	$\varepsilon_p = 0.2155(N - 7072) + 9346.539$ $R^2 = 0.9913$	10000	11502	0
R1_A	$\varepsilon_p = 1114.477\,Ln(N) - 1226.826$ $R^2 = 0.9927$	3945	8001	36	$\varepsilon_p = 0.1336(N - 3945) + 7474.168$ $R^2 = 0.9864$	10000	8810	31
R2_A	$\varepsilon_p = 1075.835\,Ln(N) - 1099.156$ $R^2 = 0.9893$	3223	7592	43	$\varepsilon_p = 0.1515(N - 3223) + 7103.268$ $R^2 = 0.9957$	10000	8618	33
R3_A	$\varepsilon_p = 1062.883\,Ln(N) - 843.671$ $R^2 = 0.9902$	3001	7666	42	$\varepsilon_p = 0.1291(N - 3001) + 7278.914$ $R^2 = 0.9824$	10000	8570	34
R4_A	$\varepsilon_p = 954.627\,Ln(N) - 980.730$ $R^2 = 0.9918$	4847	7120	53	$\varepsilon_p = 0.1436(N - 4847) + 6424.536$ $R^2 = 0.9868$	10000	7860	46

Note: _A: Level A,

ε_p: Pemanent strain,

R^2: Coefficient of determination

Table 4.10: Primary and secondary regions' slope comparison

			Primary region		Secondary region	
Code	Tensile strength (kN/m) (MD ×XD)	Grid meah size (mm) Center to center of strand)	Slope	Improved slope compared to control specimen (%)	Slope	Improved slope compared to control specimen (%)
C_A	-	-	1523.9	0	0.2155	0
R1_A	$115 \times 115^{*L}$ +/- 15	$12.5 \times 12.5^{**S}$	1114.5	37	0.1336	61
R2_A	$115 \times 115^{*L}$ +/- 15	$25 \times 25^{**OL}$	1075.8	42	0.1515	42
R3_A	$115 \times 215^{*H}$ +/- 15	$12.5 \times 12.5^{**S}$	1062.9	43	0.1291	67
R4_A	$115 \times 215^{*H}$ +/- 15	$25 \times 19^{**OL}$	954.63	60	0.1436	50

^{*L}: Low level for grid tensile strength ^{**S}: Small level for grid opening size

^{*H}: High level for grid tensile strength ^{**OL}: Large level for grid opening size
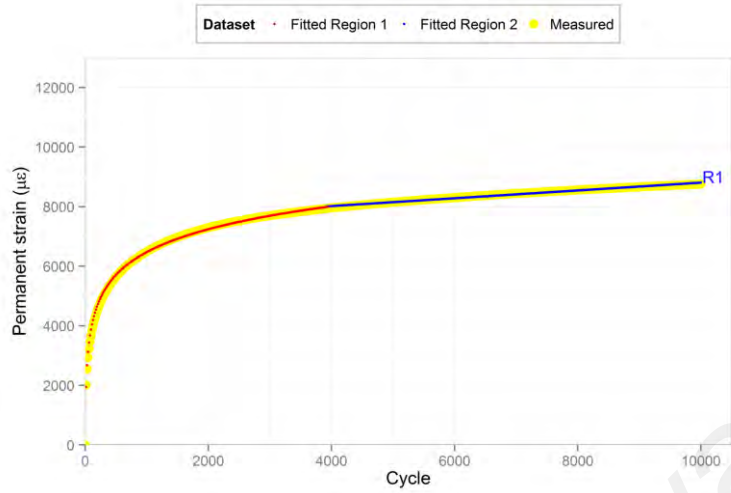
Figure 4.20: Measured and estimated permanent deformation for R1 specimen
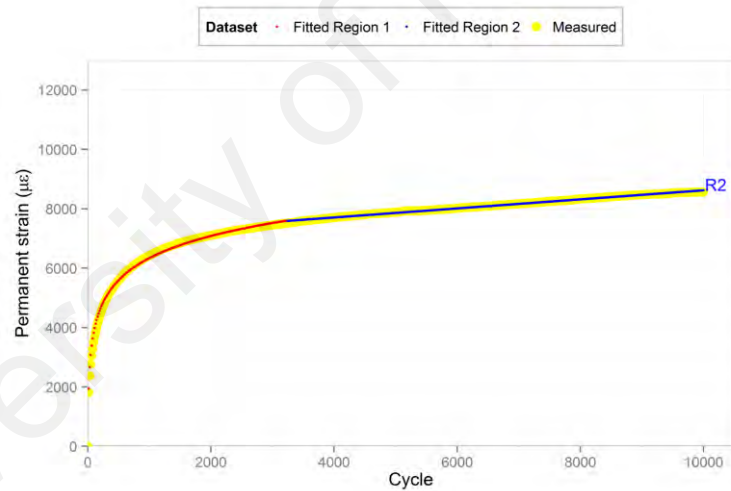
Figure 4.21: Measured and estimated permanent deformation for R2 specimen
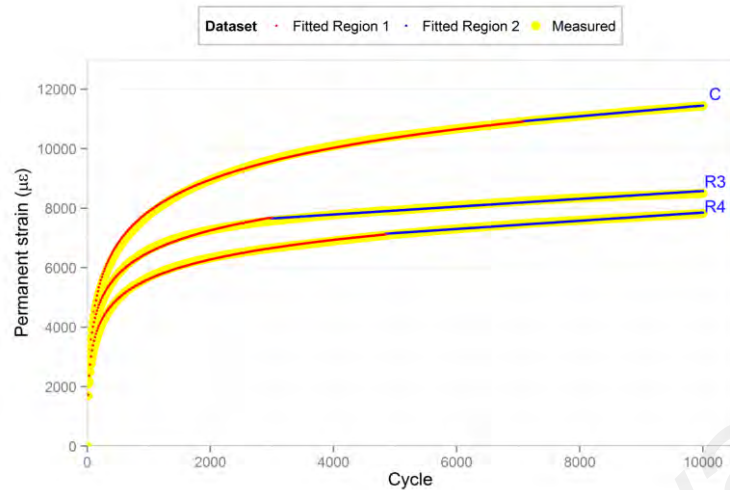
Figure 4.22: Measured and estimated permanent deformation for C, R3, & R4 specimens

Figure 4.23 is a one-to-one graph of the measured versus estimated values of permanent strain in the last cycle, including the intercept, slope and correlation coefficients. Comparing the measured and estimated permanent strain in the last cycle for each type of specimen (Figure 4.23) and the improvements in the reinforced specimens in Tables 4.9 and 4.10 as well as in Figure 4.20 - 4.22, it can be seen that the measured and estimated values were rather close to each other. We therefore, used the fitted curves from the measured values to find the turning point between the primary and secondary regions of the creep curves.
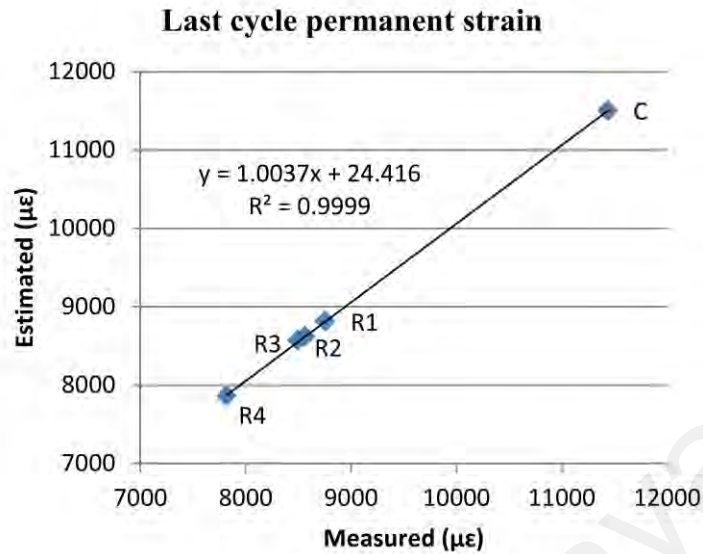
Figure 4.23: One-to one graph of measured vs. estimated permanent strain of last cycle (Level A load to rest ratio)

When only the creep curves (as shown in Figure 4.19) are taken into account, this pointed to the conclusion that enlarging the grid mesh size at the same level of tensile strength leads to better performance (resistance) within the used grids in this study. However, it can be seen from Table 4.10 that enlarging the mesh size has the effect of increasing the secondary region slope - something which does not emerge from just looking at the creep curves. In the secondary region, in which the mixture has reached to an optimum density level (Mehta et al., 2014), the presence of steeper slopes for grids with a larger mesh size but with the same tensile strength may be due to there being a lower number of grid junctions on the grid applied area. In other words, the number of stripes or threads of grid per unit area of the specimen increases as the size of the opening (mesh) is reduced, leading to greater structural and dimensional stability through the higher number of grid junctions. This could possibly explain the smaller slope in the secondary region of the creep curve.

In sum, looking at the effects of the mesh size of grids on a combination of permanent deformation and creep rate, the results suggest that larger mesh size grids performed better only in the initial stages of loading, whereas over the longer term, smaller mesh size grids will outperform large ones with same the tensile strength. These results showing small gird mesh sizes to perform better than large ones with the same tensile strengths are similar to those reported by some previous studies (Jenkins et al., 2004, September; Komatsu et al., 1998).

4.5 Summary of the Chapter

This chapter presented the testing results and data analysis of the study. Each of the objectives was investigated by analysing the relevant test results. Furthermore, the modelling part and related analysis were also presented. The chapter concluded with a comparison and discussion of each set of results.

CHAPTER 5: CONCLUSION AND FUTURE RECOMMENDATIONS

5.1 Conclusions

Using appropriate specimens prepared in a laboratory, testing methods and testing conditions, this study examined the characteristics of fibreglass geogrid reinforced asphalt concrete at two levels (high and low) of grid tensile strength and two levels (large and small) of grid opening size. This led to the following conclusions for each of the study objectives outlined in Chapter 1.

Objective 1 (Master Curve Construction)

Objective 1 was: *To construct master curves for unreinforced and fibreglass grid reinforced asphalt concrete specimens and investigate the effects of the grids on these curves..*

Asphalt concrete is a material with non-homogenous and viscoelastic behaviour that varies depending on factors such as temperature and loading frequency. The dynamic modulus is the absolute value of the complex modulus, which is calculated by dividing the maximum (peak-to-peak) stress by the recoverable (peak-to-peak) axial strain for a material. In this study, the dynamic modulus of all the specimens, including both unreinforced and fibreglass grid reinforced specimens, was determined through bending beam apparatus.

Thereafter, by constructing master curves at the reference temperature of 20℃ for each specimen type, Objective 1 was accomplished. However, by extending the constructed S-curve of the specimens to lower reduced frequencies as well as applying parameters based on the Witczak dynamic modulus model and WLF equation, we found that unlike the insignificant difference among the S-curve's upper asymptotes for different types of specimens there are big differences both among the inflection points

of the constructed curves, and among the lower asymptotes of those curves. Furthermore, the specimens reinforced with small mesh size grids displayed higher dynamic moduli than the large mesh size grids at the relevant lower asymptotes and inflection points. The same was true of the high tensile strength grids.

This suggests that, at the conditions used in this study, not only is the fibreglass grid tensile strength effective in increasing the dynamic modulus of asphalt concrete beam specimens at very low frequencies, but grid mesh size is also of considerable importance.

Objective 2 (Damage Recovery Ability of Geogrid)

Objective 2 was: *To investigate the influence of utilised fibreglass grids on the damage recovery ability of the specimens.*

To achieve this research objective, a four-point bending test apparatus was used. True healing of the tested material could not be obtained, because the time-dependent linear viscoelastic effects and non-linearity of asphalt concrete, as a viscoelastic material, could not be eliminated from the recovered stiffness. The indices obtained in this study do not therefore represent the real healing ability, but rather the damage recovery ability of the asphalt concrete specimens.

The healing phenomenon is an important factor affecting the predicted life of asphalt concrete materials. Indeed, asphalt concrete recovery is one of the main contributory factors to pavement (road surface) life prediction.

The application of sinusoidal loads in the flexural testing apparatus causes microcracks to appear at both the top and bottom of the beams. We therefore located the grids at mid-depth of the beam specimens – to provide similar conditions in terms of damage evolution at both the top and bottom lifts of the asphalt concrete beams.

In our second objective, we investigated the possible effects of geogrids applied to asphalt concrete in terms of damage recovery capability of asphalt concrete. The damage recovery ability of the material was measured in two phases, via damage recovery indices.

In Phase I, an interrupted fatigue test was utilised, with rest times of 2, 4 and 8 minutes being applied randomly after certain amounts of stiffness reduction, only the specimens with small mesh size geogrids displayed recovery of damage after rest periods. Furthermore, among the small mesh size grids, the higher tensile strength fibreglass grids showed greater damage recovery than the low tensile strength ones. Meanwhile, there were no significant differences between the other three types of specimens.

In Phase II, the specimens were given a 32-minute rest period at certain levels of damage during which time the recovery (if any) of the beam specimens was determined after 2, 4, 8, 16, and finally 32 minutes, respetively, through applying very low load levels so as not to cause any more damage, the results showed no significant differences in terms of healing.

Objectives 3 & 4 (Dynamic Creep Test and Creep Curve Modelling)

Objective 3 was: *To determine the separate and combined effects of fibreglass grid tensile strength and aperture size in improving the resistance to permanent deformation of unreinforced and fibreglass grid reinforced asphalt concrete specimens, and*

Objective 4 was: *To model the achieved regions of the creep curves for both unreinforced and fibreglass grid reinforced asphalt concrete specimens, and to estimate the behaviour of the primary and secondary regions and the corresponding boundary points.*

To achieve the objective 3 and 4, the dynamic creep test was conducted using a uniaxial cyclic compression test with the confinement method. Unfortunately, none of tested specimens reached the third phase of the creep curve in the course of the 10000 loading cycles conducted in this experiment. As a results, only the primary and secondary phases could be modelled; the two regions for which Ahari's model was developed.

Our results suggest that fibreglass grid reinforcement is remarkably effective in lowering the permanent deformation of asphalt concrete, probably due to the tensile forces and lateral confinement provided by such grids, at both ratios.

Secondly, our study confirms that Ahari's creep curve model can be used with both fibreglass grid reinforced, and unreinforced hot mix asphalt. In the secondary region of the creep curves, in which the optimum density of the mixture is achieved, higher tensile strengths and smaller mesh size result in gentler slope (meaning a lower permanent strain accumulation rate).

Another conclusion from our results is that increasing the tensile strength of a fibreglass grid can lead to a reduction in permanent strain, depending on the type of grid used. Moreover, not only is the tensile strength of a fibreglass gird effective in increasing the resistance of asphalt concrete to permanent deformation, but the mesh size of the grid is also of considerable importance. Our results suggests that, of the grid mesh sizes used in this study, larger mesh size fibreglass grids perform better than small ones only in the initial stages of loading. This is because enlarging the mesh size causes the creep rate to increase which eventually, in the longer terms, outweighs the smaller deformation achieved in the first stages of the creep curve.

In conclusion, the range of dynamic creep experiments we carried out suggests that smaller mesh sizes should provide more resistance to permanent deformation in the long

run. This could be due to the greater number of fibres per unit width in such smaller meshes than in the larger mesh geogrids. This finding that the best resistance to permanent deformation can be achieved by asphalt concrete reinforced grids with greater tensile strength but also with smaller mesh sizes is in line with what previous researchers have reported. Better performance of small mesh size and/or high tensile strength of the fibreglass grid reinforced specimens used in this study are similar to what observed in the results of objective one in terms of having larger dynamic moduli at low frequencies and high temperatures.

Finally, our study shows that interpreting creep curves without creep rate consideration can be misleading when the tertiary region of creep curves is not achieved in tests.

5.2 Recommendations for Future Studies

In this study, only one type of mixture with a certain aggregate gradation was used: the nominal maximum aggregate size was 9.5mm and the air void was 8% for all of the specimens. Moreover, the fibreglass grid was applied at one depth of the asphalt concrete. Further research would be useful on other types of mixture and with different target air voids (e.g. 4%); as well as testing the asphalt concrete with grids applied at different depths.

Second, in terms of performance of fibreglass grids concluded from master curves, it must be noted that four-point bending test is a non-homogeneous test. It would be helpful to try using a homogeneous test instead.

Finally, future research applying other types of damage recovery measurement to the viscoelastic properties of asphalt concrete would also be useful. Furthermore, by evaluating the damage recovery ability of more variable types of geogrids laid in different kinds of mixtures in various testing conditions a damage recovery index range can be suggested to be used for justification of using geogrids in flexible pavements. In addition, aggregate structural image analysis of the specimens (e.g. using X-ray computed tomography) can be helpful in order to investigate more in terms of mechanism of damage recovery in small mesh size grid reinforced specimens.

REFERENCES

AASHTO, S. T. (2007). Standard method of test for determining the fatigue life of compacted hot-mix asphalt (HMA) subjected to repeated flexural bending, *American Association of State and Highway Transportation Officials, Washington, DC.*

Abtahi, S., Sheikhzadeh, M., & Hejazi, S. (2009). Fiber-reinforced asphalt-concrete-A review. *Construction and Building Materials, 24*(6), 871-877.

Ahari, A. S., Forough, S. A., Khodaii, A., & Moghadas Nejad, F. (2013). Modeling the primary and the secondary regions of creep curves for SBS modified asphalt mixtures under dry and wet conditions. *Journal of Materials in Civil Engineering, 26*(5), 904–911.

Al-Qadi, I., Dessouky, S., Kwon, J., & Tutumluer, E. (2008). Geogrid in flexible pavements: Validated mechanism. *Transportation Research Record: Journal of the Transportation Research Board, 2045*, 102-109.

Alataş, T., Yılmaz, M., & Kök, B. V. (2012). Comparison of permanent deformation and fatigue resistance of hot mix asphalts prepared with the same performance grade binders. *Construction and Building Materials, 30*, 66-72.

Amini, F. (2005). Potential applications of paving fabrics to reduce reflective cracking (No. FHWA/MS-DOT-RD-05-174). Jackson State University.

Anderson, D. A., Christensen, D. W., & Bahia, H. (1991). Physical properties of asphalt cement and the development of performance-related specifications. *Journal of the Association of Asphalt Paving Technologists, 60*.

ASTM D3515-00 (2000a). Standard specification for hot-mixed,hot-laid bituminous paving mixtures, *ASTM International, West Conshohocken, PA, www.astm.org.*

ASTM D8-00 (2000b). Standard terminology relating to materials for roads and pavements, *ASTM Intrnational, West Conshohocken, PA, www.astm.org.*

ASTM D2726-00 (2000c). Standard test method for bulk specific gravity and density of non-absorptive compacted bituminous mixtures, *ASTM Intrnational, West Conshohocken, PA, www.astm.org.*

ASTM C215-00 (2000d). Standard test method for fundamental transverse, longitudinal, and torsional resonant frequencies of concrete specimens, *ASTM International, West Conshohocken, PA, www.astm.org.*

ASTM D3203-00 (2000e). Standard test method for percent air voids in compacted dense and open bituminous paving mixtures, *ASTM Intrnational, West Conshohocken, PA, www.astm.org.*

ASTM D4439-00 (2000f). Terminology for geosynthetics, *ASTM International, West Conshohocken, PA, www.astm.org.*

ASTM D2041-00 (2000g). Theoretical maximum specific gravity and density of bituminous paving mixtures, *ASTM International, West Conshohocken, PA, www.astm.org.*

Austin, R., & Gilchrist, A. (1996). Enhanced performance of asphalt pavements using geocomposites. *Geotextiles and Geomembranes, 14*(3), 175-186.

Baek, J., & Al-Qadi, I. (2008). Mechanism of overlay reinforcement to retard reflective cracking under moving vehicular loading. In *RILEM International Conference on Cracking in Pavements (6th: 2008: Chicago, Ill.).*

Barksdale, R. D. (1972, September). Laboratory evaluation of rutting in base course materials. In *Third International Conference on the Structural Design of Asphalt Pavements, Grosvenor House, Park Lane, London, England. (Vol. 1. No. Proceeding)*, (1).

Barksdale, R. D. (1991). *Fabrics in asphalt overlays and pavement maintenance* 171.

Bazin, P., & Saunier, J. (1967, January). Deformability, fatigue and healing properties of asphalt mixes. In *Intl Conf Struct Design Asphalt Pvmts*.

Bennert, T. A. (2009). Dynamic modulus of hot mix asphalt (No. FHWA-NJ-2009-011).

Berg, R. R., Christopher, B. R., & Perkins, S. (2000). Geosynthetic reinforcement of the aggregate base/subbase courses of pavement structures (No. GMA White Paper II).

Bertuliene, L., Oginskas, R., & Bulevicius, M. (2011, May). Research of rut depth in asphalt pavements reinforced with geosynthetic materials. In *Proceedings of the 8th International Conference Environmental Engineering*, *Lithuania*.

Bohuslav, T. R. (2008). Pavement design guide, *Texas Department of Transportation*.

Bonnaure, F., Huibers, A., & Boonders, A. (1982). A laboratory investigation of the influence of rest periods on the fatigue characteristics of bituminous mixes. *Journal of the Association of Asphalt Paving Technologists, 51*, 104-128.

Bonnaure, F., Huibers, A., & Boonders, A. (1983). Etude en laboratoire de l'influence des temps de repos sur les caractéristiques de fatigue des enrobés bitumineux. *REV GEN ROUTES AERODR,* (595).

Brown, S., Thom, N., & Sanders, P. (2001). A study of grid reinforced asphalt to combat reflection cracking (with discussion). *Journal of the Association of Asphalt Paving Technologists, 70*.

Button, J., & Lytton, R. (2007). Guidelines for using geosynthetics with hot-mix asphalt overlays to reduce reflective cracking. *Transportation Research Record: Journal of the Transportation Research Board, 2004*(1), 111-119.

Canestrari, F., Belogi, L., Ferrotti, G., & Graziani, A. (2015). Shear and flexural characterization of grid-reinforced asphalt pavements and relation with field distress evolution. *Materials and Structures, 48*(4), 959-975.

Carpenter, S., & Shen, S. (2006). Dissipated energy approach to study hot-mix asphalt healing in fatigue. *Transportation Research Record: Journal of the Transportation Research Board, 1970*, 178-185.

Castro, M., & Sánchez, J. A. (2006). Fatigue and healing of asphalt mixtures: discriminate analysis of fatigue curves. *Journal of transportation engineering, 132*(2), 168-174.

Chang, D., Ho, N., Chang, H., & Yeh, H. (1999). Laboratory and case study for geogrid-reinforced flexible pavement overlay. *Transportation Research Record: Journal of the Transportation Research Board, 1687*, 125-130.

Chehab, G., Kim, Y., Schapery, R., Witczak, M., & Bonaquist, R. (2002). Time-temperature superposition principle for asphalt concrete with growing damage in tension state. *Journal of the Association of Asphalt Paving Technologists, 71*.

Christensen, D. W., & Anderson, D. A. (1992). Interpretation of dynamic mechanical test data for paving grade asphalt cements (with discussion). *Journal of the Association of Asphalt Paving Technologists, 61*.

Collin, J., Kinney, T., & Fu, X. (1996). Full scale highway load test of flexible pavement systems with geogrid reinforced base courses. *Geosynthetics International, 3*(4), 537-549.

Cominsky, R., Killingsworth, B., Anderson, R., Anderson, D., & Crockford, W. (1998). Quality control and acceptance of superpave-designed hot mix asphalt (No. Project D9-7 FY'93) *NCHRP Report 409*. Washington, DC., USA.

Daniel, J., & Kim, Y. (2001). Laboratory evaluation of fatigue damage and healing of asphalt mixtures. *Journal of Materials in Civil Engineering, 13*(6), 434-440.

De La Roche, C. (1996). *Module de rigidité et comportement en fatigue des enrobés bitumineux: expérimentations et nouvelles perspectives d'analyse* (Doctoral dissertation), École Central de Paris, Paris, France.

Doucet, F., & Auger, B. (2010). Complex Modulus Determination of Asphalt Mixes at the Ministère des Transports du Québec (No. RTQ-10-01).

Dougan, C. E., Stephens, J., Mahoney, J., & Hansen, G. (2003). E*-Dynamic modulus: Test protocol-problems and solutions (No. CT-SPR-0003084-F-03-3).

Elseifi, M. A., & Al-Qadi, I. L. (2004). A simplified overlay design model against reflective cracking utilizing service life prediction. *Road Materials and Pavement Design, 5*(2), 169-191.

EN_CEN 12697-33 (2003). Bituminous mixtures. Test methods for hot mix asphalt. Part 33: Specimen prepared by roller compactor, *Comité Européen de Normalisation.*

EN_CEN 12697-26 (2004). Bituminous mixtures - Test methods for hot mix asphalt Part 26: Stiffness, *Comité Européen de Normalisation.*

EN_CEN 12697-25 (2005). Bituminous mixtures - Test methods for hot mix asphalt Part 25: Cyclic compression test, *Comité Européen de Normalisation.*

Ferrotti, G., Canestrari, F., Pasquini, E., & Virgili, A. (2012). Experimental evaluation of the influence of surface coating on fiberglass geogrid performance in asphalt pavements. *Geotextiles and Geomembranes, 34*, 11-18.

Francken, L., & Clauwaert, C. (1987, July). Characterization and structural assessment of bound materials for flexible road structures. In *Proceedings 6th International Conference on the Structural Design of Asphalt Pavements*, *Ann Arbor* 130-144.

Francken, L., & Verstraeten, J. (1998). Interlaboratory test program on complex modulus and fatigue (No. RILEM REPORT) 181-216.

Fwa, T., Tan, S., & Zhu, L. (2004). Rutting prediction of asphalt pavement layer using C-ɸ model. *Journal of transportation engineering, 130*(5), 675-683.

Gabra, R., & Horvli, I. (2006). *Simplified testing method for evaluation of asphalt mixtures for their susceptibility to permanent deformation*. *Unpublished manuscript*. Retrieved from: www.nvfnorden.org

Goodrich, J. L. (1991). Asphaltic binder rheology, asphalt concrete rheology and asphalt concrete mix properties (with discussion). *Journal of the Association of Asphalt Paving Technologists, 60*.

Grabowski, W., & Pozarycki, A. (2008). Energy absorption in large dimension asphalt pavement samples reinforced with geosynthetics. *Foundations of Civil and Environmental Engineering,* (11), 17-28.

Halim, A., Haas, R., & Phang, W. (1983). Geogrid reinforcement of asphalt pavements and verification of elastic theory. *Transportation Research Record: Journal of the Transportation Research Board,* (949), 55–65.

Hayton, B. (1998). Bitumen rheology and the bohlin dynamic shear rheometer. *Scott Wilson Pavement Engineering*, 1-13.

Hongu, T., & Philips, G. (1990). New fibers Ellis Horwood series in polymer science and technology, *New York, Springer*.

Hosseini, H., Darban, A., & Fakhri, K. (2009). The effect of geosynthetic reinforcement on the damage propagation rate of asphalt pavements. *Scientia Iranica*, 26-32.

Huang, Y. H. (1993). *Pavement analysis and design*.

Hufenus, R., Rueegger, R., Banjac, R., Mayor, P., Springman, S., & Brönnimann, R. (2006). Full-scale field tests on geosynthetic reinforced unpaved roads on soft subgrade. *Geotextiles and Geomembranes, 24*(1), 21-37.

Jacobs, M. M. J. (1995). *Crack growth in asphaltic mixes*, Delft University of Technology, Netherlands.

Jenkins, K. J., Dennison, P., Ebels, L. J., & Mullins, L. S. (2004, September). 3-D polymer grid reinforcement of asphalt for rut resistance. In *Proceedings of the 8th Conference on Asphalt Pavements for Southern Africa (CAPSA'04)*.

Jiang, H., Wu, S., Qiu, J., & Wei, W. (2010). Self healing asphalt concrete-state of the art. *Journal of Wuhan University of Technology, 32*(17), 67-70.

Kaloush, K., & Witczak, M. (2002). Tertiary flow characteristics of asphalt mixtures (with discussion and closure). *Journal of the Association of Asphalt Paving Technologists, 71*, 248-280.

Kaloush, K. E., Witczak, M. W., Way, G. B., Zborowski, A., Abojaradeh, M., & Sotil, A. (2002). Performance evaluation of Arizona asphalt rubber mixtures using advanced dynamic material characterization tests (No. Final Report).

Kalyoncuoglu, S., & Tigdemir, M. (2011). A model for dynamic creep evaluation of SBS modified HMA mixtures. *Construction and Building Materials, 25*(2), 859-866.

Kandhal, P. S., & Chakraborty, S. (1996). Evaluation of voids in the mineral aggregate for HMA paving mixtures (No. 96-4) 78-101.

Kausch, H., Petrovska, D., Landel, R., & Monnerie, L. (1987). Intermolecular interaction in polymer alloys as studied by crack healing. *Polymer Engineering & Science, 27*(2), 149-154.

Kenis, W. J. (1978). Predictive design procedures, VESYS users manual (No. FHWA-RD-77-154).

Khodaii, A., Fallah, S., & Moghadas Nejad, F. (2009). Effects of geosynthetics on reduction of reflection cracking in asphalt overlays. *Geotextiles and Geomembranes, 27*(1), 1-8.

Khodaii, A., & Mehrara, A. (2009). Evaluation of permanent deformation of unmodified and SBS modified asphalt mixtures using dynamic creep test. *Construction and Building Materials, 23*(7), 2586-2592.

Kim, B., & Roque, R. (2006). Evaluation of healing property of asphalt mixtures. *Transportation Research Record: Journal of the Transportation Research Board,* (1970), 84-91.

Kim, K., Doh, Y., & Lim, S. (1999). Mode I reflection cracking resistance of strengthened asphalt concretes. *Construction and Building Materials, 13*(5), 243-251.

Kim, Y.-R., Little, D., & Lytton, R. (2003). Fatigue and healing characterization of asphalt mixtures. *Journal of Materials in Civil Engineering, 15*(1), 75-83.

Kim, Y., & Park, T. S. (2013). Reinforcement of recycled foamed asphalt using short polypropylene fibers. *Advances in Materials Science and Engineering, 2013*.

Kim, Y., Whitmoyer, S., & Little, D. (1994). Healing in asphalt concrete pavements: Is it real? *Transportation Research Record,* (1454).

Kim, Y. R. (2009). *Modeling of asphalt concrete*: McGraw-Hill Professional.

Kim, Y. R., & Lee, Y.-C. (1995). Interrelationships among stiffnesses of asphalt-aggregate mixtures (with discussion). *Journal of the Association of Asphalt Paving Technologists, 64.*

Kim, Y. R., Little, D. N., & Benson, F. C. (1990). Chemical and mechanical evaluation on healing mechanism of asphalt concrete (with discussion). *Journal of the Association of Asphalt Paving Technologists, 59.*

Komatsu, T., Kikuta, H., Tuji, Y., & Muramatsu, E. (1998). Durability assessment of geogrid-reinforced asphalt concrete. *Geotextiles and Geomembranes, 16*(5), 257-271.

Kutay, M., Gibson, N., & Youtcheff, J. (2008). Use of pseudostress and pseudostrain concepts for characterization of asphalt fatigue tests. *Chapter 30, pavement cracking: mechanisms, modeling, detection, testing and case histories*, 305-314.

Laurinavičius, A., & Oginskas, R. (2006). Experimental research on the development of rutting in asphalt concrete pavements reinforced with geosynthetic materials. *Journal of civil engineering and management, 12*(4), 311-317.

Lee, K. W., Gundapuneni, S. K., & Singh, A. (2010). Effects of asphalt binder grade on the performance of Rhode island hot-mix asphalt (No. FHWA-RIDOT-RTD-09–2).

Leshchinsky, B., & Ling, H. (2012). Effects of geocell confinement on strength and deformation behavior of gravel. *Journal of geotechnical and geoenvironmental engineering, 139*(2), 340-352.

Ling, H., & Liu, Z. (1999). Performance of geosynthetic-reinforced asphalt pavements. *Journal of geotechnical and geoenvironmental engineering, 127*(2), 177.

Ling, H. I., & Liu, Z. (2001). Performance of geosynthetic-reinforced asphalt pavements. *Journal of geotechnical and geoenvironmental engineering, 127*(2), 177-184.

Little, D., Lytton, R., Williams, D., & Chen, C. (2001). Microdamage healing in asphalt and asphalt concrete, Volume I: Microdamage and microdamage healing, Project summary report (No. FHWA-RD-98-141).

Little, D., Lytton, R., Williams, D., Chen, C., Kim, Y., & Lee, H. (1998). Fundamental properties of asphalts and modified asphalts—task K: microdamage healing in asphalt and asphalt concrete. *FHWA Final Report, 1*.

Little, D. N., Lytton, R. L., Chairl, B., Williams, D., & Kim, Y. R. (1998). An analysis of the mechanism of microdamage healing based on the application of micromechanics first principles of fracture and healing.

Liu, Q. (2012). *Induction healing of porous asphalt concrete* (Doctoral dissertation, Delft University of Technology).

Luo, X. (2012). *Characterization of fatigue cracking and healing of asphalt mixtures*, (Doctoral dissertation, Texas A&M University).

Lytton, R. (1989). Use of geotextiles for reinforcement and strain relief in asphalt concrete. *Geotextiles and Geomembranes, 8*(3), 217-237.

Lytton, R. L., Uzan, J., Fernando, E. G., Roque, R., Hiltunen, D., & Stoffels, S. M. (1993). Development and validation of performance prediction models and specifications for asphalt binders and paving mixes (Vol. 357) (No. SHRP-A-357).

M. Signore, J. (2012). Long-life pavements concepts and lab testing. http://slideplayer.com/slide/3426070/

Mahrez, A., Karim, M., & Katman, H. (2003). Prospect of using glass fiber reinforced bituminous mixes. *Journal of the Eastern Asia Society for Transportation Studies, 5*, 794-807.

Mahrez, A., Karim, M. R., & Katman, H. (2005). Fatigue and deformation properties of glass fiber reinforced bituminous mixes. *Journal of the Eastern Asia Society for Transportation Studies, 6*, 997-1007.

Majidzadeh, K., Aly, M., Bayomy, F., & El-Laithy, A. Implementation of a pavement design system: Volumes 1 & 2. *Research Project EES, 579*.

Matthew, W., Michael, M., Mena, S., & Waleed, Z. (2013). Validating an endurance limit for HMA pavements: Laboratory experiment and algorithm development. Appendix 2 endurance limit for HMA based on healing phenomena using viscoelastic continuum damage analysis (No. NCHRP 9-44 A).

Maurer, D., & Malasheskie, G. (1989). Field performance of fabrics and fibers to retard reflective cracking. *Geotextiles and Geomembranes, 8*(3), 239-267.

Mc Elvaney, J., & Pell, P. (1973). Fatigue damage of asphalt. Effect of rest periods. *Highways and Road Construction, 41*(1766).

Medani, T., & Huurman, M. (2003). Constructing the stiffness master curves for asphaltic mixes (No. 7-01-127-3).

Mehta, Y., Guercio, M. C., & McCarthy, L. (2014). Determine viscoelastic mechanical properties of warm mix asphalt (WMA)-reclaimed asphalt pavement (RAP) mixes under high stresses in airfield flexible pavements and its impacts on design life.

Meyer, N., & Elias, J. (1999, March). Design methods for roads reinforced with multifunctional geogrid composites for subbase stabilization. In *Kunststoffe in der Geotechnik, Technical University Munich*.

Mirzahosseini, M. R., Aghaeifar, A., Alavi, A. H., Gandomi, A. H., & Seyednour, R. (2011). Permanent deformation analysis of asphalt mixtures using soft computing techniques. *Expert Systems with Applications, 38*(5), 6081-6100.

Mirzapour Mounes, S., Karim, M. R., Khodaii, A., & Almasi, M. H. (2014). Improving rutting resistance of pavement structures using geosynthetics: An overview. *The Scientific World Journal, 2014*.

Mirzapour Mounes, S., Karim, M. R., Mahrez, A., & Khodaii, A. (2011). An overview on the use of geosynthetics in pavement structures. *Scientific Research and Essays, 6*(11), 2234-22418.

Molenaar, A. A. A. (2009). Design of flexible pavements *Structural Design of Pavements*.

Monismith, C. L., Ogawa, N., & Freeme, C. R. (1975, January). *Permanent deformation characterization of subgrade soils due to repeated loading*. In *54th Annual Meeting of the Transportation Research Board*, *Washington District of Columbia*.

Montepara, A., Tebaldi, G., & Costa, A. (2007, September). *A surface steel reinforcement for asphalt pavements using 3D finite element model*. In *4th International Siiv Congress*, *Palermo (Italy)*.

Montestruque, G., Rodrigues, R., Nods, M., Elsing, A., Petit, C., Al-Qadi, I., & Millien, A. (2004). Stop of reflective crack propagation with the use of PET geogrid as asphalt overlay reinforcement. In *Fifth International RILEM Conference on Reflective Cracking in Pavements* 231-239.

NCHRP (2011). A manual for design of hot mix asphalt with commentary (No. 673).

Nur, M. A., Khattak, M. J., & Bhuyan, M. R.-U.-K. (2013). Rutting model for HMA overlay treatment of composite pavements. *ISRN Civil Engineering, 2013*.

Ong, G., & Fwa, T. (2005). Analysis and design of vertical-drainage geosynthetic-reinforced porous pavement for roads and car parks. *Journal of the Eastern Asia Society for Transportation Studies, 6*, 1286-1301.

Palmeira, E. M. (2007). Geosynthetics in road engineering. *IGS Leaflets on Geosynthetics Applications, IGS Education Committee*. Available at www. geosyntheticssociety. org

Partl, M., Bahia, H., Canestrari, F., De la Roche, C., Di Benedetto, H., Piber, H., & Sybilski, D. (2013). Advances in inter-laboratory testing and evaluation of bituminous materials: state-of-the-art report of the RILEM technical committee (Vol. 9) (No. STAR 206-ATB).

Perkins, S. W. (1999). Mechanical response of geosynthetic-reinforced flexible pavements. *Geosynthetics International, 6*(5), 347-382.

Prager, S., & Tirrell, M. (1981). The healing process at polymer–polymer interfaces. *The Journal of Chemical Physics, 75*(10), 5194-5198.

Rahimzadeh, B. (2002). *Linear and non-linear viscoelastic behaviour of binders and asphalts* (Doctoral dissertation, University of Nottingham).

Raithby, K. D., & Sterling, A. B. (1970). The effect of rest periods on the fatigue performance of a hot-rolled asphalt under reversed axial loading and discussion. In *Association of Asphalt Paving Technologists Proc*.

Rowe, G., Baumgardner, G., & Sharrock, M. (2008, July). A generalized logistic function to describe the master curve stiffness properties of binder mastics and mixtures. In *45th Petersen asphalt research conference, Laramie, Wyoming*, (Vol. 1416).

Rutting, *Local Government & Municipal Knowledge Base*, from http://www.lgam.info/rutting

Saraf, C., & Majidzadeh, K. (1973, June). Dynamic response and fatigue characteristics of asphaltic mixtures. *Fatigue and Dynamic Testing of Bituminous Mixtures* In *Seventy-sixth Annual Meeting of the American Society for Testing and Materials*, *Philadelphia* 95.

Saraf, C., Majidzadeh, K., & Tribbett, W. (1996). Effect of reinforcement on fatigue life of asphalt beams. *Transportation Research Record: Journal of the Transportation Research Board,* (1534), 66-71.

Sayegh, G. (1967, January). Viscoelastic properties of bituminous mixtures. In *Intl Conf Struct Design Asphalt Pvmts*.

Schapery, R. (1984). Correspondence principles and a generalized J-integral for large deformation and fracture analysis of viscoelastic media. *International Journal of Fracture, 25*(3), 195-223.

Shen, S., & Carpenter, S. H. (2007). Dissipated energy concepts for HMA performance: fatigue and healing *Center of Excellence for Airport Technology* (No. 29) COE Report.

Si, Z., Little, D. N., & Lytton, R. L. (2002a). Characterization of microdamage and healing of asphalt concrete mixtures. *Journal of Materials in Civil Engineering, 14*(6), 461-470.

Si, Z., Little, D. N., & Lytton, R. L. (2002b). Evaluation of fatigue healing effect of asphalt concrete by pseudostiffness. *Transportation Research Record: Journal of the Transportation Research Board,* (1789), 73-79.

Sias, J. E. (1996). *Rate-dependent stiffnesses of asphalt concrete used for field to laboratory prediction and fatigue and healing evaluation* (Master thesis, North Carolina State University).

Siriwardane, H., Gondle, R., & Kutuk, B. (2010). Analysis of flexible pavements reinforced with geogrids. *Geotechnical and Geological Engineering, 28*(3), 287-297.

Sivilevičius, H., & Petkevičius, K. (2002). Regularities of defect development in the asphalt concrete road pavements. *Journal of civil engineering and management, 8*(3), 206-213.

Sobhan, K., Genduso, M., & Tandon, V. (2005, June). Effects of geosynthetic reinforcement on the propagation of reflection cracking and accumulation of permanent deformation in asphalt overlays. In *Proceedings of the 3rd LACCEI International Latin American and Caribbean Conference for Engineering and Technology (LACCET'05) Advances in Engineering and Technology: A Global Perspective*, Cartegena, Columbia 1-9.

Tayfur, S., Ozen, H., & Aksoy, A. (2007). Investigation of rutting performance of asphalt mixtures containing polymer modifiers. *Construction and Building Materials, 21*(2), 328-337.

Asphalt Technology SDN. BHD, (2003), *Penetration grade bitumen*, Lot 11930, Jalan Perajurit, Telok Gong, 42000 Port Klang, Selangor Darual Ehsan, Malaysia.

Thakur, J. K., Han, J., Pokharel, S. K., & Parsons, R. L. (2012). Performance of geocell-reinforced recycled asphalt pavement (RAP) bases over weak subgrade under cyclic plate loading. *Geotextiles and Geomembranes, 35*, 14-24.

Thomas, G. B., Finney, R. L., Weir, M. D., & Giordano, F. R. (2001). *Thomas' calculus*: Addison-Wesley.

Tseng, K.-H., & Lytton, R. L. (1989). Prediction of permanent deformation in flexible pavement materials. *Implication of Aggregates in the Design, Construction, and Performance of Flexible Pavements, ASTM STP, 1016*, 154-172.

Van Dijk, W., & Visser, W. (1977). Energy approach to fatigue for pavement design. In *Association of Asphalt Paving Technologists Proc*, (Vol. 46).

Van Gooswilligen, G., De Hilster, E., & Robertus, C. (1994). Changing needs and requirements for bitumen and asphalts. In *Proceedings of the 6th Conference on Asphalt Pavements for Southern Africa, Held Cape Town October 1994. Vol 2*.

Verhaeghe, B., Myburgh, P., & Denneman, E. (2007, September). Asphalt rutting and its prevention. In *Proceedings of the 9th Conference on Asphalt Pavements for Southern Africa (CAPSA'07), Gaborone, Botswana*.

Verstraeten, J. (1991). Fatigue of bituminous mixes and bitumen thixotropy. In *Proc. XIX th World Road Congress, AIPCR, Marrakech, Maroc* 766-769.

Virgili, A., Canestrari, F., Grilli, A., & Santagata, F. (2009). Repeated load test on bituminous systems reinforced by geosynthetics. *Geotextiles and Geomembranes, 27*(3), 187-195.

Von Quintus, H. L., Mallela, J., Weiss, W., Shen, S., & Lytton, R. L. (2009). Techniques for mitigation of reflective cracks (No. AAPTP 05-04). Atlantic city, New Jersey.

Whitmoyer, S., & Kim, Y. (1994). Determination of elastic properties of asphalt concrete using vibrational analysis. *ASTM J. Test. Eval, 22*(2), 139-148.

Williams, M. L., Landel, R. F., & Ferry, J. D. (1955). The temperature dependence of relaxation mechanisms in amorphous polymers and other glass-forming liquids. *Journal of the American Chemical Society, 77*(14), 3701-3707.

Witczak, M. (2001). Development of the 2002 guide for the design of new and rehabilitated pavements-flexible pavements overview. *Hot topics*.

Witczak, M., Andrei, D., & Houston, W. (2004). Guide for mechanistic–empirical design of new and rehabilitated pavement structures *Appendix GG-1: Calibration of permanent deformation models for flexible pavements* (pp. 1-91).

Wool, R., & O'connor, K. (1981). A theory crack healing in polymers. *Journal of applied physics, 52*(10), 5953-5963.

Yang, X., Han, J., Pokharel, S. K., Manandhar, C., Parsons, R. L., Leshchinsky, D., & Halahmi, I. (2012). Accelerated pavement testing of unpaved roads with geocell-reinforced sand bases. *Geotextiles and Geomembranes, 32*, 95-103.

Yang, Y., Bai, S., & Wu, H. (2014). An experimental investigation into the dynamic behaviors of geogrid-reinforced subgrade soils. *Advanced Civil, Urban and Environmental Engineering, 157*, 211.

Zhang, Z., Roque, R., Birgisson, B., & Sangpetngam, B. (2001). Identification and verification of a suitable crack growth law (with discussion). *Journal of the Association of Asphalt Paving Technologists, 70*.

Zheng, C., & Aysar, N. (2007). Experimental study on fatigue crack growth in both plain and reinforced asphalt concretes. *Journal of the Eastern Asia Society for Transportation Studies, 7*, 2039-2050.

Zhou, F., Scullion, T., & Sun, L. (2004). Verification and modeling of three-stage permanent deformation behavior of asphalt mixes. *Journal of transportation engineering, 130*(4), 486-494.

Zielinski, P. (2013). Investigations of Fatigue of Asphalt Layers with Geosynthetics. *Archives of Civil Engineering, 59*(2), 247.